Supercapacitor Assisted Bicycle for the future of efficient mobility

A thesis

submitted in partial fulfilment

of the requirements for the degree

of

Master of Engineering

at

The University of Waikato

by

Don Charles Uvindra Sirimanne

THE UNIVERSITY OF
WAIKATO
Te Whare Wānanga o Waikato

2021

Abstract

With the world becoming more aware about climate change and being climate conscious, the move away from conventional gasoline powered mobility is accelerated. The public, looking for alternate methods of transportation, are taking up bicycle riding for its low carbon impact and health aspects. As a result, electrically assisted bicycles powered by Li-ion batteries have risen in popularity for the added convenience they allow. This newfound interest allows for more development in the e-mobility sector. This is where a supercapacitor assisted bicycle (SCA-Bicycle) fits in. Compared to existing bicycles in the market a supercapacitor assisted bicycle, due to the nature of supercapacitors, allows the user to store a portion of the energy used while riding on level terrain and use it to assist the user when navigating positive gradient terrain. Supercapacitors can undergo limitless charge-discharge cycles and unlike Li-ion batteries do not need charging to be heavily regulated. This results in a fit and forget system with minimal maintenance required for the onboard electronics. Along with sustainable ingredients, the energy density of supercapacitors has reached closer to lead-acid batteries while newer development has achieved capacity of Li-ion batteries. This rapid pace of development along with the benefits they provide show that supercapacitors will be the future of energy storage.

Another avenue supercapacitors allow, due to their low internal resistance, is brake energy recovery. When braking is applied, while traversing negative gradient slopes, energy is usually lost as heat. This is due to the use of conventional friction braking. A brake energy recovery system enables the storing of this lost energy for later use. This allows for efficient cycling of the energy available for the rider and results in a mode of transport with minimal energy waste.

Acknowledgements

I would like to express my sincere gratitude to my supervisor, Dr. Nihal Kularatana for directing me through the course of my studies. Prof. Nihal Kularatna enforces a heavy emphasis on practical engagement of electronics, always backed by the phrase “burning is learning.” By encouraging us to build many circuits and with as many successful and failed attempts allowed us to build our confidence in the technical materials we learnt. A big weight is placed on the simple fundamentals and allowed me to identify new and innovative solutions. Along with his industry experience he has also instilled passion within us due to his regular tea-time stories, basically showing that if one is motivated, the sky is the limit.

I would also like to acknowledge our technical officer, Benson Chang for providing access to the lab rooms and also providing components and equipment whenever I needed them.

Table of Contents

List of Figures

List of Tables

Chapter 1 :Introduction

With an increasing awareness of the world to climate change and consumers becoming climate conscious, a move away from conventional gasoline powered mobility is accelerated. With exploring alternate methods of transportation some have taken up bicycle riding for the low carbon impact on the environment and the added bonus of better health. As a result a new segment in the market has opened up for electrically assisted bicycles for the added convenience they allow. The basic construction of these E-bikes consists of an energy storage device, mostly a Li-ion battery, providing energy to an electric motor. The position of the electric motor separates the E-bikes on the market. One type is the hub-drive and as the name suggests has the electric motor in either the front or rear wheel hubs. The other type is the mid-drive which includes a motor that is connected to the pedals. One of the main disadvantages of existing E-bikes is the limited range due to capacity of the battery. To increase range bigger batteries are needed which then increases the weight carried by the bicycle. The added weight of the batteries will then require the bicycle frame to be stronger which will add more weight resulting in a bicycle harder to ride without the electric assist.

1.1 New type of electrically assisted bike

The bicycles is an old technology that is still a fairly effective machines at transporting people. Even so the average human can generate only a limited amount of power for self-propulsion. This can be experienced by anyone riding a bicycle up an incline or against strong headwinds. This issue was somewhat relieved by the use of multi-gear bicycles allowing for changing the torque sent to the wheels. With battery technology and motors becoming efficient and cheaper, E-bikes entered the market to deal with the demanding power requirements. Therefore, E-bikes are in high demand resulting in more developments in the e-mobility sector.

This led to the development of the supercapacitor assisted bicycle (SCA-Bicycle), an electrically assisted bike with the use of a new type of energy storage device, supercapacitors. The concept was to store energy while riding on flat ground and riding downhill and then utilize this energy for riding uphill, the most demanding aspect of bicycle riding. Supercapacitors have very low internal resistance (ESR) compared to Li-ion batteries, allowing for high power charging and discharging

while having lower losses. Another advantage is the reduced weight. A battery powered bike needs to store enough energy for the whole ride and therefore requires larger batteries. A supercapacitor assisted bike need to store only the energy required for a single hill climb which can then be charged fast while riding downhill, requiring a smaller capacity.

1.2 Project Development and objectives

For building a prototype an existing E-bike kit was obtained, which consisted of a front mounted in-hub brushless DC (BLDC) motor and a motor controller. The battery was replaced by a supercapacitor bank.

The main objectives of the project are,

- To access the viability of a supercapacitor bank to provide a hill climb assist.
- To develop an effective charging system to harvest energy into the supercapacitor bank while riding.
- To develop a brake energy recovery system for more energy harvesting.
- To complete objectives within the time frame of a Master programme of study.

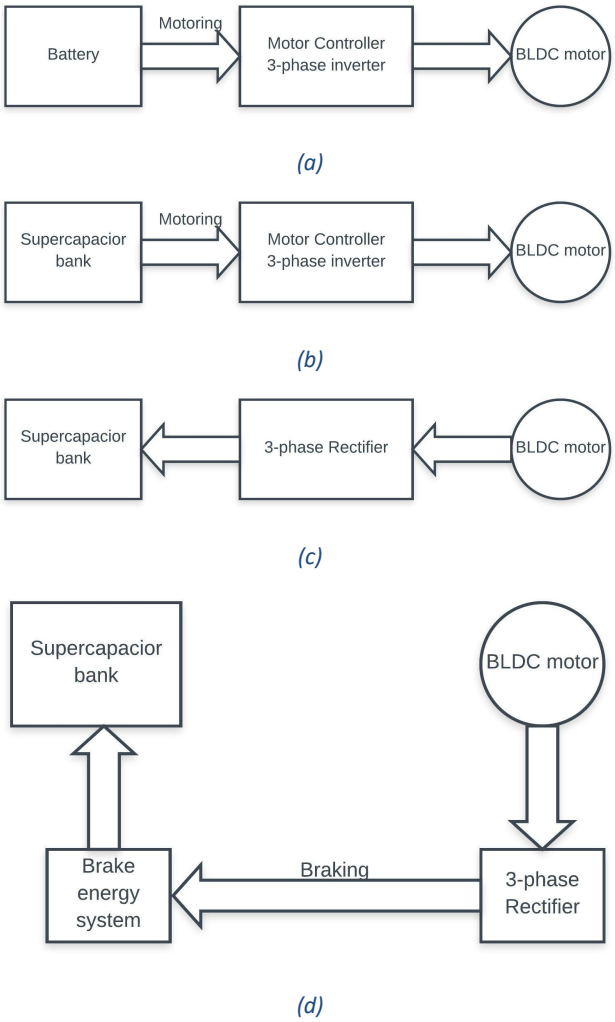

Figure 1.1: Block diagram of: (a) Existing commercial E-bikes. (b) Supercapacitor bank replacing battery. (c) Energy generation during flat ground riding. (d) Brake energy recovery when riding downhill.

1.3 Thesis structure

The following chapters explore the technical developments that aided in the development of the supercapacitor assisted bicycle prototype.

Chapter 2 Covers the basics of motor operation and the different types available along with their respective benefits for specific applications and their pitfalls.

Chapter 3 Explores the various types of energy storage devices used in electricity. This chapter details the capabilities and limitation of each type along with their application and future trends

Chapter 4 Details the numerous available power conversion techniques. This chapter explores the evolving of the basic regulators to the more efficient switching converters.

Chapter 5 Combines the technical knowledge explored in the earlier chapters to develop the supercapacitor assisted bike concept.

Chapter 6 Reports on the objectives achieved and future areas of development.

Chapter 2 : Electricity meets Mechanical power: The Humble motor / Electro-magnetism for motion

This chapter explores the basic principles of motor operation and the different types of motors available. Each type of motor is explored for their individual benefits for applications while also looking into their pitfalls.

2.1 Fundamentals of electric motors.

Electric motors are used every day in many household equipment starting from washing machines and vacuum machines to small power tools like electric drills. A bare bones electric motor is constructed of an arrangement of copper coils and steel laminations. There are several important general principles and guidelines to follow in analyzing the basic mechanisms of an electric motor operation.

Faraday's law of induction, a basic law of electromagnetism, governs the fundamental operating principle of an electric motor. This law predicts how a magnetic field interacts with and electric circuit to create an electromotive force (EMF). Electromotive force is defined as electromagnetic work done on a unit charge when it has travelled one round of a conductive loop. This force can be demonstrated by placing a compass near a current carrying wire. Replacing the compass with a bar magnet as shown in figure 2.1 will show the force on the wire to be minimal.

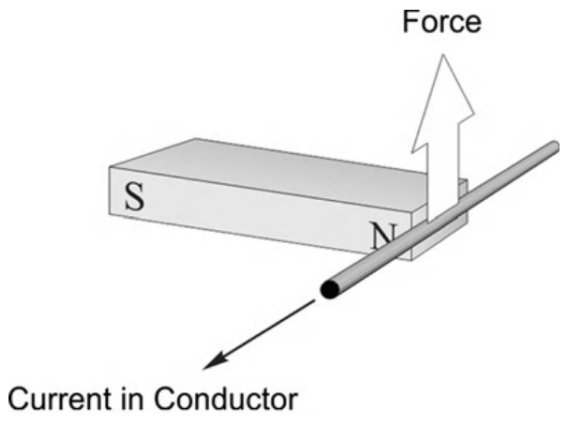

Figure 2.1: Force produced on a current carrying conductor. [1]

To get a useful force from the motor you need a strong magnetic field and a lot of conductors, carrying as much current as possible, to interact with that field. This force is greatest when the conductor is perpendicular to the magnetic field [1] [2]. By experimenting it is also found that this maximum force doubles when the current through the conductor is doubled and when both current and magnetic field is doubled cause the force to multiply by a factor of four. This relationship is expressed by the expression,

$$F = BIl \tag{2.1}$$

where, F is the force on a wire of length l carrying a current I that is exposed to a uniform magnetic flux density B.

2.1.1 Magnetic flux density

A bar magnet has a magnetic field surrounding it. This field consists of flux lines. To observe the said flux lines, we can devise a simple experiment. By placing a sheet of paper above a bar magnet and dropping iron filings on the sheet of paper would arrange the iron filings as shown in figure 2.2. If we place a small compass along these flux lines, we can see the compass needle change direction. This shows that the flux lines have a direction as shown. By convention the flux lines are said to be positively directed from the N to the S of the magnet. It should however be mentioned that the magnetic flux lines form closed loops.

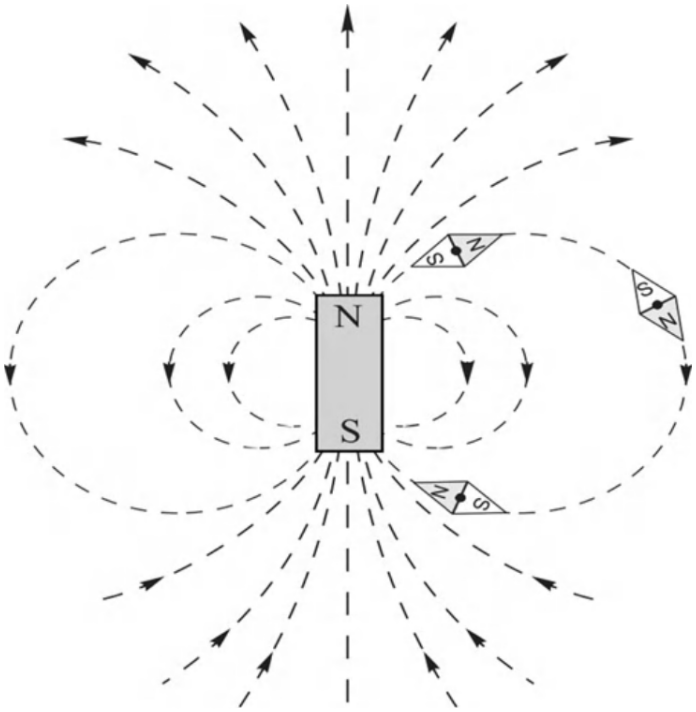

Figure 2.2: Magnetic Flux lines of a bar magnet.[1]

Flux plots also provide us information of the intensity of the magnetic field. It is believed that in between each flux line there is an equal amount of magnetic flux. Therefore, when the flux lines are closer to each other we obtain a higher density of magnetic flux. We obtain the vector quantity flux density (**B**) by using the following expression,

$$\boldsymbol{B} = \frac{\Phi}{A} \tag{2.2}$$

where Φ is the magnetic flux while A is the cross-sectional area in between the flux lines.

We can also obtain a magnetic field by passing current through a multi-turn coil of wire. For each turn a field pattern is produced and when these fields are superimposed we obtain a field that is substantially increased and that which resembles that of a bar magnet. Since bar magnets are more costly compared to coils, the magnetic fields of most motors are produced by coils. These coils need to create large magnetic fields which is done by arranging the coils and their associated magnetic circuit favorably.

2.1.2 Magnetic Ohm's law

To increase the flux density, we can increase the current in the coil or add more turns. The ability for a coil to produce flux is quantified in terms of its magnetomotive force (m.m.f). The m.m.f of the coil is the product of the number of turns (N) and the current (I). A given m.m.f can be obtained by either large number of thin wires carrying a low current or a small number of thick wires carrying a large current.

The magnetic flux created is proportional to the m.m.f driving it. By introducing the idea of reluctance (S). Reluctance quantifies the difficulty of the magnetic flux to complete the circuit. The magnetic Ohm's law is presented by the following expression,

$$Flux = \frac{m.m.f}{Reluctance} \tag{2.3}$$

To obtain a high flux for a given m.m.f we need to reduce the reluctance, and this is done by using a good magnetic material, magnetic steel. Air is bad magnetic material and therefore has a high reluctance. This gives a path for the flux lines to follow and therefore most of the flux lines ae confined the steel rather than the air surrounding coil. Therefore, we can guide the flux where we need by shaping the steel.

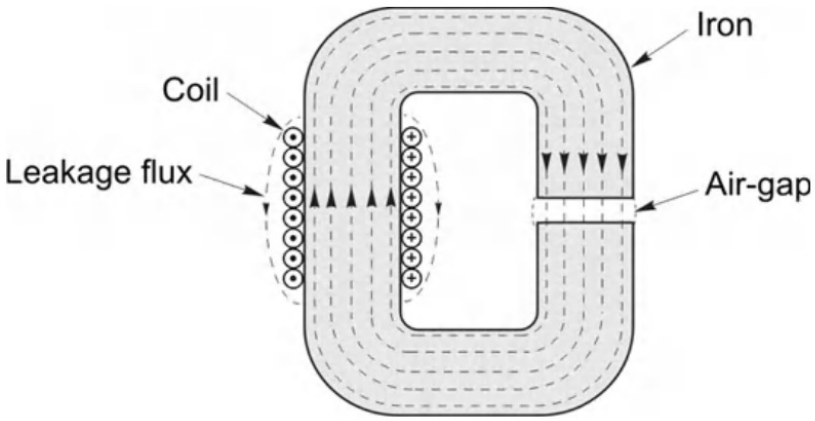

Figure 2.3: Flux lines inside a low-reluctance magnetic circuit [1]

2.1.3 Torque production

Figure 2.3 shows the magnetic circuit with its flux lines. The air gap region is where the force producing conductors of the motor are placed. The flux density is unform across the cross-section of the steel due to the low reluctance compared to that of air. When the air gap is relatively small the flux jumps across without expanding out into the air, as shown in Figure 2.2, providing with a flux density as high as it was inside the steel.

With the magnetic circuit designed to produce a high flux density we need to obtain maximum force from it. Therefore we need to arrange a set of conductors such that positive current flows under a N-pole and vice versa, as shown in figure 2.4 (a).

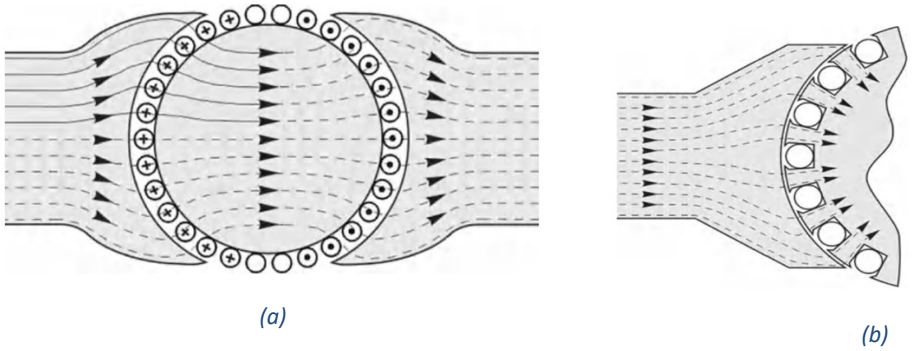

(a) *(b)*

Figure 2.4: (a) current carrying conductor on rotor, (b) slotting to accommodate conductors [1]

This arrangement of conductors provide another limitation on design. The size of the conductors are limited by the spacing between the air gap which will restrict the maximum current capabilities of the force carrying conductor and also affect the flux density. To mitigate this limitation “slotting”, as shown in Figure 2.4(b), was developed that allowed the air gap to be as minimal as possible and hence the reluctance to be minimal. This provided the added benefit of the force from the conductors to the sides of the slots, which are more capable than the conductors at transferring torque to the shaft.

2.2 Types of Electric motors

We now know the torque generated by an electric motor is due to the interaction between a current carrying conductor and a magnetic field, produced either by a magnet or an electromagnet. Electric motors are also classified into two main categories below depending on how they are powered.

1. Direct current motors (DC)
2. Alternating current motors (AC)

Earlier electric vehicles used DC motors for propulsion. AC motors are highly efficient and have a higher power density and better reliability than DC motors [2]. This has resulted in Ac motors to be found for propulsion in electric vehicles to electricity generation in power stations. While AC motors are used in the realm of medium to high power applications, DC motors are still favoured for low power applications due to their ease of control and cost.

2.3 Direct current motors (DC)

DC motors as the name suggests uses Direct current to operate. The main DC motor most people first encounter is the brushed permanent magnet (PM) DC motor. The permanent magnet provides the magnetic flux. The current inside the brushed motor flows from the stator, stationery part, to the rotor, rotating part, of the motor by using mechanical brushes and commutators, as shown in Figure 2.5. Another DC motor is the wound field motor. These motors generate the magnetic field using an electromagnet while the rest of the motor construction matches that of the brushed PM motor. This motor provides the benefit of weakening the magnetic field enabling high speed operation. These motors can be found in low power applications such as windshield wipers and window shutters in cars.

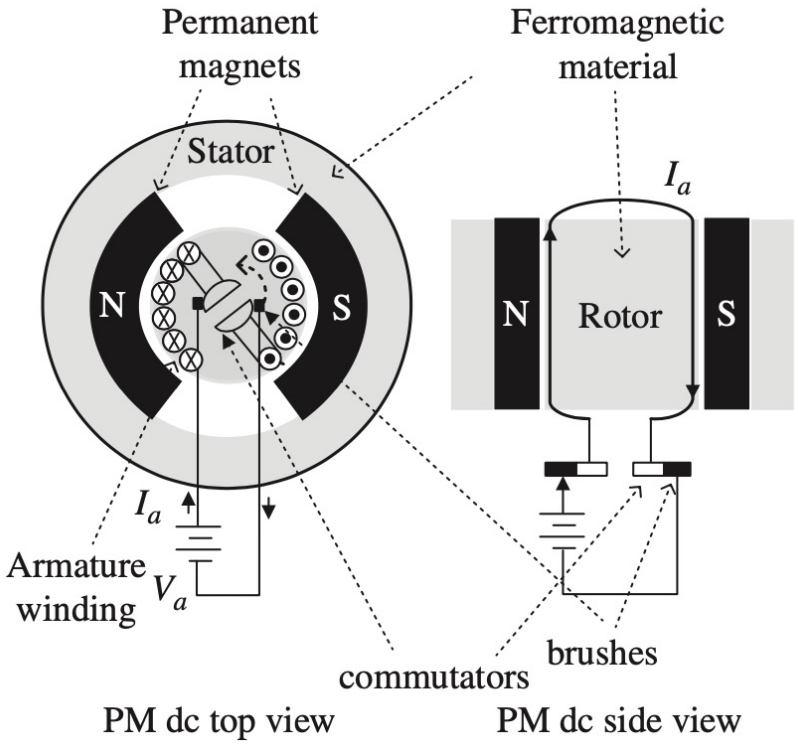

Figure 2.5: Permanent DC motor structure [2]

The stator contains the permanent magnets with an even number of poles excited alternately north and south in sequence. The rotor contains the armature winding that carries the current which creates the torque. The armature winding contains a number of coils across the rotor spanning 180 electrical degrees, from a north pole to a south pole. For the motor to produce torque and continue rotating the direction of current at the north pole should be in one direction while other side has current in the opposite direction. This is taken care of by the use of the brushes and commutators. The commutator is a cylinder formed by copper segments mounted on the armature shaft. The brushes connected to the power source and left touching the commutator cylinder providing current to the armature. Taking the example of the two pole motor shown in figure 2.5, the current flowing through the armature winding results in a torque which rotates the rotor. When the rotor completes half a cycle the current in the armature will alternate and change the direction of the current and this will continue providing continuous rotation. Although the brushes and commutators provide a solution for alternating the direction of the current, it is also the main point of failure for the motor. There is significant wear and tear in the brushes and commutators due to the friction on the contact surface. With the friction a build-up of conducting carbon dust is also observed between the commutator pieces. This results in reduced lifetime, regular maintenance as well as loss in efficiency of the motor.

2.3.1 Types of DC motors

Conventional DC motors are characterized as shunt, series, or compound connected [3][4]. Each type of motor has specific and different characteristics and the type of motor used depends on the mechanical requirement of the load.

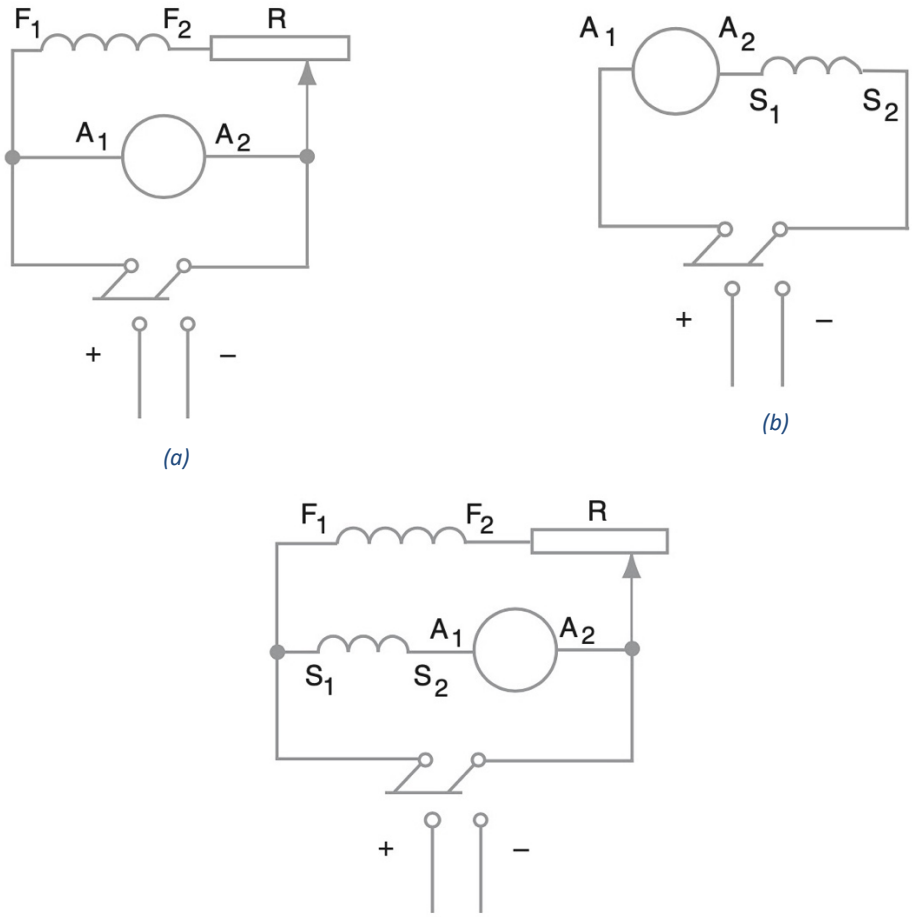

Figure 2.6: Types of Dc motors; (a) Shunt motor, (b) Series Motor, (c) Compound motor[4]

The shunt motor has field windings consisting of many turns of small wire forming the concentrated field pole winding. The field windings might be in parallel with the armature (shunt), or separately connected across a voltage supply. By controlling the current through the winding the flux can be controlled which has an important effect on the output of the motor.

The series motor has field windings consisting of few turns of large wires and it is connected in series with the armature. The field flux is controlled by the applied voltage and load torque which determines the current in the armature. As the load torque affects the current the series connected

motor is considered a constant power motor. Series motor is used for loads that require maximum torque when starting. The torque limit is set by placing a series resistance in the armature or adjusting the applied voltage. Due to the motor's torque-speed relationship the motor shouldn't run unloaded, in which case the speed will increase dramatically and destroy the rotor.

The compound winding motor has both a shunt winding and a series winding. The majority of the flux is due to the shunt windings with additional excitation from the series winding. Cumulative compounding is when the series winding field add to the flux produced by the shunt winding or differential compounding when subtracted. Cumulative compounding provides the best parts of both shunt and series by contributing to the flux resulting in high starting torque and the general speed-torque characteristic of the shunt motor.

2.4 Alternating current motors (AC)

The development of the AC motor is credited to the brilliant inventor Nikola Tesla. Tesla envisioned a motor that would remove the need for brushes and commuters. His idea consisted of feeding a three-phase ac voltage and currents to create a spinning magnetic field within the motor. The AC motor was instrumental in the development of the current electricity grid [2].

The most common type of motor used in homes, business and industry are induction motors due to their rugged construction and reliable operation. Induction motors get their name from the method of transfer of power from the primary winding of the stator to the rotor. The stator is a doughnut shaped stack of steel laminations with insulated slots holding the stator coils.

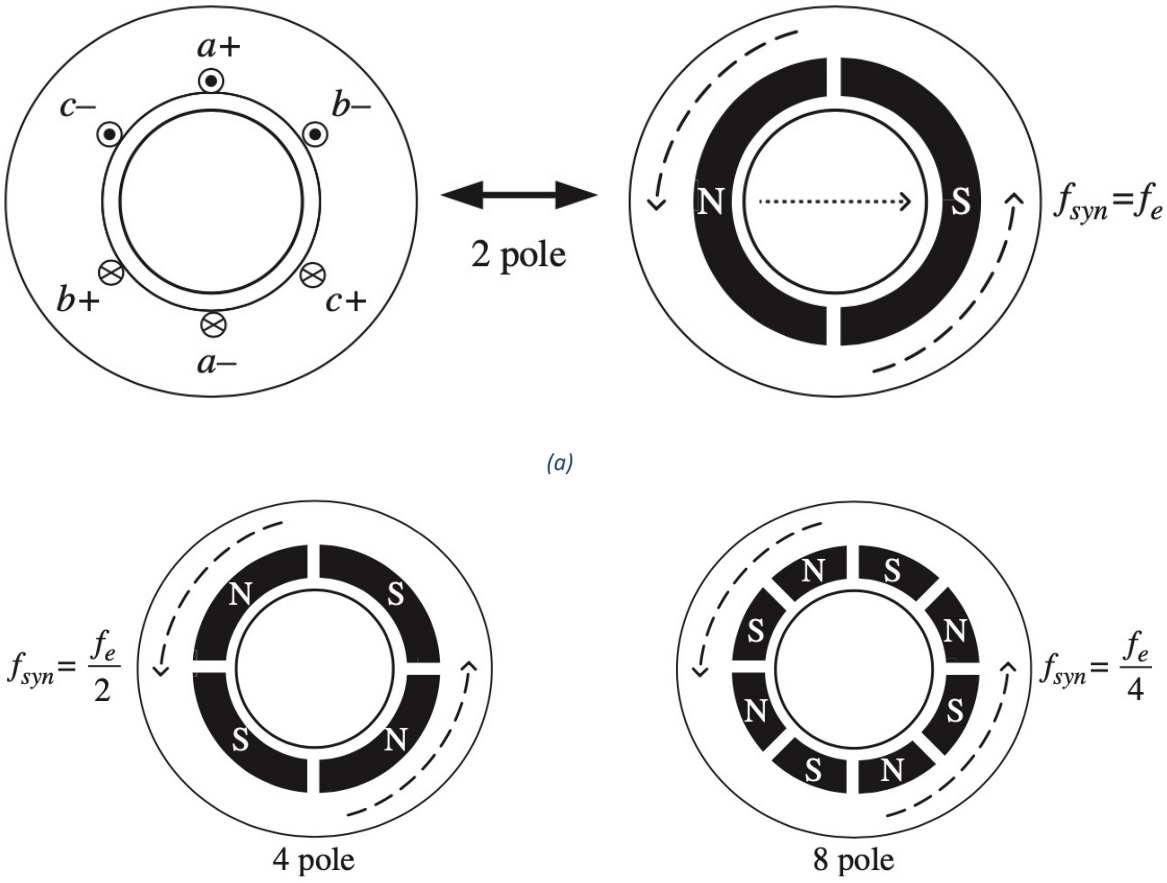

Figure 2.7:The spinning magnetic field of AC motor for various magnetic pole counts.[2]

Three winding coils, a, b and c, are placed 120° apart from each other in the stator. By providing three currents that are 120° out of phase from each other, as is provided by the AC grid, into the three individual windings a spinning magnetic field is created in the stator. The three phase windings are connected in either star (wye) or delta (mesh) configuration, as shown in figure 2.8, to form three identical groups. The spinning magnetic field can be modelled by a spinning magnet as shown in figure 2.7(a). The magnetic field can then interact with a magnetic field of a rotor, either generated by a electromagnet or permanent magnet, to generate an electromechanical torque. The spinning magnetic field will induce the rotor current with which it will interact, the basis of the induction motor.

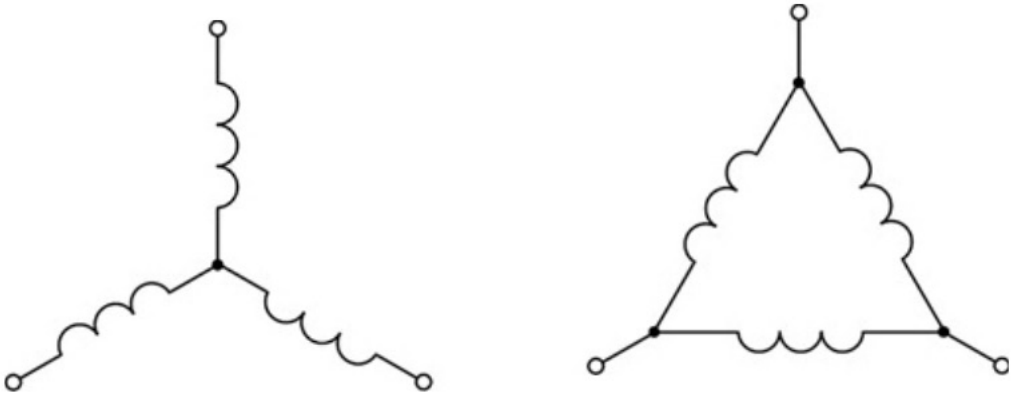

(a) *(b)*

Figure 2.8: (a) star (Wye) configuration, (b) Delta (Mesh) configuration [1]

The induction motor is usually designed to have more than one magnetic pole pair. The conductors can be rearranged in the stator slots to make multiple pole motors. Four pole and eight pole motor with their equivalent stator magnetic fields are shown in figure 2.7(b). The four pole motor has two pole pairs and the rotating magnetic field will take two electrical cycles for a complete rotation. The eight pole motor has 4 pole pairs resulting in the rotating magnetic field requiring four electrical cycle for a complete rotation. The frequency of the rotating magnetic field is the synchronous frequency f_{syn}. The synchronous frequency can be calculated by the following expression,

$$f_{synchronous} = \frac{frequency\ of\ power\ supply}{number\ of\ pole\ pairs} \tag{2.4}$$

A more useful measure of the AC motor is the synchronous speed N_s, which is given by the expression,

$$N_s = \frac{120f}{p} \tag{2.5}$$

Where f is the frequency of the power supply and p is the number of pole pairs. Table 2.1 shows the synchronous speed for commonly used pole pairs. The speeds for 50 Hz and 60 Hz supply is shown as the electrical grid of parts of the world utilize one of these frequencies.

Table 2.1: Synchronous speed, in rev/min [1]

Pole-pairs	50 Hz	60 Hz
2	3000	3600
4	1500	1800
6	1000	1200
8	750	900
10	600	720
12	500	600

By increasing the number of pole pairs for a given speed we can supply the motor with a high frequency power supply. This allows for the size and weight of the motor to decrease and therefore is favoured for automotive applications.

2.4.1 Types of AC motors

AC motors come in two different flavours, asynchronous and synchronous motors. They both consists of similar stators but have different rotor configurations.

In an asynchronous motor the spinning magnetic field operates at a different frequency from the current with which it interacts for torque generation. The squirrel cage induction motor is an example of an asynchronous motor. Here the current supplied to stator generates a spinning magnetic field. The rotor, shown in Figure 2.9(a), is made of a stack of slotted steel laminations which are approximately equal to the length of the stator. Copper or aluminium bars are mounted near the surface of the rotor and they are shorted to resemble a squirrel cage. The spinning magnetic field induces voltages and current on the rotor which again interacts with the spinning magnetic field producing torque.

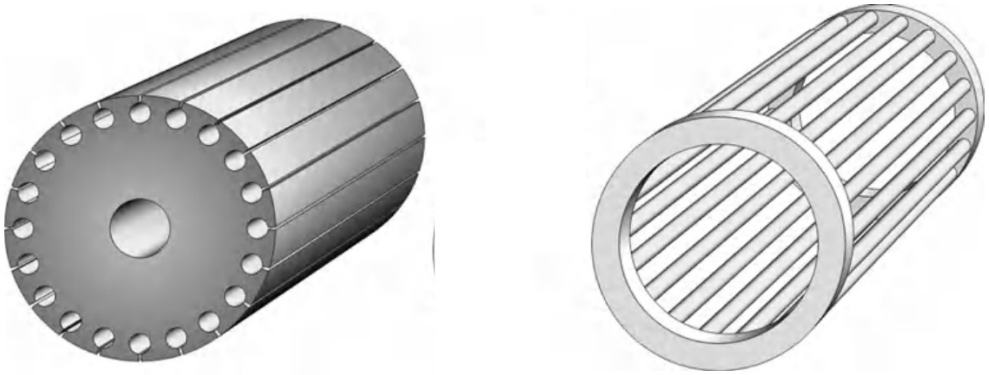

(a) *(b)*

Figure 2.9: Rotor construction: (a) slotted steel laminations, (b) copper bars resembling cage[1]

In a synchronous motor the spinning magnetic field and current operate at the same frequency. Synchronous motor consisting permanent magnets have rotors containing several pairs of permanent magnet poles. The current supplied to the stator then interacts with the magnetic field of the magnets to produce torque. Technological advances of permanent magnets and power electronics have led the way for high-power density motors. The magnets are either placed on the surface or in the interior of the rotor. For the propulsion system of electric vehicles the interior permanent magnet ac motor is used. The interaction between the magnetic flux and the current supplied generates a magnet torque while the interaction between the iron material and supplied current produce a reluctance torque.

2.5 Brushless Direct Current motor (BLDC)

The BLDC motor provides the benefits of a DC motor by operating with a DC power supply while having the longevity and minimal maintenance of AC motors. The BLDC motor works similar to a permanent magnet AC motor. Whereas the stator contains the permanent magnets of the AC motor, the BLDC motor contains them in the rotor and the stator contains the current carrying conductors. This motor uses electronics commutation to switch the stator field. The motor uses sensors to determine the rotor position and the inverter triggers adjusting the supply voltage to provide proper level of voltage to the stator poles to maintain speed and direction. A schematic for BLDC control is shown in Figure 2.10.

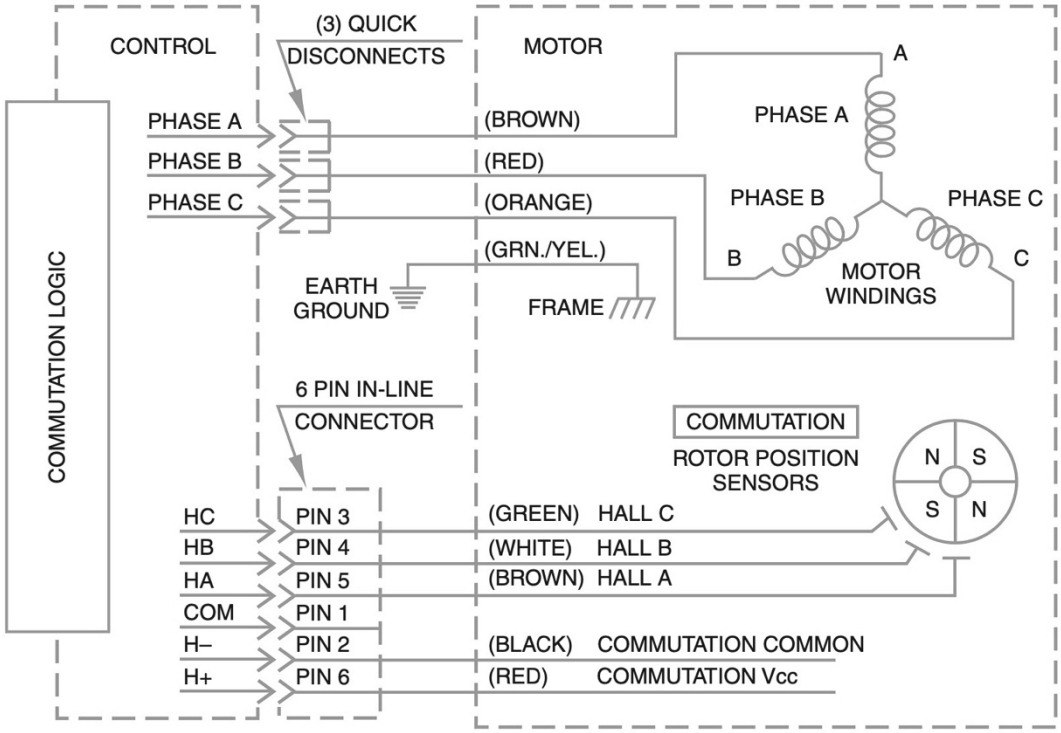

Figure 2.10: BLDC motor control schematic[4]

The torque on a BLDC motor is controlled by adjusting the armature winding current. The flux density distribution is approximately trapezoidal in shape. The torque can be found by the expression,

$$Torque = K_T I \tag{2.6}$$

Where K_T is the motor torque constant and I is the current in the windings. Similarly the back emf of the motor can be found by the expression,

$$EMF = K_E \omega = K_E \frac{2\pi N}{60} \tag{2.7}$$

Where K_E is the motor voltage constant, ω is the rotor speed in radians per second and N is the rotor speed in revolutions per minute. It should be mentioned that for most motors K_E and K_T are equal.

Chapter 3 : Storing Coulombs in Chemical reactions or Electrostatic fields

This chapter explores the various energy storage devices used for electricity comparing their energy storage capabilities and power capabilities along with discussing the limitations of each type of energy storage device. We also explore the past techniques to more recent developments in the field and what the future trends will look like.

3.1 Fundamentals of Energy Storage Devices

An energy storage device, as the name implies, is used to store energy in one form or the other so that energy can be extracted later. Energy, which is an important concept in physics, is the ability to do work. Work, *W*, is described as a force *F* moving an object by a distance, Δx, in the same direction as the force, given by the expression below.

$$W = F\Delta x \tag{3.8}$$

The first law of thermodynamics states that the change in internal energy of a system is equal to the work done by the system. This also falls in line with the law of conservation of energy in that energy can neither be created or destroyed and energy can only transfer from one form to another. Along with the multitude of energy forms, different units are used to be applicable for the field. For example the British Thermal Unit (BTU) used for temperature regulating systems. For the field of electricity the commonly used unit for energy is the kilowatt-hours (kWh), while the fundamental unit is the Joule (J).

Apart from storing energy an energy storage device should also be capable of releasing the stored energy at an appropriate rate, or power rating. Power is the rate of change of energy measured in watts (W). Average power, $\bar{P}$, is expressed by,

$$\bar{P} = \frac{\Delta W}{\Delta t} \tag{3.9}$$

For electrical systems the power consumed or generated can be measured based on the terminal voltage, *V*, and current, *I*, passing through an electrical component by,

$$P = VI \tag{3.10}$$

3.1.1 Simplified equivalent circuit of an energy storage device

Obtaining a simple energy device with a constant terminal voltage of *V* volts and an energy storage capacity of *E* there is a finite internal resistance, r_{int}, which results in the equivalent circuit shown in Figure 3.1(a). By connecting a load with resistance, R_L, we obtain a closed circuit, as shown in Figure 3.1(b), aiding us in analysing the energy storage device.

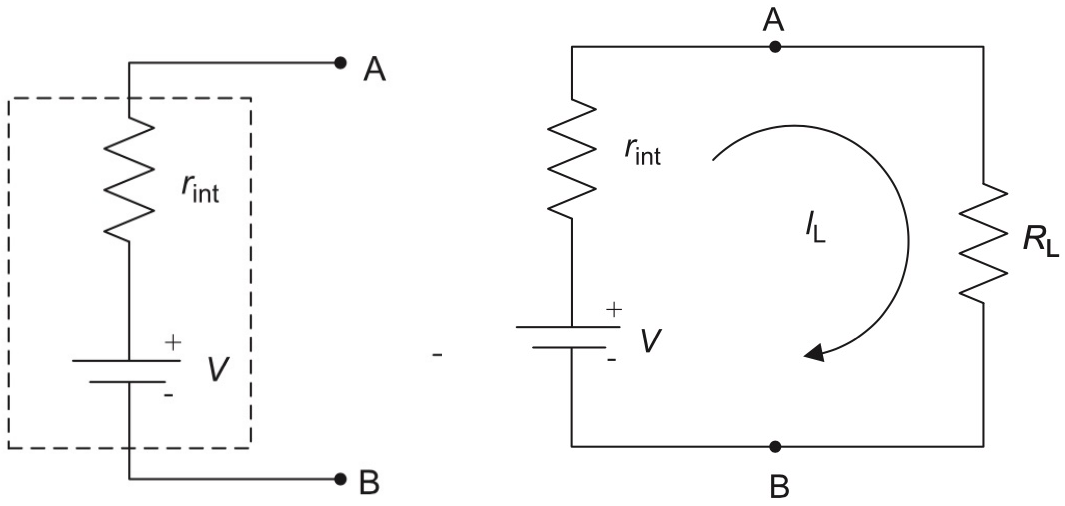

(a) *(b)*

Figure 3.1: Energy storage device (a) represented by a constant voltage source and fixed internal resistance (b) closed circuit formed with external load [6, p. 41]

We can analyse the circuit by applying ohm's law.

$$I_L = \frac{V}{R_L + r_{int}} \tag{3.11}$$

Voltage of the load, V_L, is found to be,

$$V_L = \frac{VR_L}{R_L + r_{int}} = \frac{V}{1 + \frac{r_{int}}{R_L}} \tag{3.12}$$

From Equation (3.5) we can observe that the useful voltage appearing at the load increases with a high open-circuit voltage but decrease as the internal resistance increases. Therefore, a good energy device should have a low internal resistance and a high open-circuit voltage. An expression for the power expended by the load can now be found by combining Equation (3.4) , (3.5) and (3.3)

$$P_L = I_L V_L = \frac{V}{R_L + r_{int}} \frac{V}{1 + \frac{r_{int}}{R_L}} = \frac{V^2}{R_L} \left[\frac{1}{\left(1 + \frac{r_{int}}{R_L}\right)^2} \right] \tag{3.13}$$

The power supplied to a load therefore depends on the open-circuit voltage and the internal resistance of the energy device, with an ideal source with zero internal resistance provide a maximum power output of V^2/R_L. However, in practice the maximum power output is restricted by the internal resistance of the energy source. Part of the energy is converted and wasted as heat generated due to the internal resistance. The maximum possible load power occurs when $R_L = r_{int}$ where, the maximum possible power output is $V^2/4R_L$. Many modern supercapacitor families have very low internal resistance which allow these devices to supply large amounts of power to a load when fully charged to the rated voltage [6, p. 42]. Batteries on the other hand have an internal resistance that increases while discharging resulting in the available power to drop.

3.1.2 Short term energy storage in power electronic systems.

Couple of basic components are used in power electronics for short term energy storage. One such component is the inductor. Energy is stored in an inductor by creating a magnetic field, which is

generated when current flows through the inductor. The energy stored, E_L, in an inductor, of inductance L, by passing a current of I is given by,

$$E_L = \frac{1}{2} LI^2 \tag{3.14}$$

As the energy is stored due to the current passing through the inductor, this energy cannot be physically transported after disconnecting the circuit.

The other component in question is the capacitor. Energy storage is associated with an electrostatic field based on electric-charge storage. When a voltage source is connected to the capacitor, its voltage rises exponentially to the value of the voltage source. The energy stored, E_C, in a capacitor of capacitance C, by a DC voltage source of V volts is,

$$E_C = \frac{1}{2} CV^2 \tag{3.15}$$

Because of the nature of energy storage if the capacitor has no significant leakage, the energy can be transported after disconnecting the circuit. Practical capacitors have high leakage currents and therefore dissipates this energy in the form of heat in the large leakage resistance.

3.1.3 Long term energy storage solutions

The energy storage devices mentioned in the previous section is used mainly for circuit level design. To accommodate longer term energy storage, such as a backup for when a power failure occurs, there a several devices used [6, p. 47].

- Electro-chemical devices such as batteries
- Supercapacitor banks
- Flywheels
- Fuel cells and their energy source

Electro-chemical batteries allow for the storage of energy for few minutes to a few hours. Supercapacitors are the bigger cousins of capacitors and as such behave similar. They have much higher capacitances compared to capacitors allowing for more energy to be stored. The internal resistance of supercapacitors are much lower compared to batteries, allowing for high power. Usually supercapacitors and batteries are used together to obtain the best characteristics of both.

Flywheels use a rotating mass to store energy based on the speed of rotation and the inertia of the rotor. The energy stored in the rotor, E_k of a flywheel rotating at a high speed of ω with a moment of inertia J is given by,

$$E_k = \frac{1}{2} J \omega^2 \tag{3.16}$$

The rotors are usually made to keep the mass low while increasing its inertia with newer systems using light weight carbon-fibre and other composite materials for construction.

Fuel cells converts the chemical energy of a fuel directly to electrical energy by means of an electrochemical process. Fuel and an oxidizing agent are separately and continuously supplied to the two electrodes of the cell, as shown in Figure 3.2. An electrolyte is placed between the two electrodes to conduct ions from one electrode to the other. The electrons released from the fuel under catalyst flow through the external circuit to the cathode, due to the potential difference between the electrodes, where they combine with the oxygen and produce an exhaust.

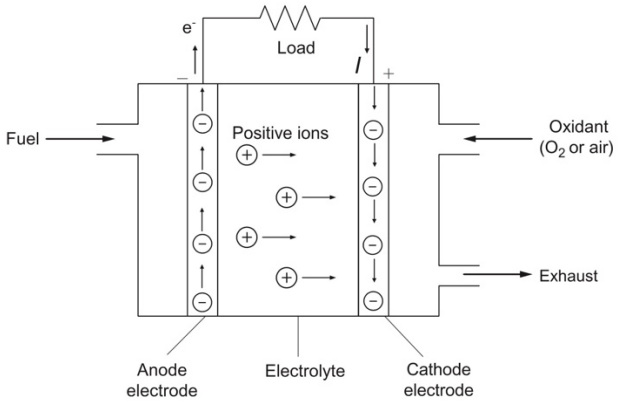

Figure 3.2: Operation of a fuel cell.[6, p. 52]

Rather than being an energy storage device, the fuel cell is an energy converter. It taps into the energy stored in the fuel to provide energy.

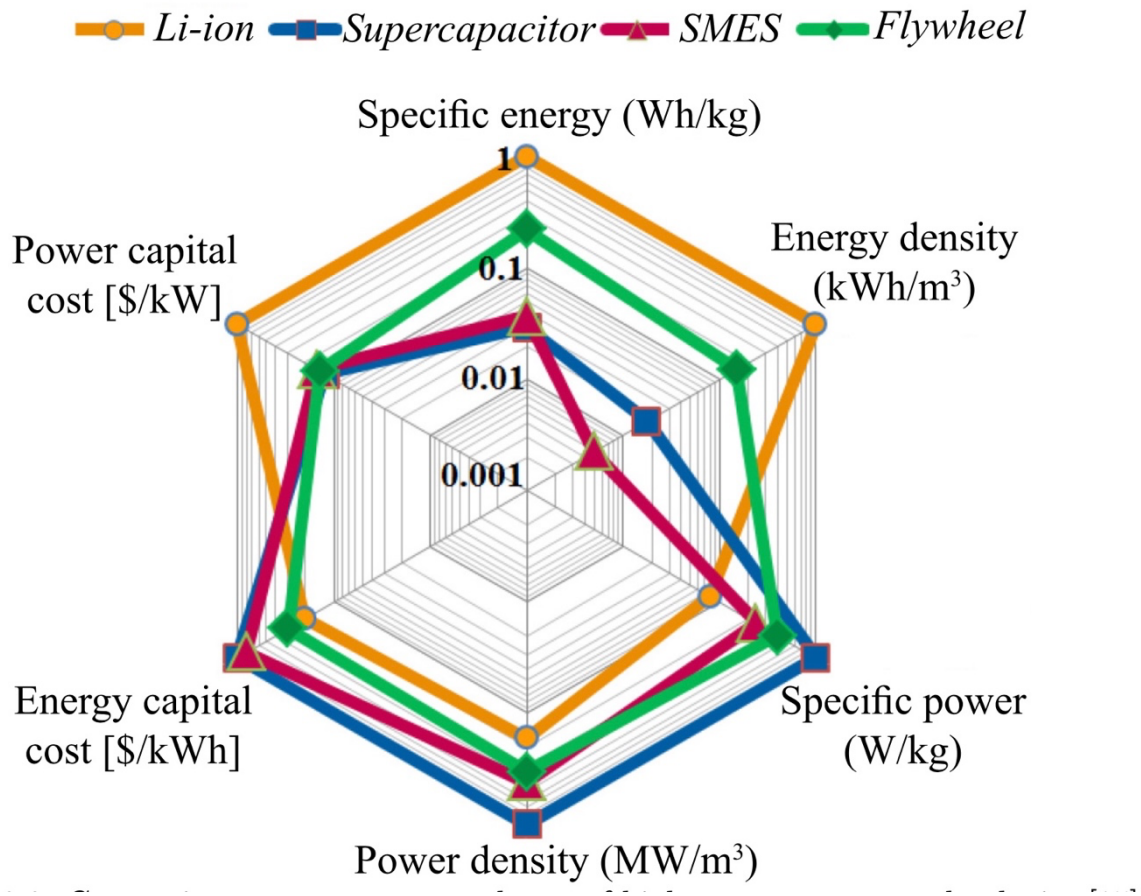

Figure 3.3:Comparison of power, energy and cost of long-term storage techniques [15]

3.1.4 Technical Specifications of energy storage devices.

With various energy storage devices available, it is required to characterise them by a general set of specification that will allow an engineer to choose a device depending on the requirements of the application, especially size and power.

Energy density is the energy stored per unit volume or weight. It is called gravimetric energy density when weight is used and volumetric energy density when volume is used. The units are watt-hour per kilogram and watt-hour per liter respectively.

Power density is the maximum power delivered per unit volume or weight. Just like with energy density when volume is used it is called volumetric power density and gravimetric power density when weight is used. The units are Watts per litter and Watts per kilogram respectively.

Cycle life is the number of times a device can withstand deep discharge and recharge repetitively, using the manufacturer's recommendations, before capacity depreciates below specifications.

Cyclic energy density considers the energy density over the service life of an application. It is defined as the product of energy density and the cycle life at said energy density. The units are watt-hour-cycles per kilogram for gravimetric or watt-hour-cycles per liter for volumetric.

Self-discharge rate states how long an energy storage device be stored and still provide the required capacity. Batteries have lower self-discharge rates than supercapacitors. Self-discharge is measured in terms of percentage of capacity loss per month or years in terms of energy lost.

3.1.5 Ragone plot

The two main specifications used to compare the performance of energy storage devices are the energy density and power density. To provide a visual comparison of these specifications a Ragone plot, as shown in Figure 3.4, is used with the devices located in characteristic regions.

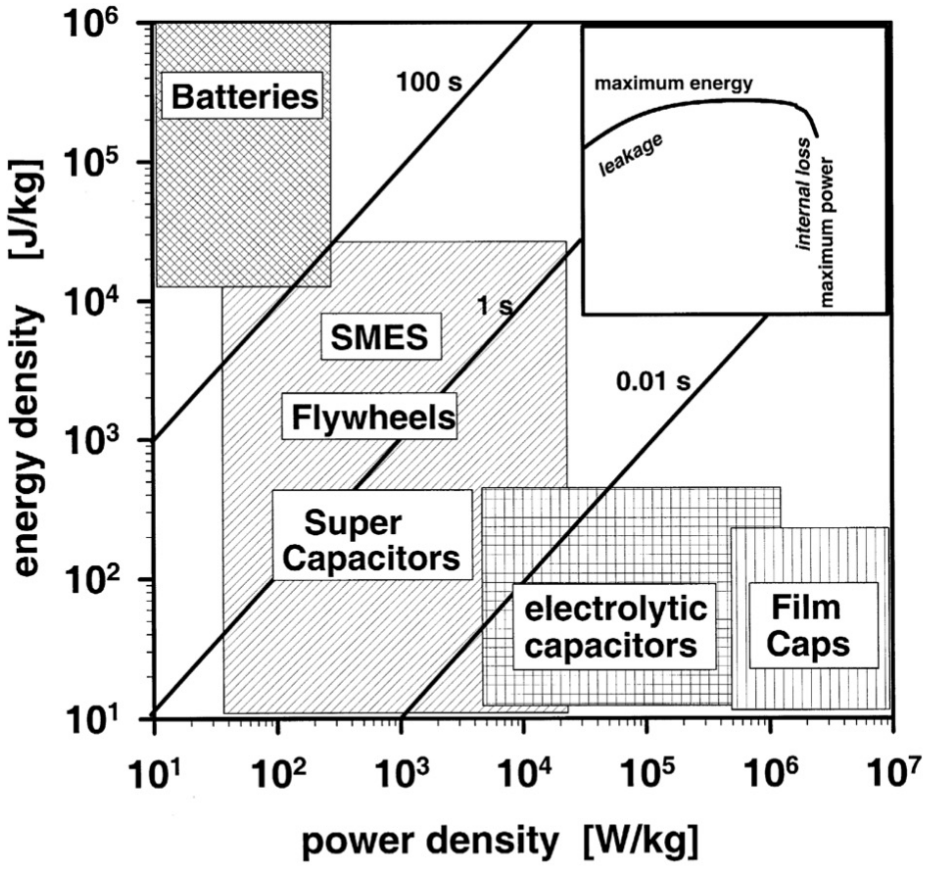

Figure 3.4: Ragone plot [16]

The regions are related to specific applications by energy and power requirements. Internal losses and/or leakage etc. determine the boundaries of the regions. In the log-log plane of Figure 3.4, the straight lines correspond to time where, as observed batteries are used for long time applications while film capacitors are used for short time applications. The Ragone plot provides the power limits of a storage device and the optimum working region for said device, shown by the part of the curve where both energy and power are high.

3.2 Rechargeable batteries.

An electric battery stores and converts electrochemical energy to electrical energy. Rechargeable battery chemistries are based on variations of lead acid, nickel-based and lithium based systems. The choice of battery technology used depends on the size, weight, cycle life, operating range and cost. A comparison of major battery chemistries is shown in Table 3.1.

NiCd batteries were used to power rechargeable consumer electronics until cadmium came under regulatory scrutiny. With the technology having matured newer chemistry of NiMH entered the market with an increase in energy density. This technology was later beaten by Li-ion based chemistry, which is seen in all portable consumer electronics in recent times. However, Li-ion have the tendency to be damaged easily if battery is not managed properly. Fail-safe circuits are required to protect against over-current or over-temperature conditions that will otherwise can lead to catastrophic failure, such as the exploding Samsung note 7 devices. Therefore, Li-batteries have strict charge and discharge controls in place.

Table 3.1:Battery chemistry specifications [6, p. 76]

Parameter	Unit/ conditions	Sealed lead acid	NiCd	NiMH	Li-ion	Li-polymer	Li-iron phosphate
Average cell voltage	V	2.0	1.2	1.2	3.6	1.8-3.0	3.2-3.3
Self-discharge	% month	2-4%	15-25%	20-25%	6-10%	18-20%	
Cycle life	Cycles to reach 80%	500-2000	500-1000	500-800	1000-1200		1500-2000
Overcharge tolerance		High	Med	Low	Very Low		
Internal resistance		Low	Very Low	Moderate	High (coke electrode) Highest (graphite electrode)		
Energy by volume	Watt-hour/liter	70-110	100-150	200-350	200-330	230-410	200
Energy by weight	Watt-hour/kg	30-45	40-60	60-80	120-160	120-210	100

3.3 Lithium based rechargeable battery.

The demand for portable electric devices resulted in the development of lithium based batteries. They had almost double the energy density of nickel based batteries resulting on light weight energy packs. The cell voltage was also three times that of nickel based batteries resulting in fewer cells for a given voltage requirement. Because of the high-energy density and declining costs of manufacturing and battery management circuits Li-ion cells are seen in every portable consumer electronics. Figure 3.5 shows a capability of Li-ion cells compared to other battery chemistries.

The anode of a Li-ion cell is a material capable of acting as a reversible Li-ion reservoir and is usually a form of carbon. The cathode can also act as a reversible Li-ion reservoir with $LiCoO_2$, $LiNiO_2$, or $LiMn_2O_4$ as preferred materials due to their high oxidation potentials. The cathode reaction generates a half-cell voltage of approximately 1 v, while the anode half-cell reaction generates -3 V for an overall voltage of approximately 4V [2, p. 76].

Lithium-titanate (LiT) batteries replace the carbon in the anode with titanium. This allows for significantly improved lifetime of the battery and the reduced internal resistance improves it power capability. This however results in a low voltage and low specific energy compared to Li-ion cell and cost more due to the titanium. The carbon anode is replaced Silicon-based alloys to achieve higher energy density.

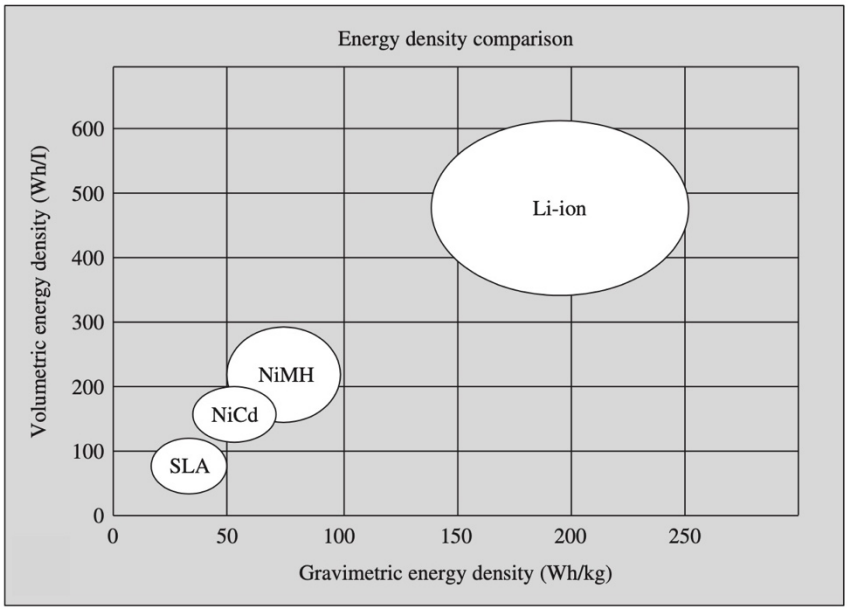

Figure 3.5: comparison of Li-ion with other chemistries [6, p 88)

Li-ion cells looks to be superior than the rest. However, lithium cells cannot tolerate overcharge and over discharge conditions. Commercially available Li-ion batteries have protection circuits that limit charging and discharging voltages to avoid reducing the cycle life and damage to the cells.

Li-ion batteries use coke or graphite for its anode material, each providing different discharge profiles, as shown in Figure 3.6. The graphite anode discharge is observed to be flat during the majority of discharge cycle and therefore have more energy available for a given voltage. The coke anode has a more sloped discharge profile.

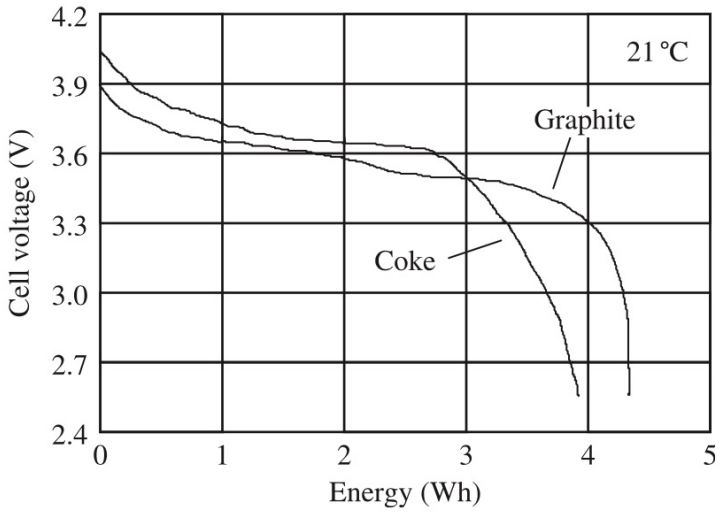

Figure 3.6: Li-ion discharge profile

3.4 Supercapacitors for energy storage.

Capacitors store energy in an electrostatic field. Common capacitors have capacitance values in the range of microfarads with a wide range of voltage ratings. This allows them to be used for filtering and temporary energy storage. Due to their micro scale capacitances the energy stored is quite small.

Recently a new family of capacitors called electrochemical capacitors were developed with high capacitances, in the range of 0.1 to over 50,000 F, albeit with voltages at 2 to 4V. These electrochemical capacitors are called supercapacitors, ultracapacitors or electrochemical double-layer capacitors (EDLCs). They store charge in an electrical double layer at the interface between a high surface area electrode and an electrolyte. Individual cells are connected in series in supercapacitor banks to obtain high voltage levels. Table 3.2 shows a comparison of electrolytic capacitors and supercapacitors. Supercapacitors are able to provide power bursts in short durations

and have life cycles close to several million, compared to batteries. As it stands, supercapacitors are 10 times more capable in terms of specific power rating and about 10 times smaller compared to rechargeable batteries in terms of gravimetric energy density rating [6, p. 199]. The demand for supercapacitors have increased due to increased demand from smaller devices, such as mobile phones, and larger systems, such as electric vehicles. They have also become attractive for the clean energy sector as supercapacitors are more environmentally friendly than batteries.

Table 3.2: Comparison of capacitor families [6, p. 49]

Energy storage limit	Capacitor type	Manufacturer	Parameters			
			Capacitance	Terminal voltage (V)	Short circuit current (A)	ESR (mΩ)
< 1 J	Electrolytic	RSS	2200uF	16	104	153
1-5 J	Supercap	Maxwell	1 F	2.7	3.85	700
		Cap-xx	2.4 F	2.3	115	20
	Electrolytic	Corner	2200uF	50	704	71
		Dubilier				
5-50 J	Supercap	Maxwell	10 F	2.5	14	180
		Cap-xx	1.2 F	4.5	112.5	40
		Nesscap	10 F	2.3	33	70
	Electrolytic	Cornell	82,000uF	16	1441	11.1
		Dubilier				
		VICOR	270uF	200	325	614
>50 J	Supercap	Maxwell	350 F	2.7	840	3.2
		Nesscap	120 F	2.3	144	16
>10 kJ	Supercap	Samwha	3000F	3.0	13,000	0.23
		Electric				

3.4.1 Supercapacitor behaviour

Supercapacitors are based on the same simple principles applicable to electrostatic capacitors. A higher capacitance is created in an electrostatic capacitor where larger area plates combines with shorter distance between plates. In supercapacitors, the electrical double layer formed next to a large-area electrode and an electrolyte is used.

The electrodes of a supercapacitor are made of a porous carbon, such as active carbon. This is due to the high electrical conductivity, low cost and high chemical stability with a large specific surface area afforded. The large surface area is due to the distribution of the pores. While energy storage is achieved in batteries via reduction and oxidation reactions creating electron transfer between the chemicals, supercapacitors base their energy storage on charge separation happening at an electron-electrode interface. In an electrode the different pore sizes are mixed and in each pore an electrical double layer is formed, giving the simple case of a capacitor plate with a very high surface area [6, p. 201].

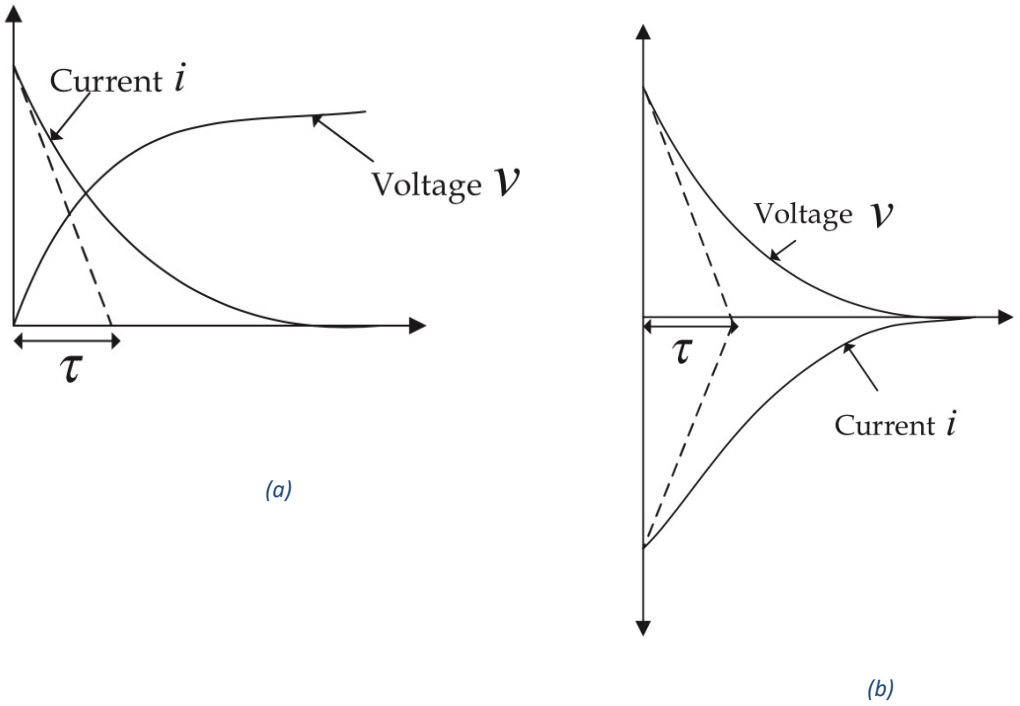

Figure 3.7: Capacitor voltage and current behaviour (a) charging (b) discharging

Equations that model the behaviour of electrolytic capacitors can be used for supercapacitors as well. For charging a capacitor, assuming the initial voltage is zero, we obtain the following Equations for current, *i*(t) and voltage, *v*(t).

$$i(t) = \frac{V_{in}}{R} e^{-\frac{t}{RC}} \tag{3.17}$$

$$v(t) = V_{in}\left[1 - e^{-\frac{t}{RC}}\right] \tag{3.18}$$

Where V_{in} is the input voltage, R is the total resistance of the circuit and capacitance C.

For discharging a capacitor the Equations for current, *i*(t) and voltage, *v*(t) are,

$$v(t) = V_C e^{-\frac{t}{RC}} \tag{3.19}$$

$$i(t) = \frac{V_C}{R} e^{-\frac{t}{RC}} \tag{3.20}$$

Where V_C is the initial voltage of the capacitor.

The charging and discharging behaviour of capacitors is shown in Figure 3.6. When discharging the current behaves same as it was charging but now flows out of the capacitor.

The rate at which a capacitor charges depend on the product of the total resistance of the circuit and capacitance. This quantity is referred to as the time constant, τ, of the circuit and it usually takes 5 time constants to completely charge or discharge a capacitor.

$$\tau = RC \tag{3.21}$$

The total energy stored in a capacitor is given by,

$$E_C = \frac{1}{2} CV^2 \tag{3.22}$$

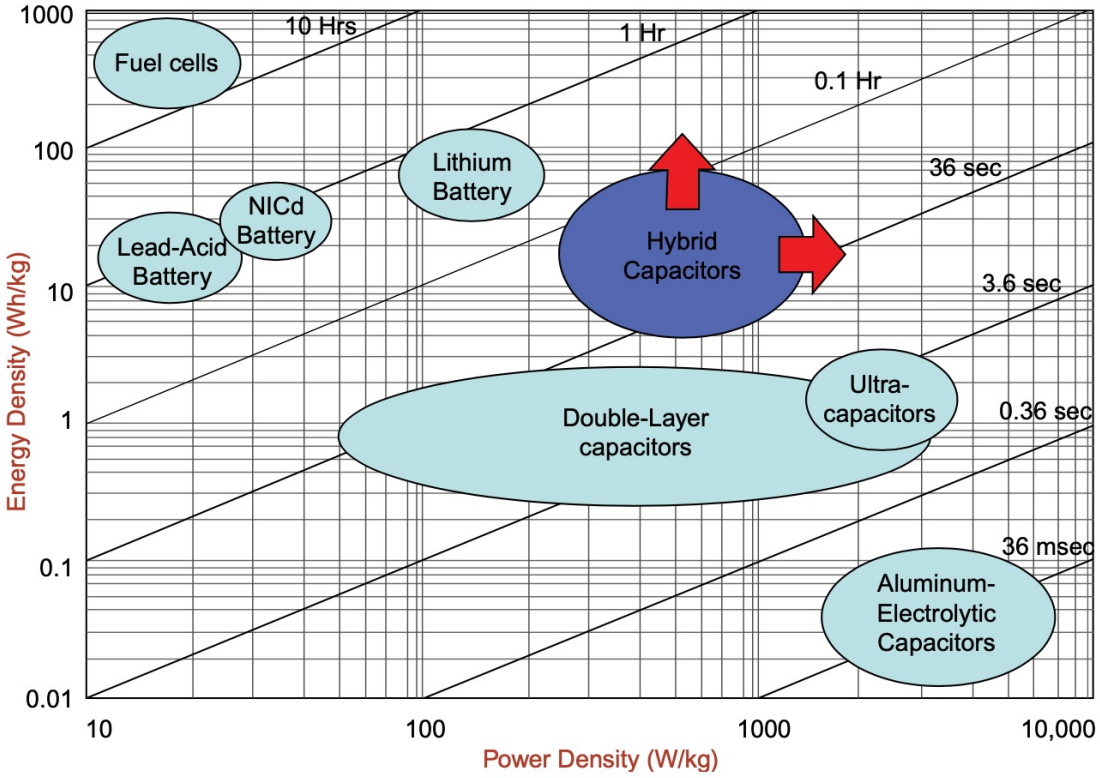

Figure 3.8: Ragone plot updated with capacitor families [6, p.242]

A Ragone plot updated with capacitor families is shown in Figure 3.8. The supercapacitor families have a much higher energy density than electrolytic capacitors. For a size comparison Figure 3.9 contains a mixture of supercapacitors and electrolytic capacitors with their respective energy capacity.

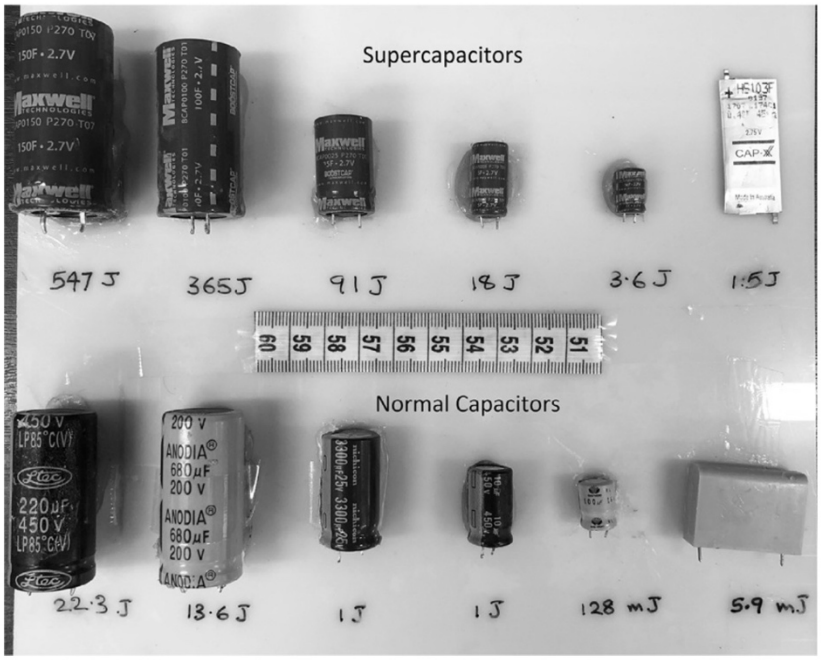

Figure 3.9: Size comparison of common capacitor and supercapacitor [6, p.243]

3.4.2 Supercapacitor Modules

The development of supercapacitor modules and larger single-cell devices can be attributed to the adoption of supercapacitors by the automotive industry[6, p.239]. The start-stop function capability of cars were mainly based of supercapacitor modules. Figure 3.10 shows the use of a supercapacitor module in a traditional internal combustion engine vehicle, that reduces the burden on the 12 V battery caused by the frequent starting of the engine for start-stop function. The battery is used to crank the engine 3-5 times a day on a car without the start-stop function, which can increase by up to 10 times if start-stop function is implemented increasing stress on the battery and hence reducing its lifetime.

Hybrid electric vehicles(HEVs) and electric vehicles(EVs) use supercapacitor modules to achieve high power without stressing the batteries. The high power density of supercapacitor module is useful when acceleration is needed.

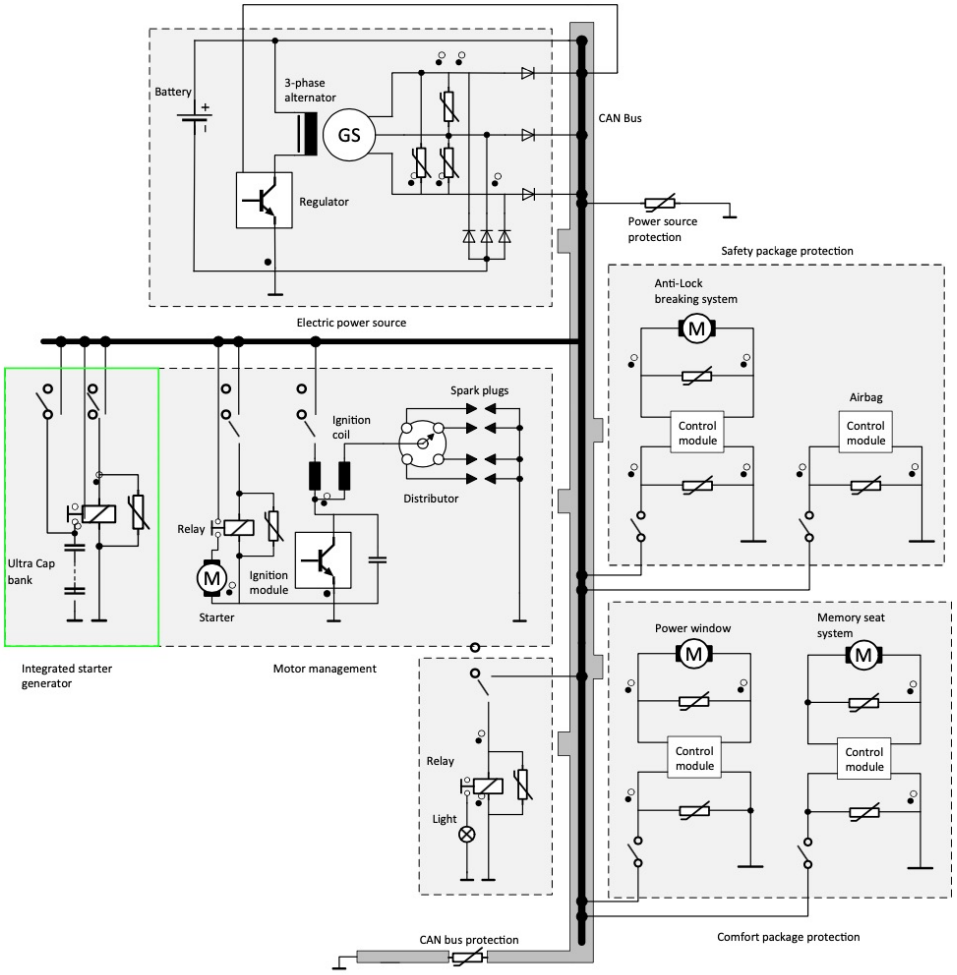

Figure 3.10: Supercapacitor module in an automotive electrical system[6, p.240]

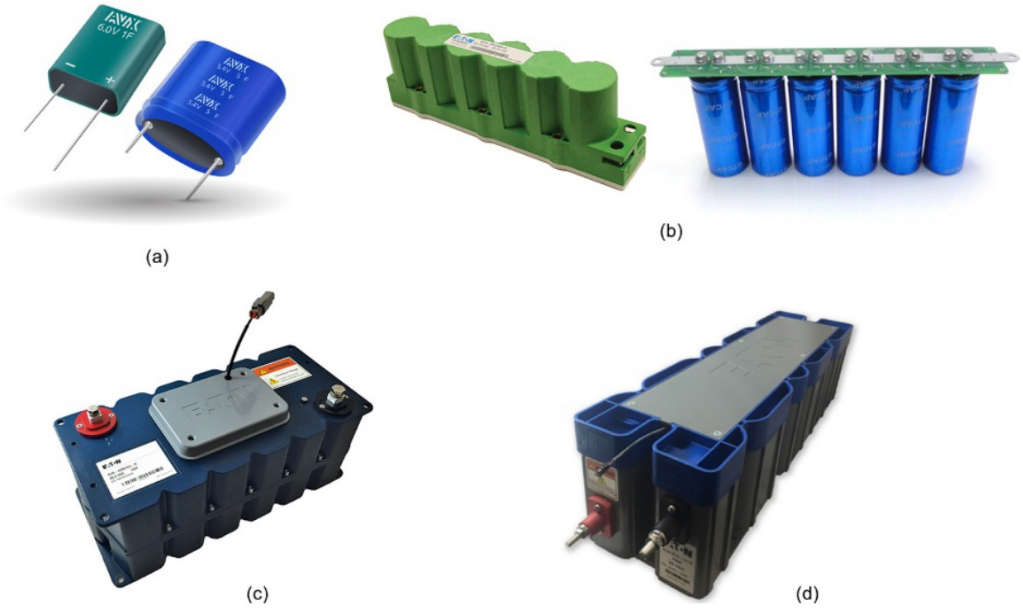

Figure 3.11: Supercapacitor modules: (a) 6 V, (b) 12 - 16 V, (c) 48 V, (d) 62 V [6, p.240]

3.4.3 Recent supercapacitor technology developments

Newer types of electrode combinations were commercialized by borrowing from Li-ion battery technologies to create asymmetrical types of supercapacitors, commercially known as hybrid supercapacitors. These achieve almost 2-3 times higher capacitance for the same canister volume, but a penalty of slightly lower cycle life is presented.

A newer family known as battery-caps or capa-batteries is introduced based on pseudo-capacitance. These achieve almost 10-25 times larger capacitance for the same canister volume. Figure 3.12 shows a comparison of three different types with same canister volume.

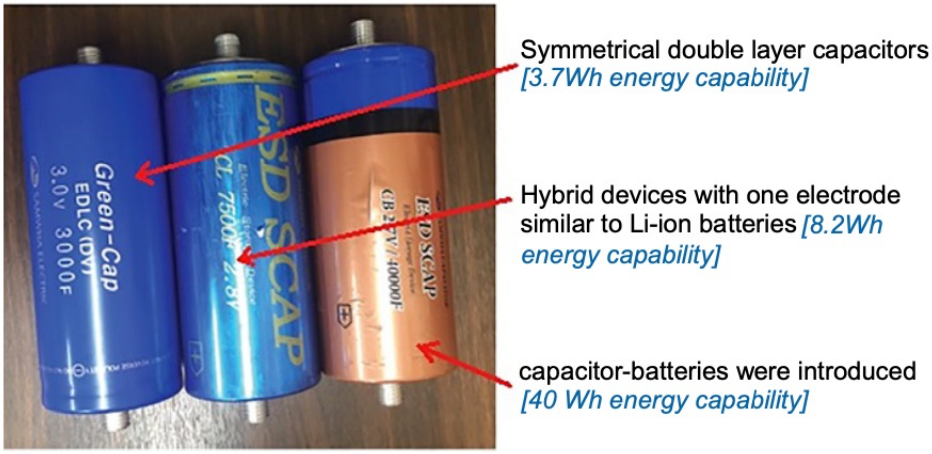

Figure 3.12: Three types of commercially available supercapacitor technologies[6, p.245]

Table 3.3: Comparison of commercially available supercapacitors[17]

Parameter	EDLCs	Hybrid SCs	CAPAbatteries
Energy density, Wh/L	5-8	10-14	50-120
Power density, W/L	8000	2500-4000	1600-3200
Cycle life, cycles	1,000,000	40,000-50,000	15,000-20,000
Rated voltage, V	2.7	2.7	2.8
Capacitance, F	1-3000	200-7500	1000-70,000

All these supercapacitor families present high volumetric power density, as observed from Table 3.3, which are significantly more than lead-acid or Li-ion batteries due to their low ESR. Batteries are also affected by the gradual increase in internal resistance with the percentage discharge of its energy. The internal resistance of a battery increases by one or two orders when discharged fully, which would be detrimental for rapid acceleration of HEVs and EVs without supercapacitor modules. Batteries also have reduced cycle life as the depth of discharge is increased compared to supercapacitors, shown in Figure 3.13.

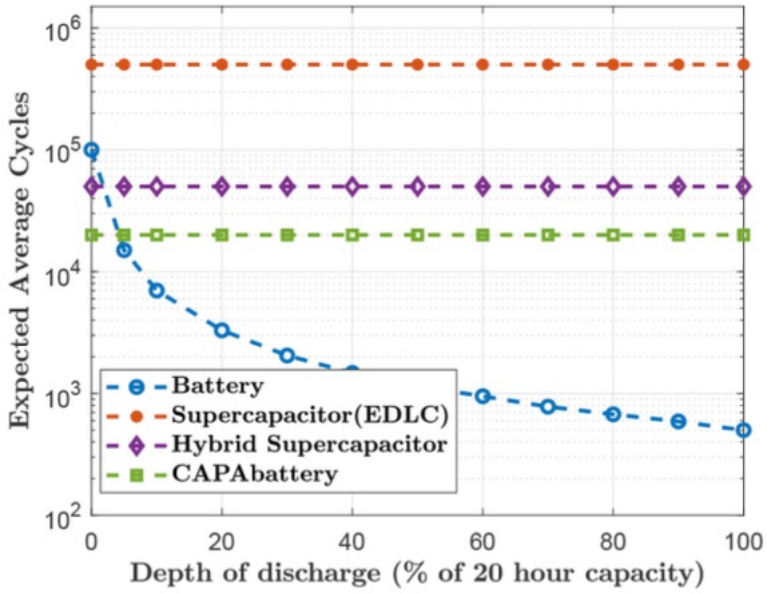

Figure 3.13: Variation of average life cycle

Chapter 4 : Power conversion

This chapter explores the various power conversion methods along with their benefits and shortfalls. We look at the evolving of the linear voltage regulator from the humble Zener diode to the development of switching regulators for efficiency at high power applications. The various active and passive components used for switching and the control mechanisms are explored as well.

4.1. Linear voltage regulator

Voltage regulation is the supplying of a steady voltage level. The simplest method of achieving this is the linear voltage regulator. This regulator is placed in between a high voltage input and the required lower voltage and gets rids of the difference by removing it as heat. Therefore the output voltage is always lower than that of the supply voltage.

4.1.1. Zener diode as a regulator.

The simplest voltage regulator is a Zener based voltage regulator, shown in Figure. Here the relatively constant reverse-breakdown voltage of the Zener diode is used for regulation. The difference between V_{in} and V_{out} is dissipated by the resistor R_S.

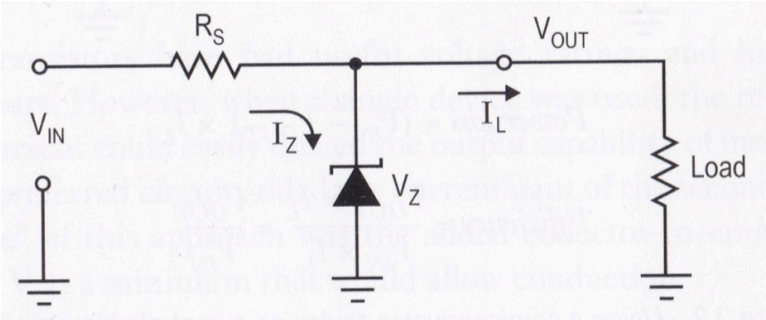

Figure 4.1: Zener diode voltage regulator. [7, p.7]

Current should pass through the Zener diode for rectification to occur and therefore I_L must be less than I_Z. The resistor carries both I_z and I_L and therefore the power loss is,

$$Power\ loss = (V_{in} - V_{out})(I_L + I_Z) + V_Z I_Z \tag{4.23}$$

There is considerable power loss when load current increases and therefore this regulator is used in low-power applications. Additional limitation is the selection of resistor R_S as it needs to be large enough to limit the current through the Zener and also be small enough to provide maximum load current. The regulated voltage is governed by,

$$\frac{V_{in} - V_{out}}{R_s} > I_L \tag{4.24}$$

This regulator has to be designed for worst case conditions to ensure proper operation. Added consideration is required for the power dissipation of the Zener as well, governed by

$$P_Z = \left(\frac{V_{in} - V_{out}}{R_S}\right) V_Z \tag{4.25}$$

Equation (4.2) and (4.3) shows that for increasing load currents the power dissipation of the Zener increases resulting in the need for a high power Zener. This situation can be improved by using an emitter follower.

4.1.2. Emitter-follower in regulation.

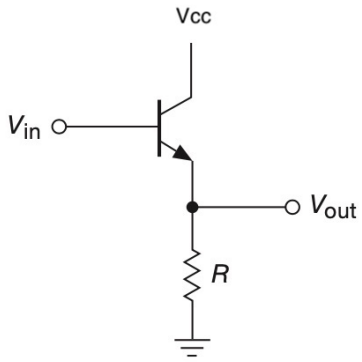

Figure 4.2: Emitter follower. [8, p. 79]

The output terminal is the emitter of the npn transistor and therefore this arrangement is called the emitter follower. The emitter follows the input, also called the base of the transistor, less one diode drop, as shown below.

$$V_{out} = V_{in} - 0.6 \tag{3.26}$$

This circuit requires less power from the input to drive a load compared to input driving the load and hence has a current gain. The input impedance is much larger compared to the output impedance. This combined with the Zener based voltage regulator, shown in Figure 4.3, provides a more capable low power voltage regulator.

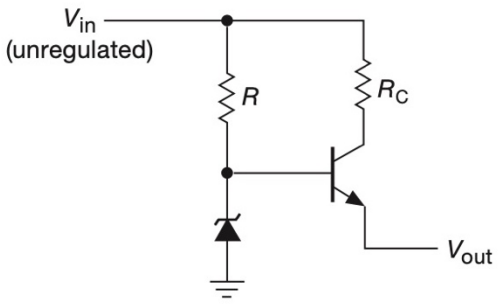

Figure 4.3: Zener regulator with emitter follower.[8, p. 82]

Here the current through the Zener is independent of the load current. The base of the transistor draws considerably low current resulting in lower power dissipation in the Zener. The resistor *R* carries only the Zener current resulting in lower power loss as well. The resistor R_C is added to limit

the current through the transistor in the case of a short circuit but is not necessary for the operation of the emitter follower.

4.1.3. Series-pass linear regulator

The emitter follower Zener regulator affords the benefit of low Zener current but has the shortfall of poor output voltage regulation as the V_{BE} of the npn transistor varies with output current. The regulated voltage is also fixed at the V_Z. An evolution of this regulator is the comparing of the output voltage to a Zener that is used as a low current voltage reference. Using a dc amplifier with a Zener reference allows the output voltage level to be adjusted according to the formula,

$$V_{out} = V_z\left(1 + \frac{R_2}{R_3}\right) \tag{4.27}$$

Due to the use of an op amp the maximum output voltage obtainable is close to V_+ and the output current is also limited to the limit of the op amp. In order to overcome this restriction, a NPN power transistor in emitter follower configuration is added allowing for higher output current.

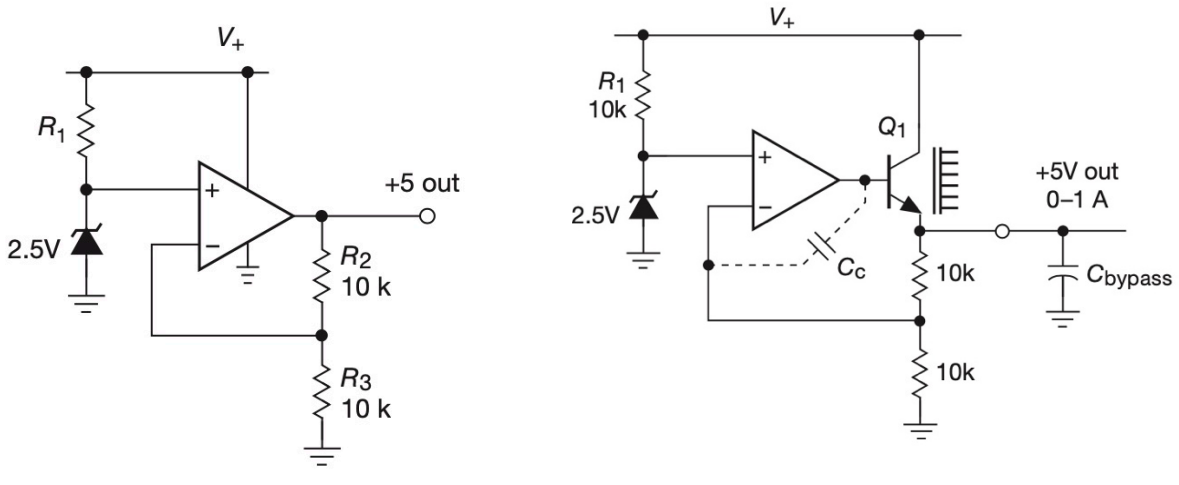

Figure 4.4: Series-pass regulator: (a) Zener with amplifier (b) Addition of a power transistor [8, p. 596]

When a single NPN transistor was used the base drive current required were higher than what the op amp could provide. Therefore transistors in a Darlington configuration was used to benefit from

the current gain of the second transistor to drive the primary. This however resulted in an addition voltage drop close to 2 V due to the added collector-to-emitter drop. Power MOSFETs with their low on-resistance can also replace the pass transistor but it has a gate-to-source threshold in several volts requiring further complexity, in the case of using a N-channel MOSFET, or increased cost, for the use of a more expensive P-channel MOSFET, in circuit design.

$$Power\ loss = (V_{in} - V_{out})I_L \tag{4.28}$$

Due to the series-pass regulator dissipates power in transistor, when the voltage difference between the input and output is larger the power loss is also larger. Therefore the linear regulator is favoured when the voltage difference or output current is comparatively lower.

4.2 Switching regulators

A switching regulator gets rid of the variable resistance of a controlled transistor with a switch which is either fully on or fully off. This allows the switches to dissipate lower power as they do no operate in the active region. To provide a steady output voltage from the chopped input voltage we use an output filter that only consists of temporary energy storage devices. The use of this output filter also results in a nearly lossless voltage regulation.

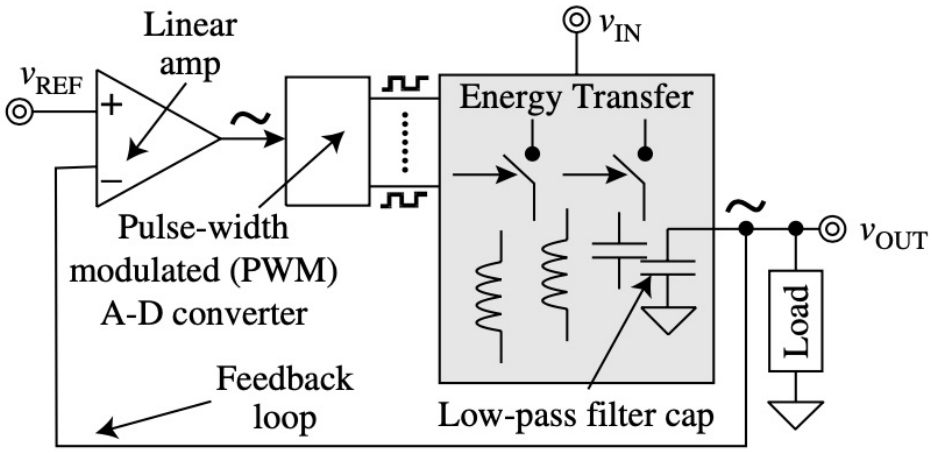

Figure 4.5: Switching regulator circuits [10, p.3]

All switching regulators consists of an inductor and transistor switch. For the operation of a switching converter the current in the inductor is increased, thereby increasing the stored energy that flows to the output during the second part.

4.2.1. Buck (Step-down) converter

The basic circuit of a buck converter is shown in Figure 4.6. It is also called the series converter due to the orientation of the switch (transistor), inductor and load. The buck converter provides a low output voltage from a high input voltage.

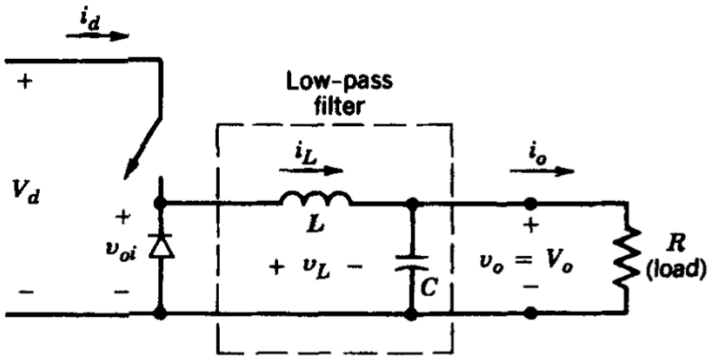

(a)

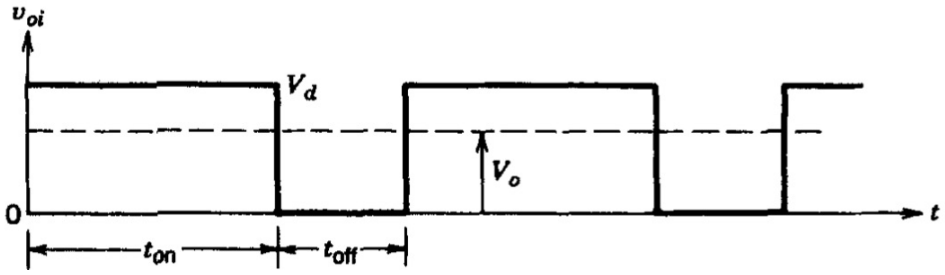

(b)

Figure 4.6: Buck converter operation[9, p.165]

The operation of the buck converter occurs in two steps. Energy from the source is both transferred to the load and stores in the inductor when the switch is conducting. The diode is reversed biased and therefore is essentially an open switch. The diode becomes forward biased when the switch is opened resulting in transferring the energy stored in the inductor. The ratio of the times when the switch is on or off determine the output voltage of the converter.

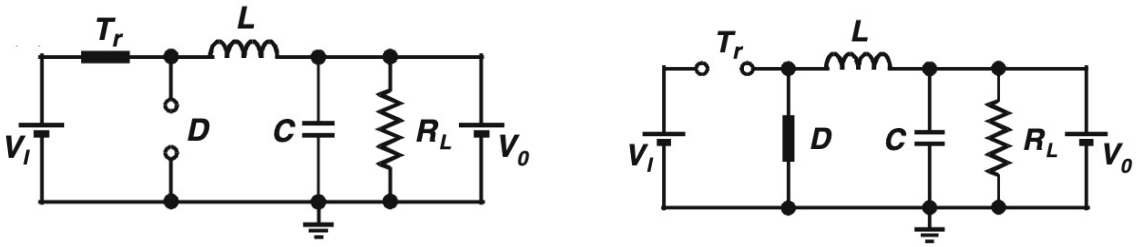

(a) *(b)*

Figure 4.7: Two step operation of buck converter: (a) Switch on (b) Switch off [11, p.215]

During the on-off period of the switch the low-pass filter observes a rectangular voltage with pulses of variable duration. The inductor passes the average voltage observed by the filter and is given by,

$$V_{average} = \frac{1}{T}\int_0^{t_{on}} V_I\, dt = V_I \frac{t_{on}}{T} = DV_I \tag{4.29}$$

Where t_{on} is the on duration of the switch with *T* being the switching period. Duty cycle, *D*, is the ratio of on duration and cycle time. The operation of the converter is separated into the two modes of operation depending on the nature of current conduction through the inductor.

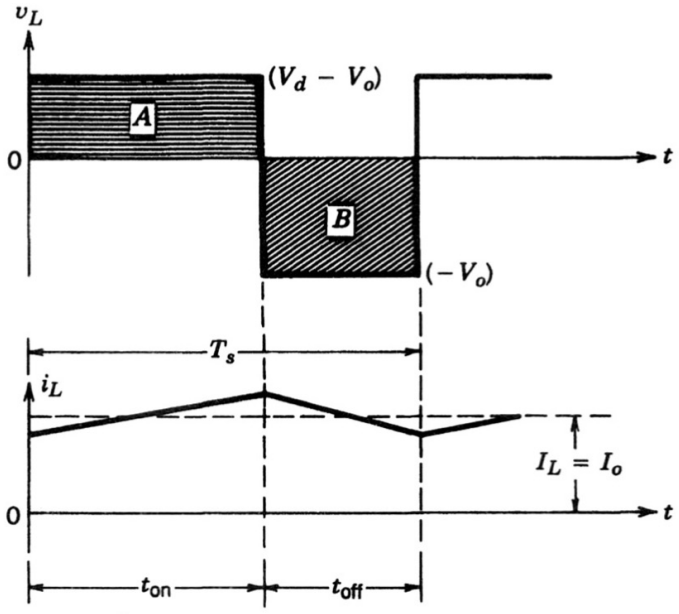

Figure 4.8: Buck converter operation at continuous conduction mode [9, p.166]

4.2.1.1 Continuous Conduction mode

When the current flow in the inductor is continuous the buck converter is said to be operating in continuous conduction mode, as shown in Figure 4.8. In steady-state operation the waveform repeats from one cycle to the next resulting in the integral of the inductor voltage over a time period to be zero.

$$\int_0^T v_L\, dt = \int_0^{t_{on}} v_L\, dt + \int_{t_{on}}^T v_L\, dt$$

From Figure 4.8 we can see,

$$(V_d - V_o)t_{on} = V_o(T - t_{on})$$

$$\frac{V_o}{V_d} = \frac{t_{on}}{T} = D \tag{4.30}$$

The boundary where continuous conduction ends is shown in Figure 4.9(a). The average inductor current at this boundary is,

$$I_{LB} = \frac{1}{2} i_{L,peak} = \frac{t_{on}}{2L}(V_d - V_o) = \frac{DT}{2L}(V_d - V_o) \tag{4.31}$$

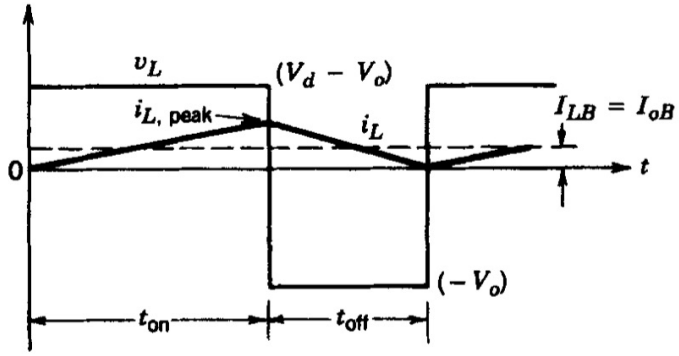

(a)

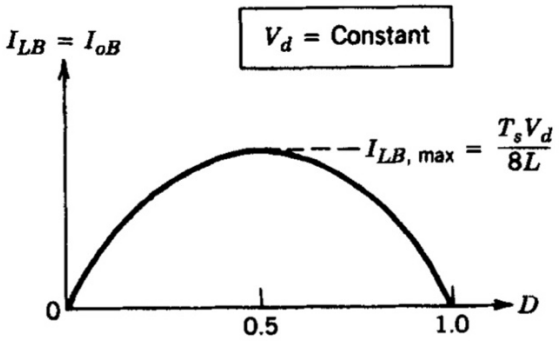

(b)

Figure 4.9: Boundary of buck converter continuous conduction mode: (a) Waveform (b) ILB vs D

4.2.1.2 Discontinuous conduction mode.

Discontinuous conduction mode occurs when inductor current goes to zero at the end of a cycle. When the output current is below the boundary current, governed by Equation (4.9), discontinuous mode occurs. By combining Equation (4.8) and (4.9) we obtain the inductor current as,

$$I_{LB} = \frac{TV_d}{2L} D(1 - D) \tag{4.32}$$

Combining Equation (4.10) with Figure 4.9 shows that maximum current required for continuous conductions occurs at D = 0.5

$$I_{LB,max} = \frac{TV_d}{8L} \tag{4.33}$$

When the inductor current is below this value the converters is said to operate in discontinuous conduction mode.

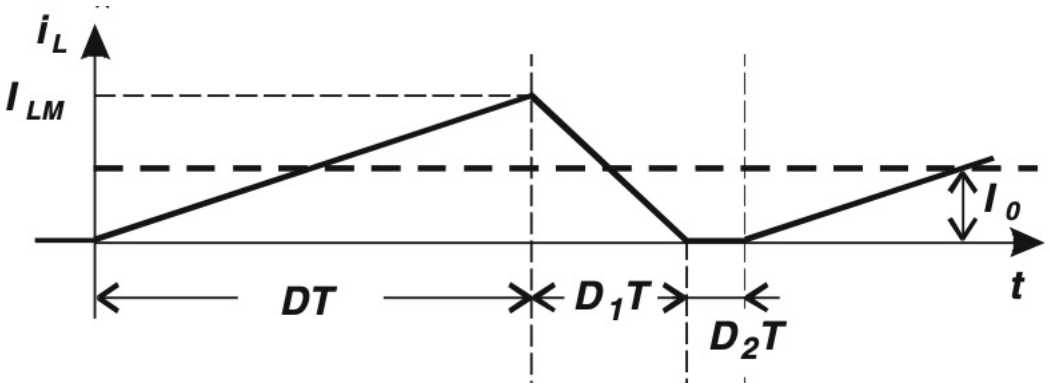

Figure 4.10: Discontinuous conduction mode of buck converter [11, p.223]

4.2.2 Boost converter

The basic circuit of a boost converter is shown in Figure 4.11. The boost converter results in an output voltage which is higher than that of the input resulting in this converters also being called a step-up converter.

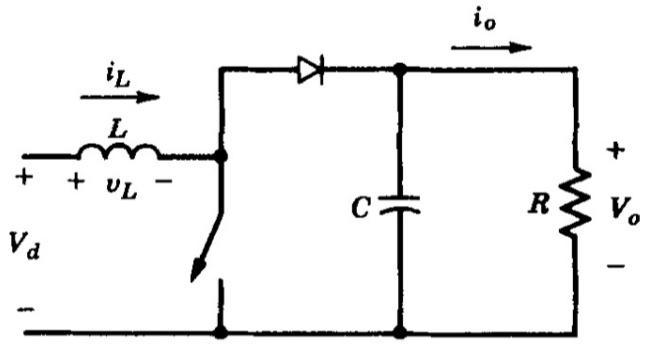

Figure 4.11: Boost converter circuit.[9, p.172]

The boost converter also operates in two steps. When the switch is on the diode is reversed biased and the inductor current ramps up storing energy. When the switch is closed the diode becomes forward biased and the output receives energy from both the inductor and the input. The boost converter is utilized when the voltage ratio is $1 < V_o/V_d < 5$.

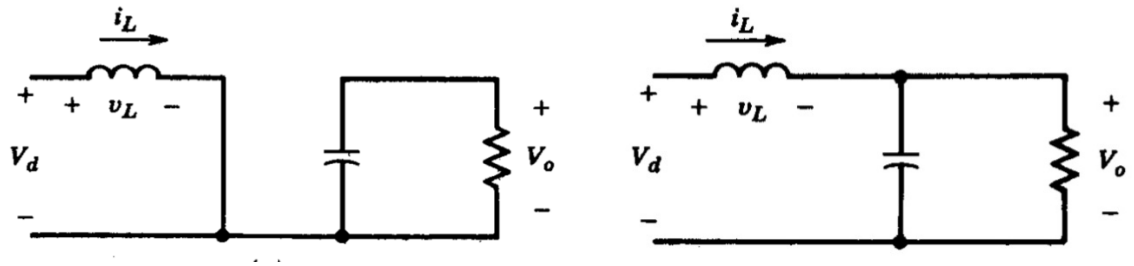

Figure 4.12: Two step operation of boost converter: (a) switch on (b) switch off [9, p. 173]

4.2.2.1 Continuous conduction mode

Continuous conduction mode here is also defined as when the inductor current is continuous. During the on-off period of the switch inductor observes a rectangular voltage with pulses of variable duration. At steady state the time integral of inductor voltage over on cycle should be zero resulting in,

$$V_d t_{on} + (V_d - V_o) t_{off} = 0$$

By simplifying above Equation we obtain

$$\frac{V_o}{V_d} = \frac{T}{t_{off}} = \frac{1}{1 - D} \tag{4.34}$$

as $T = t_{on} + t_{off}$ and $D = t_{on}/T$.

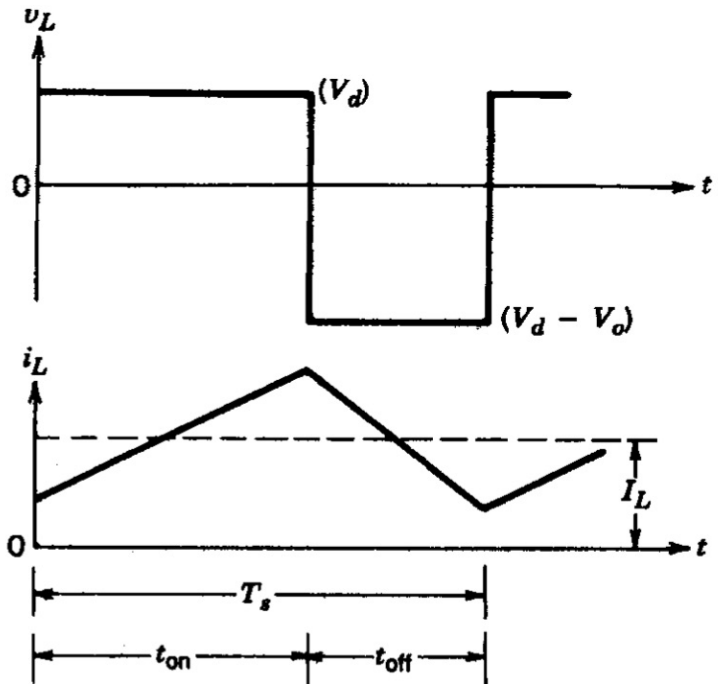

Figure 4.13: Boost converter continuous conduction mode [9, p.173]

4.2.2.2 Discontinuous conduction mode

As before when the current through the inductor drops to zero in each cycle the converter is in discontinuous conduction mode. The boundary where continuous conduction ends is shown in Figure 4.14. The average inductor current at this boundary is,

$$I_{LB} = \frac{1}{2} i_{L,peak} = \frac{1}{2} \frac{V_d}{L} t_{on}$$

$$I_{LB} = \frac{TV_o}{2L} D(1 - D) \tag{4.35}$$

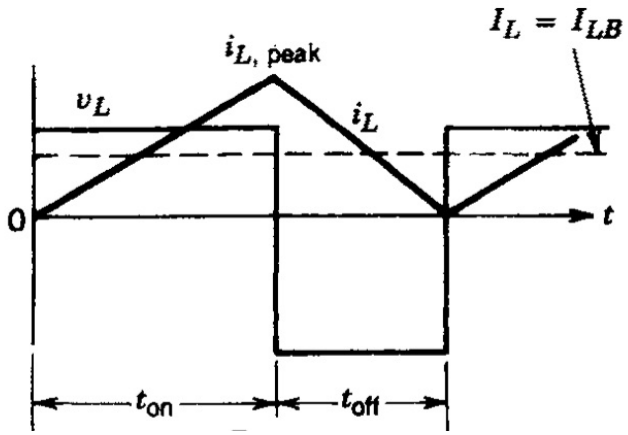

Figure 4.14: Boundary of boost converter continuous conduction mode.[9, p.174]

Maximum current required for continuous conduction is found at D=0.5 and is given by,

$$I_{LB,max} = \frac{TV_0}{8L} \tag{4.36}$$

When the inductor current is below this value the converters is said to operate in discontinuous conduction mode.

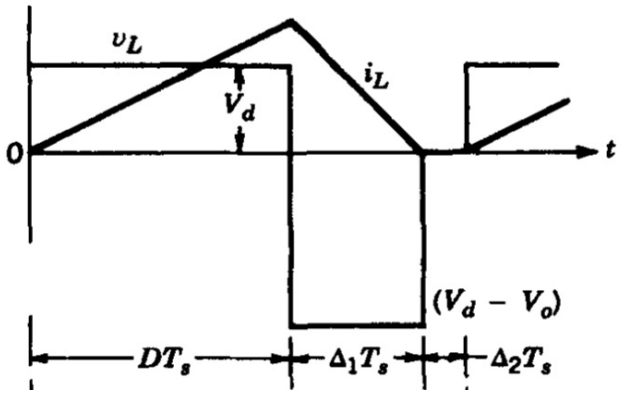

Figure 4.15: Boost converter discontinuous conduction mode

4.2.3 Switching regulator controls.

For switching regulators to operate the switches need to be turned on and off. One method of controlling the switches is called pulse width modulation(PWM). This method uses a constant frequency for switching while adjusting the ratio of on and off times.

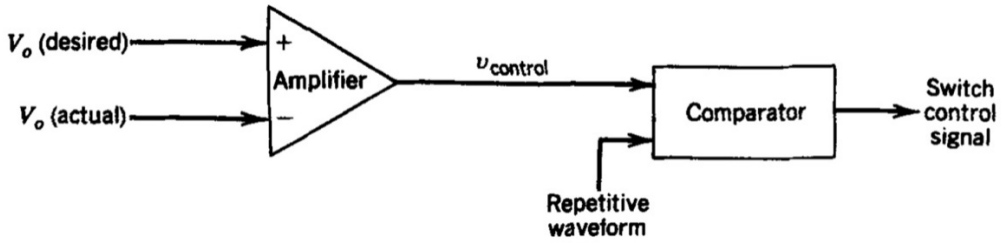

(a)

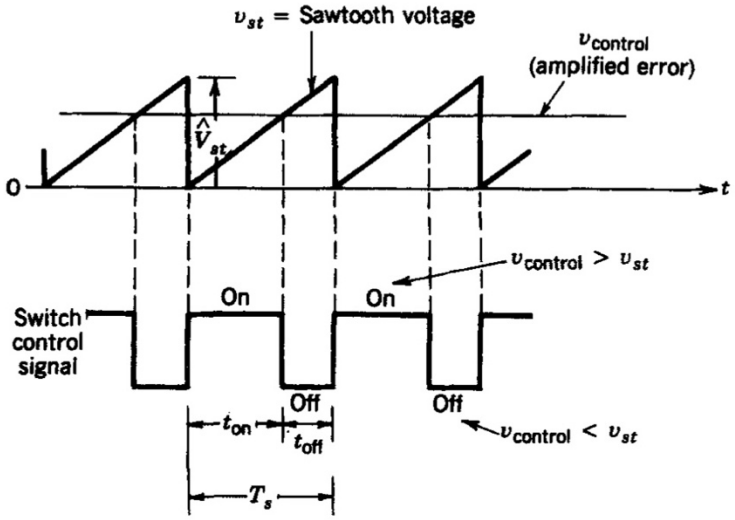

(b)

Figure 4.16: PWM: (a) Block diagram (b) comparator waveforms [9, p.163]

A sawtooth waveform with a constant amplitude sets the switching frequency. The control voltage signal is obtained by amplifying the difference between actual output and the desired output, also known as error, which is then compared with the sawtooth waveform. When the amplified error signal is greater than the sawtooth waveform the switch turns on while the switch turns off when the error signal is lower. The duty ratio is expressed as,

$$D = \frac{t_{on}}{T} = \frac{v_{control}}{V_{st}} \tag{4.37}$$

4.2.4 Miniaturizing power converters

Switch mode power supplies allow for lower volume, low weight and high efficiency power conversion as components can be smaller where high switching frequency is used. Transformers and inductors are usually the bulkiest components. The RMS voltage across a winding for a transformer is found to be,

$$V_{RMS} = 4.44 B_{max} A N f \tag{4.38}$$

Where B_{max} is the maximum flux density in the core, A is the cross-sectional area of the core, N is the number of turns and f is the operational frequency. From Equation (4.16) it can be inferred that for a required voltage if the frequency is increased, while the maximum flux density and cross-sectional area of the core are kept constant, the number of turns required can be decreased[11, p.2-2]. With increased frequency the magnetic core hysteresis loss (P_h) and Eddie current losses (P_e) can increases as,

$$P_h \propto f B_{max}^2 \tag{4.39}$$

And,

$$P_e \propto f^2 B_{max}^2 \tag{4.40}$$

Therefore, if better magnetic material with higher operational frequency is used, a small transformer can be used.

Capacitors receive the same miniaturizing advantage at higher frequencies. Capacitors are used in a power supply for the rectification and filtering stage, and for high-frequency filtering. The peak-to-peak ripple voltage ($V_{rp\text{-}p}$) when a capacitor is used for rectifier operating at a frequency f is,

$$V_{rp-p} \propto \frac{I_L}{Cf} \tag{4.41}$$

Where I_L is the average DC load current. The capacitance can be decreased when the frequency is increased for the same peak-to-peak voltage thereby reducing the size of the capacitor. For high-

frequency filtering a smaller capacitor can be used as the impedance of a capacitor (Z_C)is governed by,

$$Z_c = \frac{1}{2\pi f C}$$

Due to the switch mode supplies use transistors as switches rather than a series pass element the power dissipation is lower and therefore the required heat sinks can be made relatively small.

4.3 Charge Pump Converters

Charge pump converters, also called switched capacitor converters, uses capacitors instead of inductors or transformers for intermediate energy storage and transfer[12, p. 170]. The absence of inductors result in a cheaper converter with smaller component size and low Electromagnetic Interference (EMI). While offering extremely low operating currents, charge pump converters provide superior performance in applications processing low-level signals or that require low-noise operation.

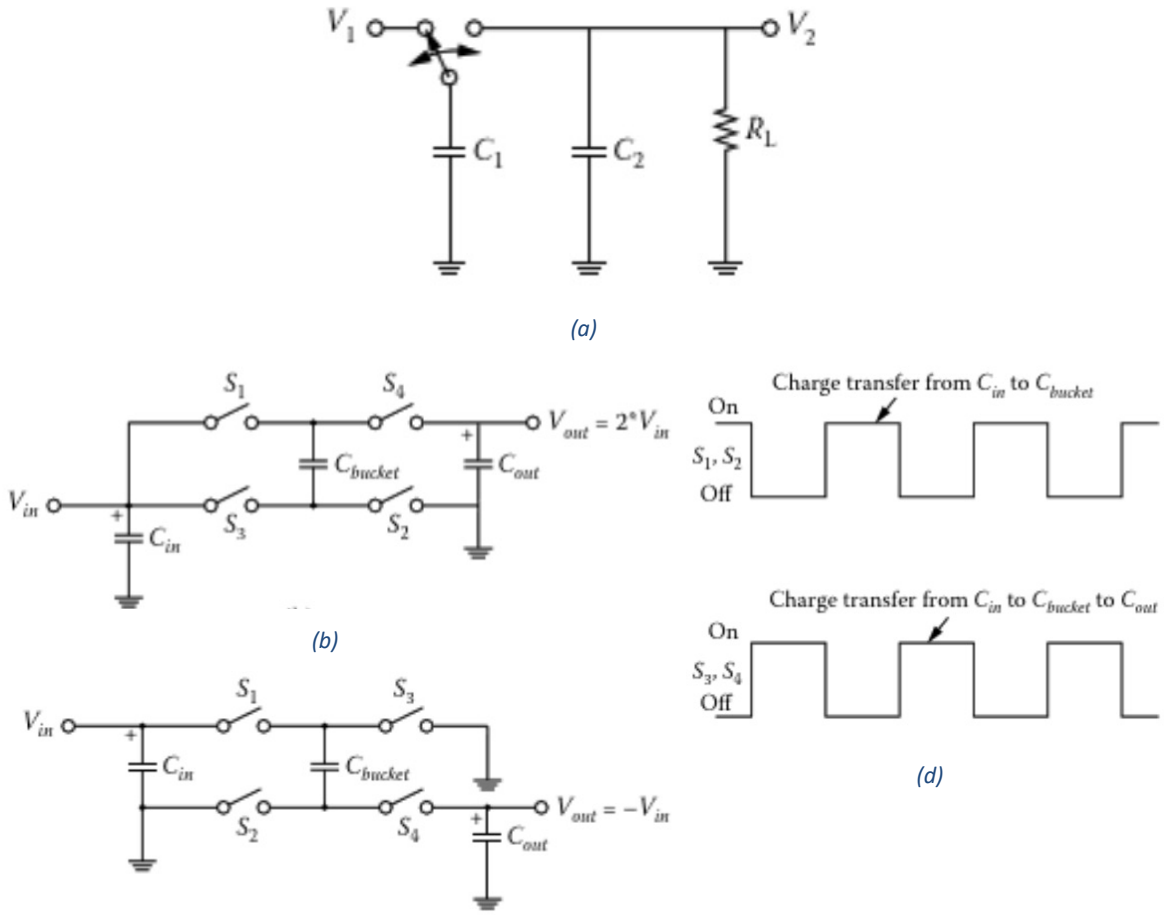

Figure 4.17:Charge pump converters: (a) Basic operation (b) Doubler (c) Inverter (d) Switch controls for doubler and inverter[12, p.171]

When the switch is in the left position in the basic charge pump converter, shown in Figure 4.17(a), capacitor C_1 charges to voltage V_1. The total charge in C_1 is then $q_1 = C_1V_1$. When the switch is moved to the right , C_1 discharges to V_2 providing the total charge on C_1 to now be $q_2 = C_1V_2$. The total charge transfer is,

$$q = q_1 - q_2 = C_1(V_1 - V_2) \tag{4.20}$$

By cycling the switch at frequency f, the current is,

$$I = fC_1(V_1 - V_2) = \frac{(V_1 - V_2)}{R_{eq}} \tag{4.21}$$

Capacitor C_2 ensures the output is held constant.

The charge pump can be used as a voltage doubler and inverter, shown in Figure 4.17(b) and (c). The timing for the switches of both configuration of converters is shown in Figure 4.17(d).

4.4 Low Dropout Regulators (LDO)

Switch mode power supplies are efficient at high power applications but they have higher noise and lower load current transient response[12, p.160]. These issues have resulted in the development of LDOs. LDOs are used to provide low-voltage power to digital circuits, where point of load regulation is required.

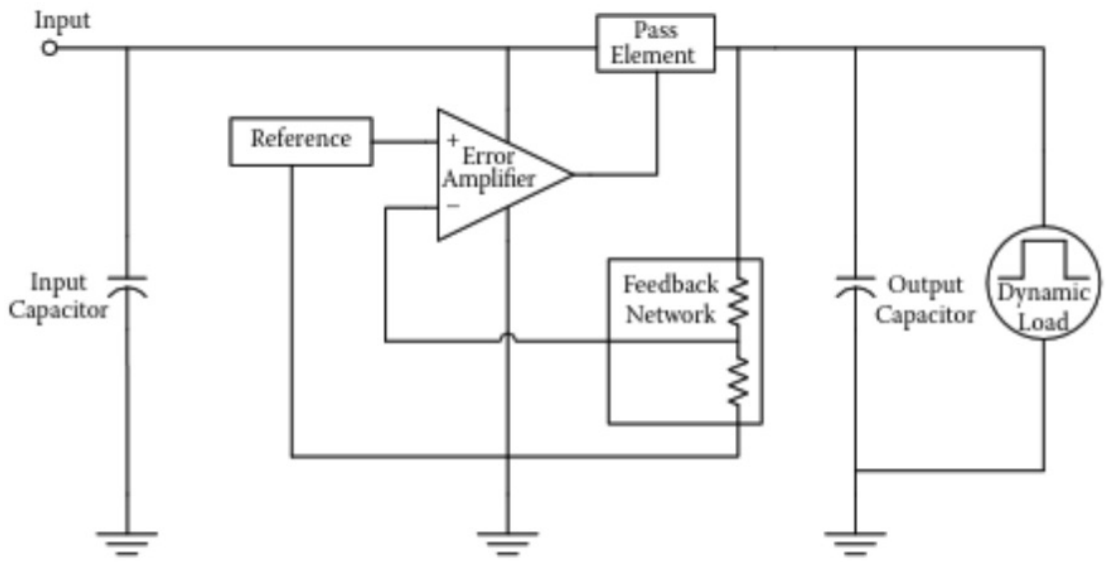

Figure 4.18: Basic LDO [12, p.162]

The main components of an LDO are the pass element, precision reference, feedback network and error amplifier. The input and output capacitors are external to the LDO. LDOs are available in multiple output voltages and current capabilities.

4.5 Supercapacitor Assisted Low Dropout Regulator (SCALDO)

A team lead by Dr. Nihal Kularatna, at the University of Waikato, designed a new power converter technique using supercapacitors as lossless voltage droppers, due to their very low ESR, in the series path of a low-dropout regulator[6, p.263]. Key features of this technique are,

- Load receives the low-noise and high-current slew rate capable DC output of a linear regulator
- Extremely low Switching frequency
- RFI/EMI issues are eliminated
- Output currents ranging from mA to over 100 A
- DC-UPS capability

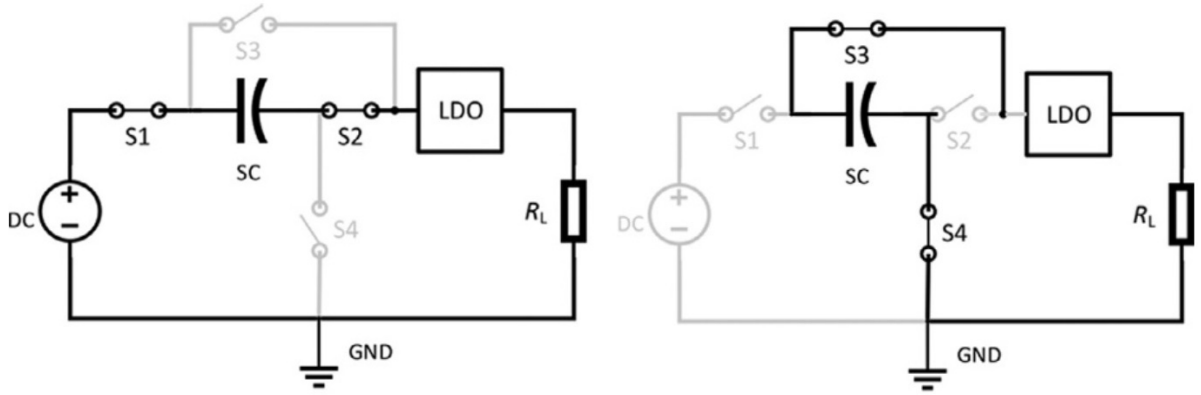

(a) *(b)*

Figure 4.19: SCALDO technique (a) minimizing series element dissipation (b) Releasing stored energy [6, p.263]

A 7 V drop across the series transistor can be observed in a typical 12-5 linear regulator. When a supercapacitor, precharged to 6 V, is placed in series the transistor sees only a 6 V input. This results in the LDO effectively working as a 6-5 V regulator with much higher efficiency. The excess energy stored in the supercapacitor during the charge phase is then released to the LDO in the discharge phase while the DC source is disconnected.

Table 4.1: Common linear regulator configurations with SCALDO [6, p.264]

DC-DC converter configuration	5-1.5 V	12-5 V	5-3.3 V	325-48 V
Efficiency without SCLADO	30%	42%	66%	14.75%
Efficiency with SCALDO	90%	84%	88%	88.6%
No. of supercapacitors	2	1	3	5
No. of switches required	7	4	10	16
Efficiency improvement factor	3	2	1.33	6
Remarks	High V_{in}/V_{out}	High V_{in}/V_{out}	Low V_{in}/V_{out}	Google 48V architecture

If the capacitor is ideal, energy is accumulated due to the load current, I_L, until the LDO reaches its minimum level before dropping the regulation capability based on the relationship[13],

$$V_{SC} = V_{SC}(0) + \frac{I_L t}{C_{SC}} \tag{4.22}$$

Where $V_{SC}(0)$ is the initial voltage across the device. Once level reached a set of low frequency switches place the supercapacitor in discharge mode.

4.6 Final thoughts on DC-DC converters

DC-DC converters are used everywhere using the traditional approaches of linear, inductor-based switch mode and switched-capacitor types. The fourth new converter technique, SCALDO allows for a high-efficiency linear DC-DC converter. All these techniques have various individual advantages compared to each other resulting in one being chosen over the other. Table 4.2 shows a comparison of all the existing converter techniques.

Table 4.2: Comparison of DC-DC converter techniques [13]

Feature	Linear regulators	Charge pump converters	Switched-mode power supplies	SCALDO
Design complexity	Low	Moderate	Moderate to high	Moderate
Cost	Low	Moderate	Moderate to high	Moderate to high
Efficiency	Low to moderate	Moderate to high	High	High
Noise	Lowest	Low	Low to moderate	Lowest
Magnetic parts	No	No	Yes	No
Output current capability	Low	Moderate	High	Moderate to High
Thermal management	Poor to moderate	Good	Best	Best
Limitations	Cannot step up	V_{in}/V_{out} ratio	Layout consideration	Number of switches

Chapter 5 : Supercapacitor assisted bicycle

This chapter explores the prototype supercapacitor assisted bicycle. It delves into the energy generation capabilities of the BLDC motor along with the ability to store energy is the supercapacitor bank. Along with a charging system for the supercapacitors, methods to control the power exerted by the rider while charging are explored to make it convenient for the rider.

5.1 Finding the BLDC motor Specifications

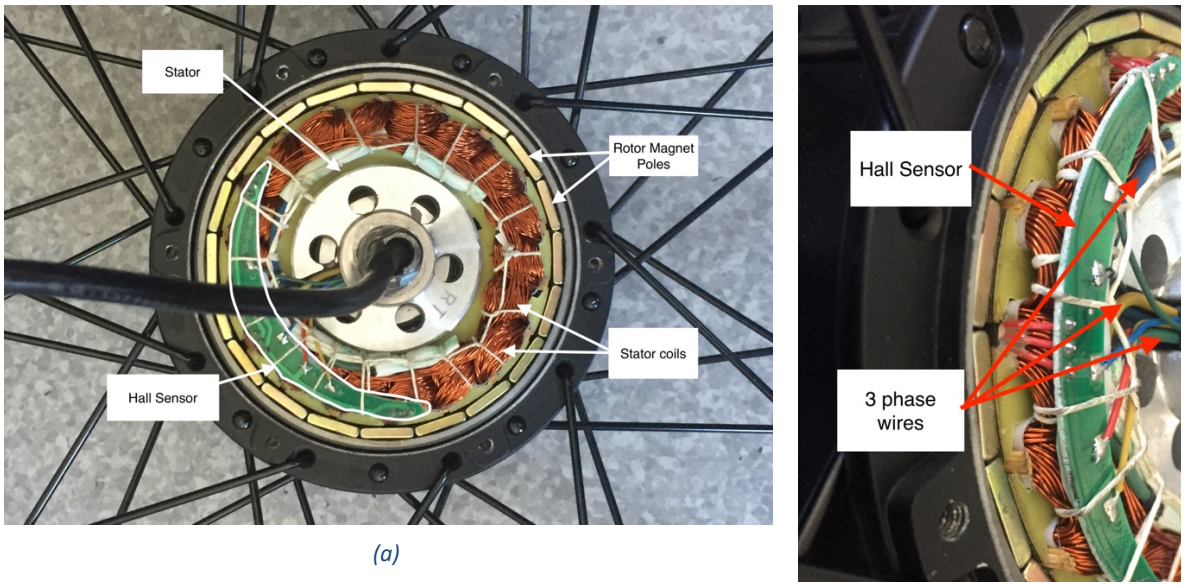

(a) *(b)*

Figure 5.1: : BLDC construction: (a) Top view (b) Side view

The commercially available E-bike kit consists of a brushless geared hub motor capable of 500 W at 36 V. Opening up the BLDC motor we are presented with the construction shown in Figure 5.1. The rotor consists of 20 “N42H” neodymium magnet poles with 18 stator coils of magnetic copper wire. A Hall sensor is used for reading the position of the magnetic poles.

By hooking up the 3 phase wires into the oscilloscope a 3 phase induced AC sine waveform can be observed. The frequency of the waveform can be found by the following equation.

$$frequency = \frac{RPM}{120} N_P \tag{5.42}$$

Where N_P is the number of poles and frequency returned in Hz. The maximum speed of motor operation is specified by manufacturer, CSC motors, to be 25 km/h or 6.94 m/s. The angular velocity, in RPM, is obtained by the following equation,

$$RPM = \frac{speed}{wheel\ radius} \frac{60}{2\pi} \tag{5.43}$$

Assuming a lossless system, the power of the motor transferred to the wheel is governed by the equation,

$$P = T_{Motor}\omega_{Motor} = T_{Wheel}\omega_{Wheel}$$

Where T is Torque and ω is the angular velocity.

For constant power input, the motor operates at a higher speed while producing lower torque while the wheel needs a lower speed at higher torque. This conversion is accomplished by the use of a reduction gear system, with the motor in this application using a 1 : 5 gear ratio. By combining equation (5.1) and (5.2) and accounting for the gear ratio we obtain the maximum frequency of the generated AC waveform to be 167.3 Hz.

An oscilloscope is used to observe the waveform of the induced voltage. The motor consists of a wye type connection and therefore the ground is inaccessible as it is inside the windings. To mitigate this a virtual ground is created by connecting resistors to each phase as shown in Figure 5.2.

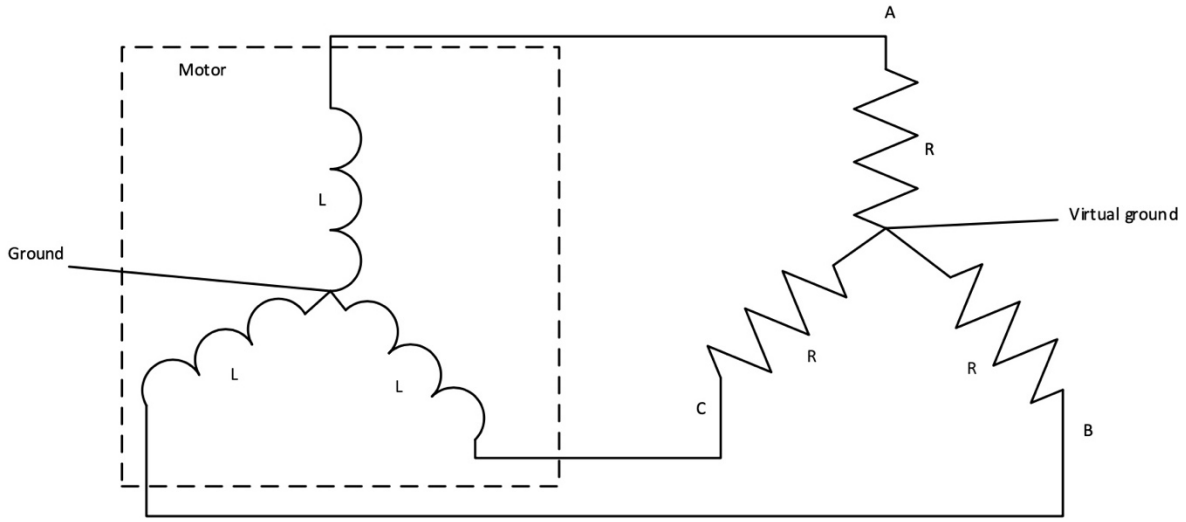

Figure 5.2: Measuring the induced waveform

Connect the two probes of the oscilloscope to any two phases marked A,B and C and the ground of the probes to the virtual ground the induced voltage can be observed. 10 kΩ resistors were used for creating the virtual ground. The motor was rotated at the max speed and the waveform, shown in Figure 5.3, was observed.

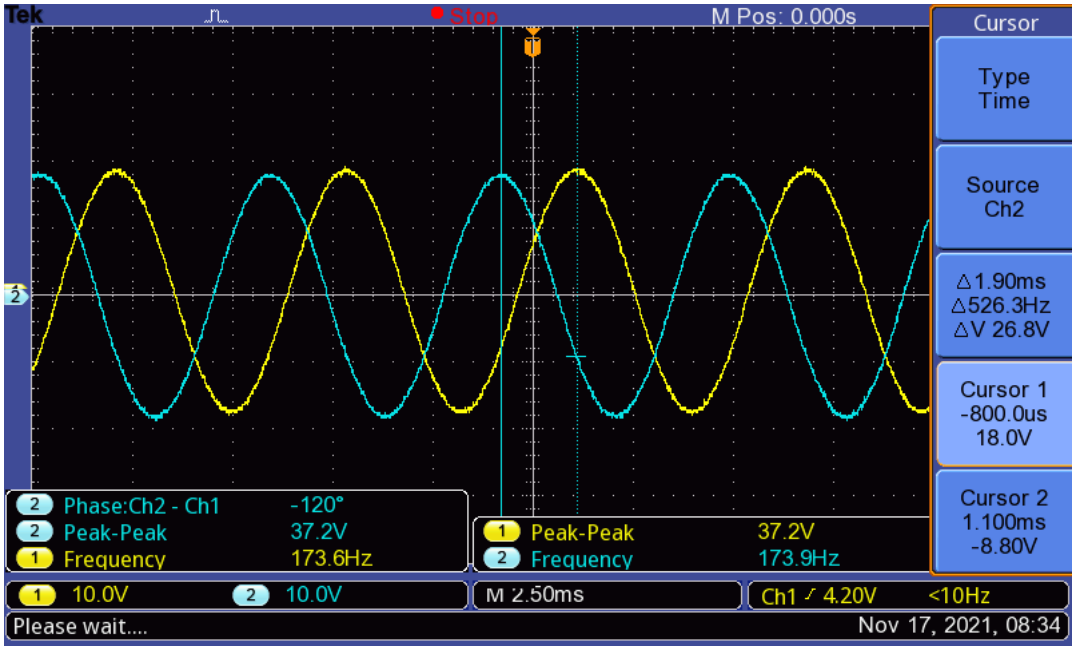

Figure 5.3: Induced voltage waveform

Phase shift between the two waveforms is found to be,

$$Phase\ shift(\emptyset) = 360 \times \frac{\Delta t}{T} = 360 \times \Delta t \times f = 360 \times (1.9 \times 10^{-3})(173.6)$$

$$\emptyset = 118.7°$$

The phase shift between two phases of the motor should be 120° resulting in a measurement error of,

$$error = \left(\frac{120 - 118.7}{120}\right) \times 100\% = 1.08\%$$

The frequency of the generated waveform differs from calculated value by,

$$error = \left(\frac{173.6 - 167.3}{173.6}\right) \times 100\% = 3.63\%$$

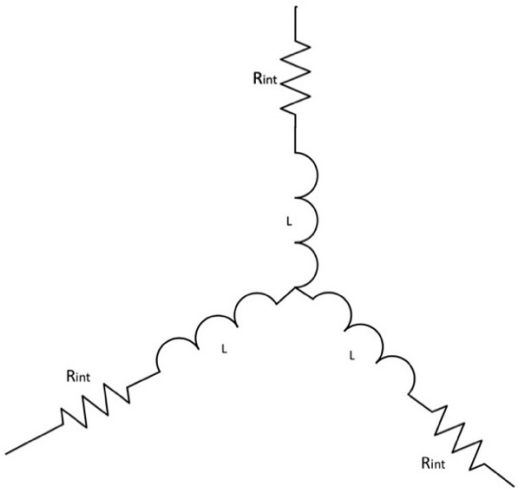

Figure 5.4: Internal components of a wye connected motor

The internal construction of the wye connection type motor is shown in Figure 5.4. To measure the values of the internal resistance and inductance of each phase an LCR meter is used. The measurements are conducted by hooking up any two phases of the motor and using a frequency close to the operating frequency of the motor. Table 5.1 shows the specifications of the motor.

Table 5.1: Motor specifications

Inductance per phase	312.4 μH
Resistance per phase	0.191 Ω
Wheel size	66 cm
Number of magnet poles	20
Number of stator coils	18
Motor max power	500 W
Operating voltage range	21-48 V
Max current	20 A

5.2 AC to DC conversion

The motor generated an induced voltage when rotated. This phenomenon is used for the generation of electricity. In the case of the BLDC motor, the induced voltage is of 3 phase AC. To store electrical energy in the supercapacitor we are in need of a DC supply. This is accomplished by using a 3 phase rectifier. The 3-phase rectifier contains of six diodes in the arrangements shown in Figure 5.5. The diodes selected for rectification depends on the frequency of the rectified signal.

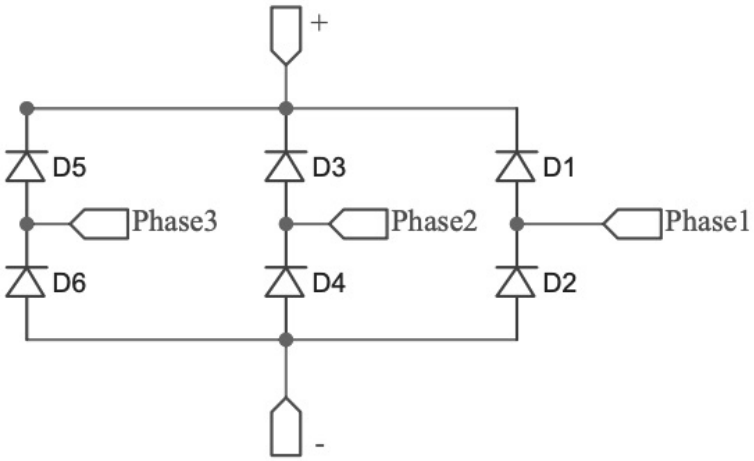

Figure 5.5: 3-phase Bridge rectifier

The general purpose P-N junction rectifier diodes are used in circuits operating at the line frequencies such as 50 or 60 Hz. The fast recovery P-N junction diodes are used with fast switching circuits, such as switch mode power supplies operating at high frequencies. Schottky diodes, while capable at high frequencies, provide a lower forward voltage drop compared to the P-N junction diodes and virtually no switching losses due to the absence of minority carrier reverse recovery. They do however have a lower blocking voltage [11, p.10]. Since the max frequency of the generated voltage is lower than 200 Hz any diode type apart from the general purpose type can be used. Due to the comparatively low voltage induced in the motor and high current requirement while enabling lower voltage loss, schottky diodes were chosen. The maximum current draw is limited to 20 A to protect the motor windings. For the choice of the power rating of the diode, the V-I curve of a diode, shown in figure 5.6, is consulted. Schottky diode specifications shown in Table 5.2.

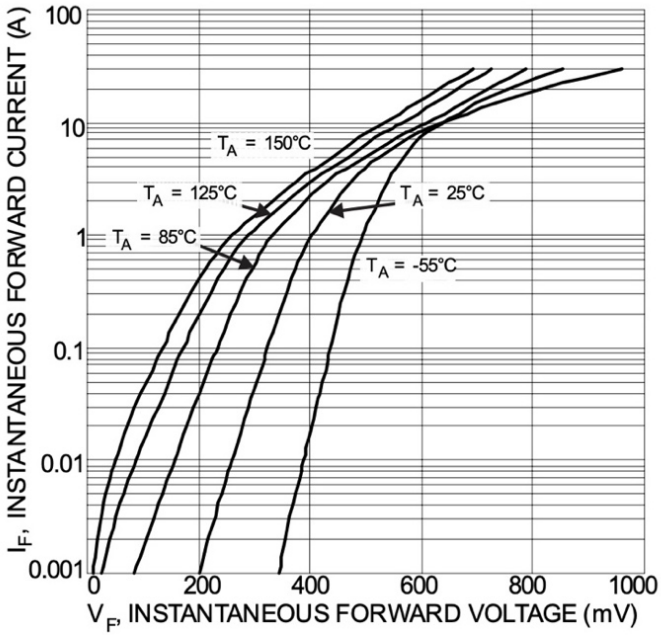

Figure 5.6: V-I curve of Schottky diode [12, p. 3]

Table 5.2: Schottky diode specifications [12]

DC blocking voltage (V)	Average rectified current (A)		Forward voltage (V) @25°C
	Per leg	total	
120	20	40	0.88

5.3 Motor constants.

The motor constants help quantify the performance of the motor. From Chapter 2 the relationships for the torque produced and the voltage induced were calculated with the assistance of K_T, motor torque constant(Nm/A), and the K_E, motor voltage constant (Vs/rad). When SI units are used K_E and K_T are the same [1, p.82]. Radian is a dimensionless quantity.

$$\frac{(newton)(meter)}{amp} = \frac{joule}{amp} = \frac{(watt)(second)}{amp} = \frac{(volt)(amp)(second)}{amp} = (volt)(second)$$

5.3.1 K_E rating

$$EMF = K_E\omega = K_E\frac{2\pi N}{60} \qquad (2.44)$$

For measuring the K_E rating of the motor the devised experiment consisted of connecting a resistive element to the output of the 3-phase bridge rectifier and rotating the wheel at specified speeds. This allowed for the plotting of the induced voltage as function of the wheel speed curve of the motor,

as shown in Figure 5.7(a). The slope of the curve provided the approximate K_E rating of the motor with respect to the wheel.

$$K_E = slope\ of\ graph = \frac{30.54 - 5.654}{250 - 50} = 0.124\frac{V}{rpm}$$

Or,

$$K_E = 1.18\frac{V}{rad/s}$$

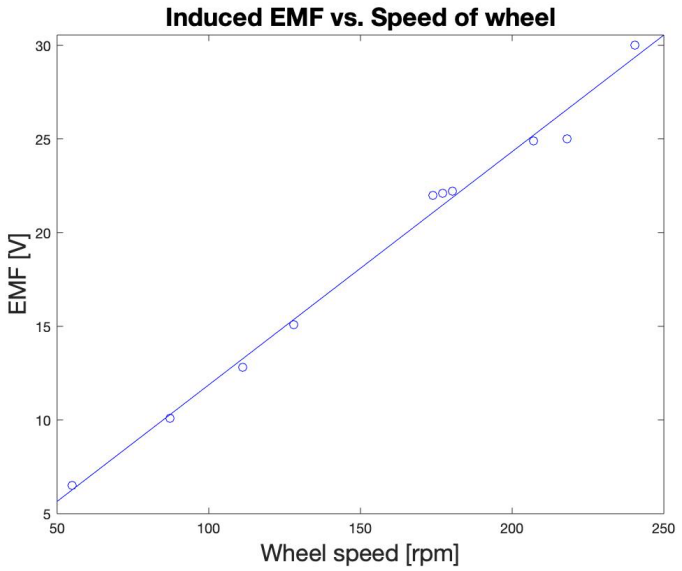

(a)

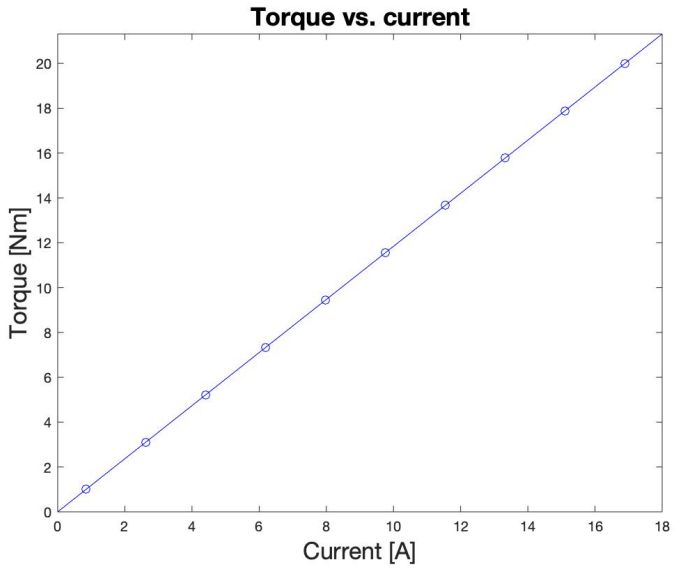

(b)

Figure 5.7: Motor relationships (a)Induced voltage vs. speed of wheel (b) Wheel torque vs motor current

5.3.2 K_T rating

K_T rating was derived utilizing the K_E rating. The K_E rating obtained was for the wheel of the motor. The K_T rating of the motor requires the K_E rating adjusted for the motor and therefore should account for the gear reduction ratio. For the purpose of electricity generation the torque exerted on the wheel is required rather than what is exerted by the motor itself. Therefore the K_T rating of the wheel is used and was found to be 1.18 Nm/A and the torque vs current characteristics were obtained by using equation 2.6, with a plot shown by Figure 5.7 (b)

$$Torque = K_T I \tag{2.6}$$

5.4 Energy used for cycling

The project was designed around the concept of storing a part of the energy used for cycling on flat ground and down inclines and utilizing it for climbing inclines. As such the kinematics of cycling is explored for calculating the available energy during cycling.

5.4.1 Kinematics of riding on flat ground

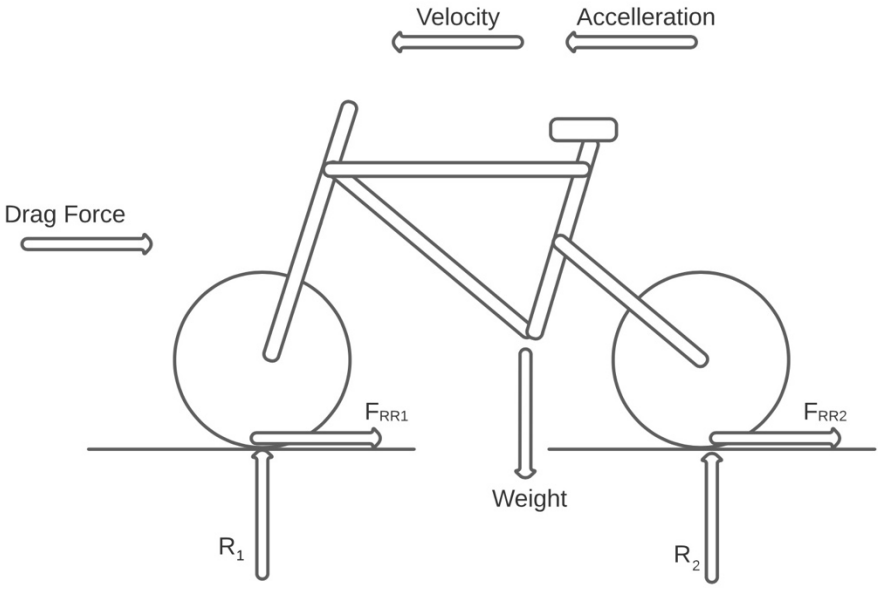

Figure 5.8: Forces acting on bicycle on flat ground

Where,

R_1, R_2 – reactant force

F_{RR1}, F_{RR2} – Rolling resistance

Figure 5.8 shows the various forces acting on a bicycle when traversing on flat ground. Drag force becomes prominent at higher speeds. The force exerted by a cyclist on the air is the mass of air encountered per unit time, multiplied by its change in velocity [13, p.125]. The mass of air encountered per unit time is proportional to the product of air density ρ, velocity *v* and frontal area *A*. This is shown in Figure 5.9. A factor of 0.5 is considered for the ability of the rider being able to cut through the air. Combined the drag force is found to be,

$$Drag\ force = F_D = \frac{1}{2}\rho_{air} C_D A v^2 \tag{5.3}$$

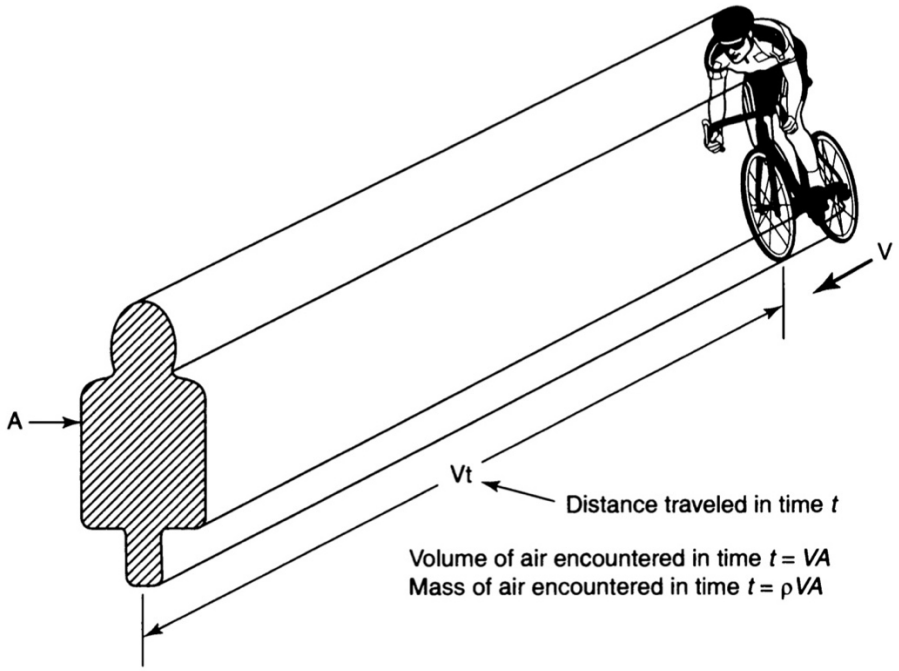

Figure 5.9: mass of air encountered by rider [13, p.126]

Observing Figure 5.8 the forces acting on the bicycle is analysed with the law of conservation of energy.

$$Energy\ exerted\ by\ rider = Drag\ energy + Rolling\ resistance\ energy$$

$$E_{rider} = (F_D + F_{RR})d$$

Where *d* is the distance travelled.

Power exerted by the rider can be found by,

$$Power\ exerted\ by\ rider = (F_D + F_{RR})v \tag{5.4}$$

F_{RR} is found by exploring the vertical component of the forces.

Vertical force components:

$$Weight = Mg = R_1 + R_2$$

Where M = mass of bicycle + mass of rider

$$F_{RR} = F_{RR1} + F_{RR2} = C_r R_1 + C_r R_2$$

$$F_{RR} = MgC_r$$

Where C_r is the coefficient of rolling resistance

Therefore the power exerted by the rider is found to be,

$$P_{rider} = \frac{1}{2}\rho_{air} C_D A v^3 + MgC_r v \tag{5.45}$$

Table 5.3 shows measured resistance and mass parameters for survey of bicycles. Since the protype in construction has similar components to an e-bike, their parameters are used for the calculations. The average speed of a cyclist was found to be 20.72 km/h or 5.756 m/s [14] according to a study done in Copenhagen, the bicycle capital of the world.

Therefore,

$$Power\ required\ on\ flat\ ground = 132.3\ W$$

This is assumed to be the maximum power that can be provided by the rider and hence the maximum power that can charge the supercapacitor bank.

Table 5.3: Measured resistance parameters [14]

Bicycle type	Road	Hybrid	Mountain	Cruiser	E-bike
C_r	0.0070	0.0079	0.0089	0.0078	0.0103
C_dA [m^2]	0.505	0.579	0.603	0.640	0.614
M [kg]	91.5	91.1	93.3	93.7	106.3
M_{rider} [kg]	75.8	73.5	75.1	74.0	74.2

5.4.2 Kinematics of riding uphill

The prototype was designed around the ability to traverse a test hill according the specifications outlined in Table 5.4.

Table 5.4: Hill climb specifications

Hill length	450m
Hill gradient	5%
Uphill speed	4.16 ms^{-1} or 14.98 km/h

The forces acting on the bicycle during a hill climb is shown in Figure 5.10.

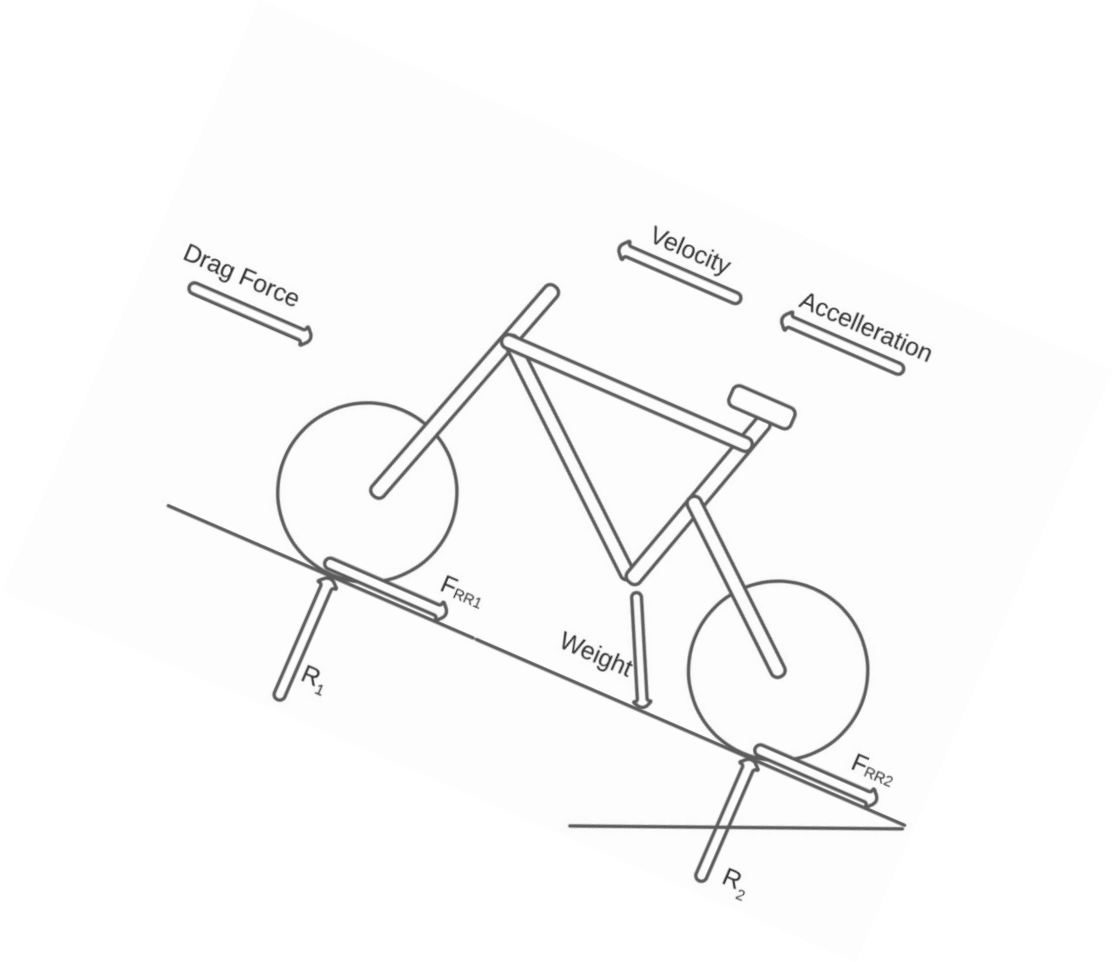

Figure 5.10: Forces acting on bicycle during hill climb

In the absence of wind and mechanical drivetrain losses [15], cyclist power *P* can be modelled as,

$$P = MgGv + MgC_r v + \frac{1}{2}\rho C_d A_f v^3 \tag{5.6}$$

Where *Mg* is the total weight (in N) of the bicycle and cyclist, C_r (unit-less) is the rolling resistance coefficient, G (unit-less) is the road grade, *v* (in m/s) is the bicycle speed, ρ (kg/m^3) is the air density, and C_d (unit-less) and A_f (m^2) are the drag coefficient and frontal area of the bicycle and cyclist.

Factoring in the parameters in Table 5.3 and 5.4 provides us the power used for climbing the hill as,

$$Power\ required\ for\ hill\ climb = 288.2\ W$$

For ease of climbing the hill, the rider should exert the same amount of power as they would be when riding on flat ground. Therefore, the power assist needed by the electric motor is found by the relationship,

$$Power\ assist = Power\ for\ hill\ climb - Power\ on\ flat\ ground$$

$$Power\ assist = 288.2 - 132.3 = 155.9\ W$$

There is also the efficiency of the motor, which is mostly in the region of 80%, to be considered. This resulted in the power provided by the supercapacitor be,

$$Power = \frac{155.9}{0.8} = 194.88\ W$$

The time taken for hill climb is found to be 108.2 seconds resulting in the total energy expended by the motor to be,

$$Energy\ used\ by\ motor = Power\ provided\ \times time$$

$$Energy\ used = 194.88\ \times 108.2 = 21.09\ kJ = 5.86\ Wh$$

5.5 Supercapacitor bank

The energy required for the hill climb assist is to be stored in a supercapacitor bank and should be done so as to power the motor. The motor controller has an operating voltage range of 21-48 V and the supercapacitor bank should hold enough energy in this range. Most double layer supercapacitors have an upper limit at around 2.7 – 3.0 V. Therefore, multiple supercapacitors need to be connected in series to obtain the required voltage. However, when connected in series the total capacitance of the bank becomes less, governed by,

$$C_{total} = \frac{C_{invidual\ cell}}{number\ of\ cells\ in\ series} \quad (5.7)$$

The motor draws a constant current. Part of the energy stored in the supercapacitor is not available for the motor due to its discharge characteristic, shown in Figure 5.11. Therefore, the energy required for the assist need to lie in the usable region of the supercapacitor.

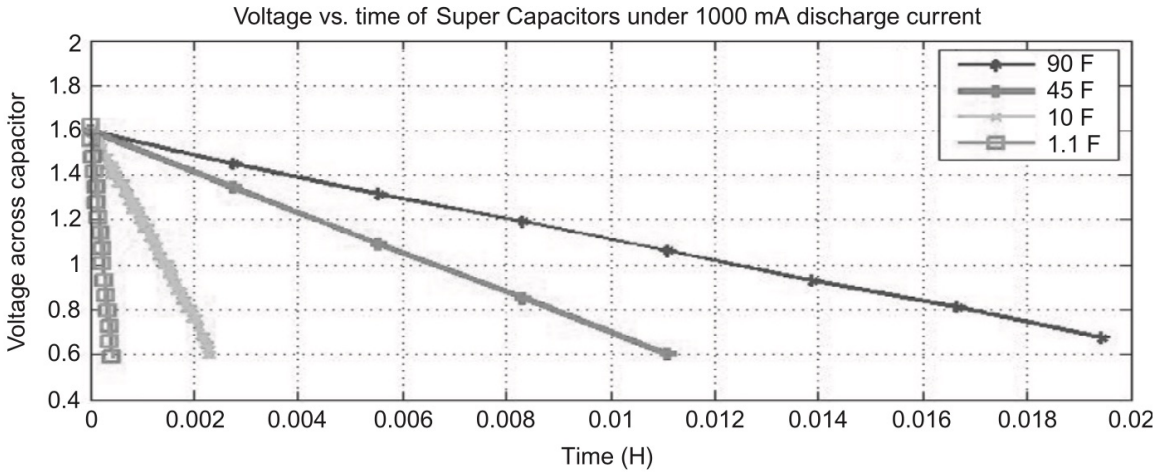

Figure 5.11: Constant current discharge curve for supercapacitors [6, p.50]

The following equation was derived to find a relationship between the usable energy and the required number of capacitors with their individual capacitance.

$$usable\ energy = \frac{1}{2}\frac{C}{n}[(nV_i)^2 - V_L^2] \tag{5.8}$$

Where C (F) is the individual capacitance, n is the number of cells, V_i the voltage rating of individual cell and V_L the lowest operating voltage.

Table 5.5 shows some available cells, with their various specifications. The previous team decided on the Illinois 470F supercapacitor, resulting in the use of 18 cells to obtain the operating range of 21 - 48 V. By using equation (5.8) the usable energy is,

$$usable\ energy = 25.08\ kJ = 6.97\ Wh$$

which provides the required energy for a successful hill climb assist.

Table 5.5: Supercapacitors and their specifications [16, p. 10]

	Voltage (V)	Unit price (NZD)	Capacitance (F)	Volume (mm^3)	Total Volume (mm^3)	ESR (mΩ)
Eaton-Electronics division	2.7	17.94	300	50.03	900.54	4.5
	2.7	20.33	400	60.61	1090.98	3.2
Illinois Capacitor	2.7	26.33	470	57.73	1039.09	3
Maxwell technologies	2.3	19.51	300	17.48	454.48	13
Vinatech	3.0	20.85	360	59.6	953.6	3
AVX	2.7	17.79	360	59.6	1072.8	6

5.6 Bicycle Power Stage.

The supercapacitors need to be charged up to 48 V while the bicycle is ridden on flat ground. This is accomplished by using the in-hub BLDC motor in its generation region. The voltage generated by the motor is directly proportional to the speed of rotation. Therefore, the motor should be rotated at speeds required to generate at least 48 V to charge the supercapacitors fully. Figure 5.12 shows the voltage generated per speed of bike. By exploring the plot of the induced voltage vs. the speed of bike, shown in Figure 5.12, it can be inferred that to reach 48 V the bike has to be travelling at speeds well over 30 km/h. This speed is much higher than the average speed of cyclist of 20.72 km/h [14]. Due to the physical limitations of an average rider, modifications should be done to achieve a higher voltage without straining the rider. To step-up the voltage the novel boost converter, explored in chapter 3, can be used. But with such a proven technique there's also the pitfall of needing multiple sensing circuits to adjust the output voltage continuously as a rider wouldn't be riding at constant speed indefinitely. A concept was explored for charging the supercapacitor bank by paying attention to the electrical systems of commercial vehicles.

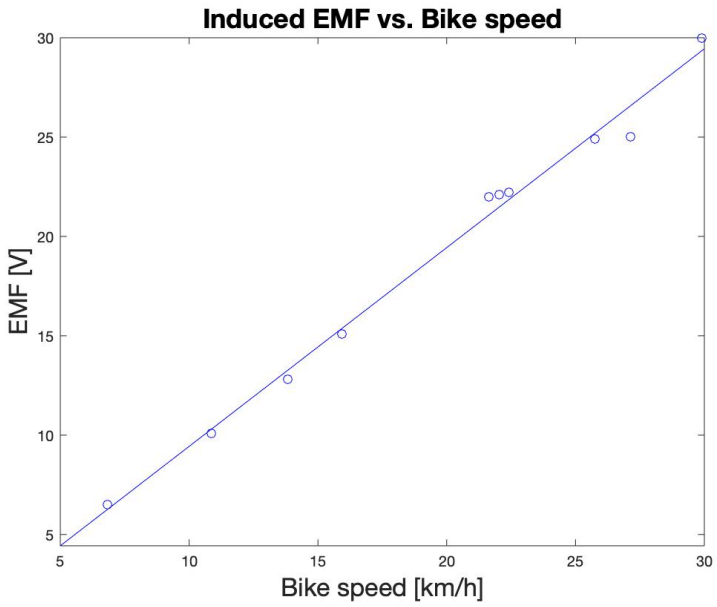

Figure 5.12: Induced voltage vs speed of bike

Heavy commercial vehicles have a combined 12/24 V system [17, p.391]. The alternator, used for electricity generation, and the electrical components operate at 12 V while the starter motor uses 24 V. The system, shown in Figure 5.13, consists of two 12 V batteries that are connected in parallel during operation of the vehicle. When the ignition switch is turned on a battery changeover relay switches the batteries in series resulting in 24 V applied to the starter motor. Afterwards the batteries connect in parallel and both are charged by the 12 V alternator.

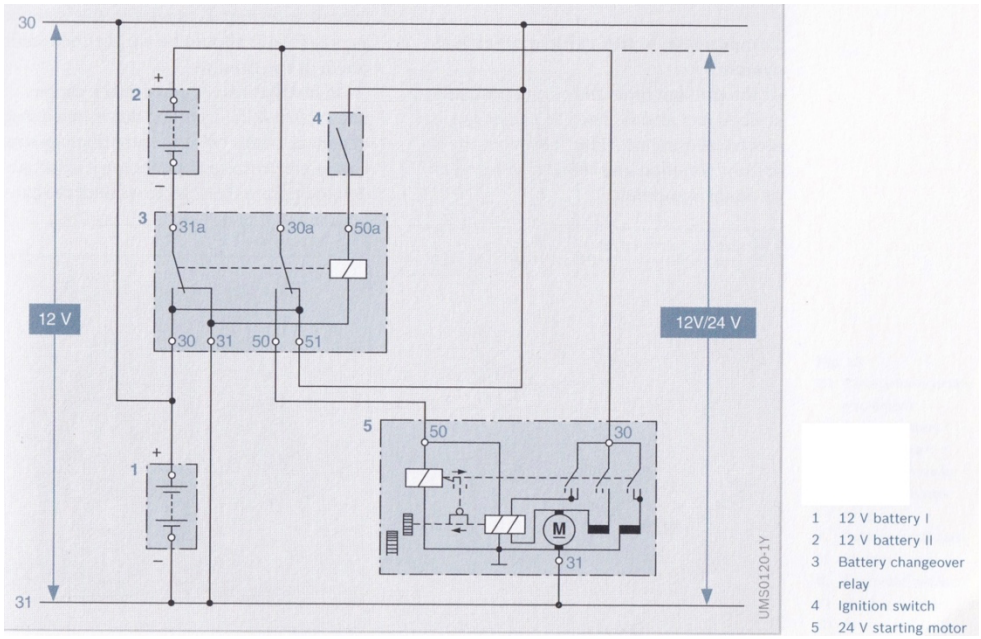

Figure 5.13: 12/24 V system of commercial vehicle [17, p.390]

From Figure 5.12 it is inferred a max voltage of 24 V is within reach of a rider traveling at around 24 km/h. Therefore, the supercapacitor bank were assembled into two equal parts capable of reaching 24 V each while charging and then combine to provide 48 V when motoring, similar to the commercial vehicle system above. The two main modes of operation is shown in in Figure 5.14 with the switches controlled for each mode.

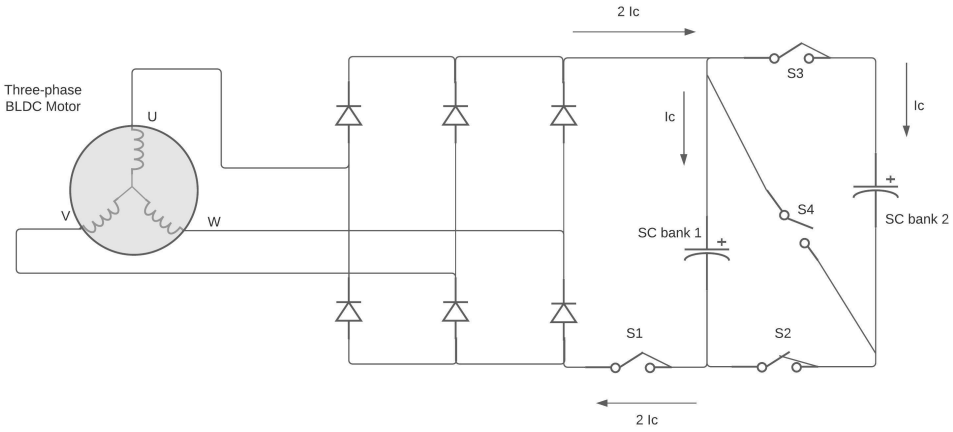

(a)

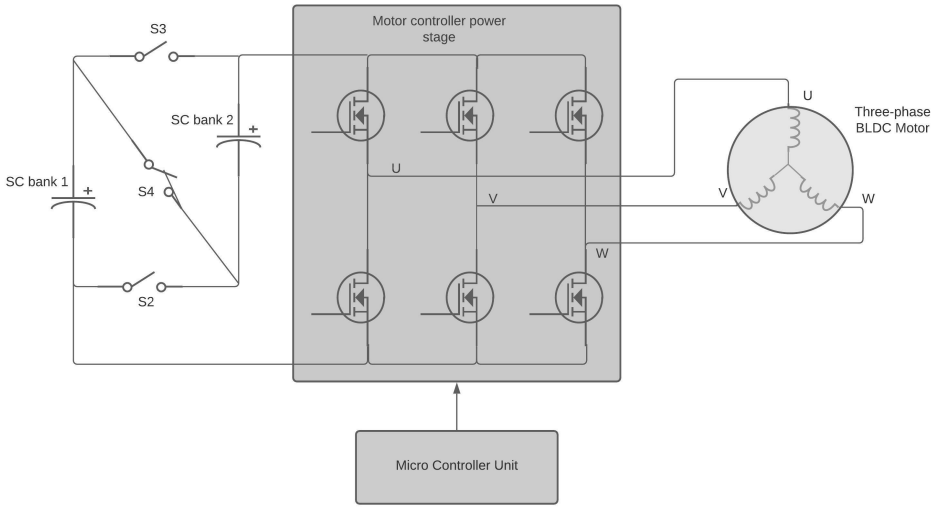

(b)

Figure 5.14: Modes of operation: (a) Charging (b) Motoring

Table 5.6: Switch states for individual mode

Mode of operation	S1	S2	S3	S4
Charging	On	On	On	Off
Motoring	Off	Off	Off	On

5.6.1 Charging Mode.

When the bicycle is set to charging mode, shown in Figure 5.14(a), switches S1, S2 and S3 are turned on while S4 is turned off. When S2 and S3 are closed it allows for the two supercapacitor banks to be connected in parallel, resulting in the two sharing current. Closing of switch S1 allows the BLDC motor to start generating electricity that is converted through the 3-phase rectifier to charge the two supercapacitor banks to equal voltages.

5.6.2 Motoring Mode

As shown in Figure 5.14(b), when set to motoring mode switches S1, S2 and S3 are all turned off while S4 is turned on. With S4 closed the two supercapacitor banks end up in series resulting in double the voltage to operate the BLDC motor.

5.7 Power converter circuit

The use of relay switches for the bicycle was deemed to be unsuitable due to the size constraints. Instead the use of power MOSFETs was explored. Attention was paid to the type of MOSFET used for each switch position weighing the ease of control and power losses. N-Channel MOSFETs are cheaper and have a lower on resistance compared to P-channel MOSFETs and are ideal to be used in low-side switching. But N-channel MOSFETs require more components and complicated design for high-side switching. Therefore, P-channel MOSFETs were placed as high-side switches, S3 and S4, while N-channel MOSFETS were placed as the low-side switches, S1 and S2.

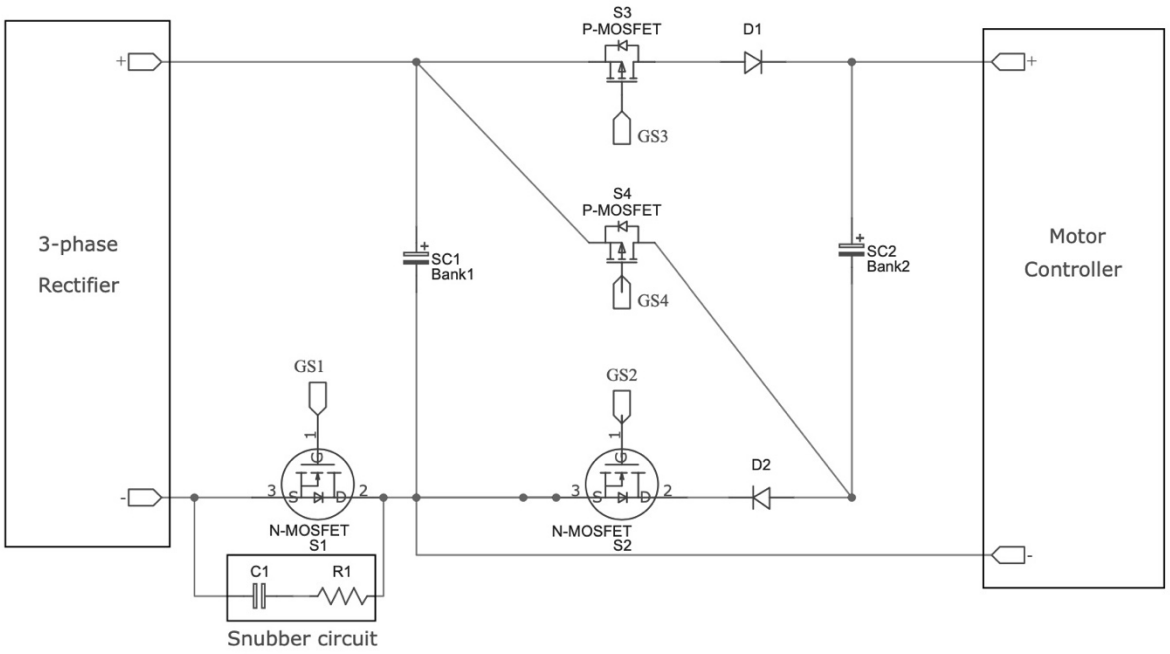

Figure 5.15: Power stage

MOSFETs block current only in one direction. When the series connection of the banks are made, diode D1 blocks the stepped up voltage from charging the supercapacitor bank 1. Diode D2 acts to stop the motor controller from consuming power just from supercapacitor bank 2.

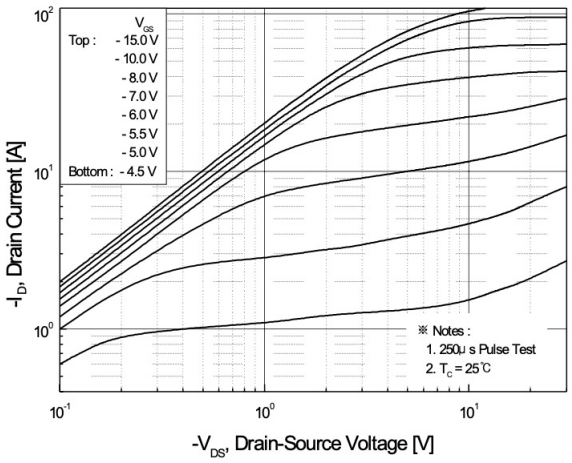

(a)

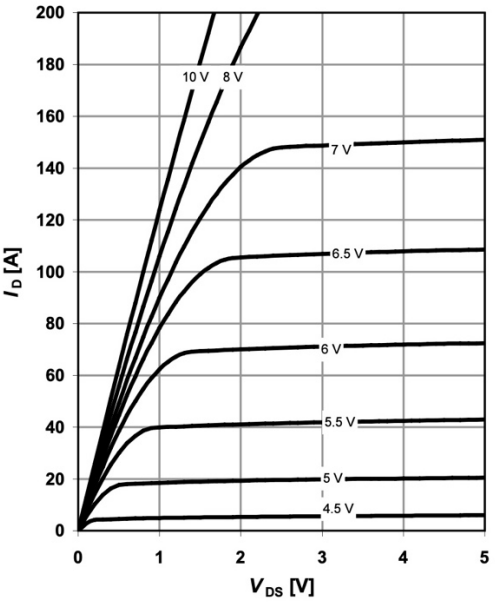

(b)

Figure 5.16: Typical output characteristics (a) P-Channel MOSFET[20] (b) N-Channel MOSFET[19]

5.7.1 Control circuit

MOSFETs are voltage controlled devices. The control circuit should be designed to accommodate correct voltage levels for operation of the MOSFETs. The typical output characteristics of the MOSFETs are shown in Figure 5.16. MOSFETs turn on when V_{GS} passes a certain threshold voltage. As seen from the plots in Figure 5.16, the resistance of the MOSFET decreases with increasing V_{GS}. Therefore, V_{GS} should be run at the highest voltage possible to reduce losses. The lowest voltage achieved by the system is 11 V and therefore V_{GS} of -10 V for the P-channel MOSFET and V_{GS} of 10 V for the N-channel MOSFET was chosen. This is done by utilizing the simple Zener diode regulator, as shown in Figure 5.17, due to the low power requirements of driving the MOSFET gates. A 9.4 V rail was also obtained by utilizing an emitter-follower.

Table 5.7: Specifications of MOSFETs used[19][20]

	P-Channel MOSFET	N-Channel MOSFET
I_D -Drain Current continuous	-27 A	50 A
V_{DSS} – Drain-Source Voltage	-60 V	60 V
$R_{DS(on)}$ – On Resistance	0.07 Ω @V_{GS} = -10 V	9 mΩ @V_{GS} = 10 V
$V_{GS(th)}$- Gate Threshold Voltage	-2 V < V_{GS} < -4 V	2 V < V_{GS} < 4 V
P_D- Power Dissipation	120 W	71 W
Q_g -Gate Charge total	36 nC	33 nC

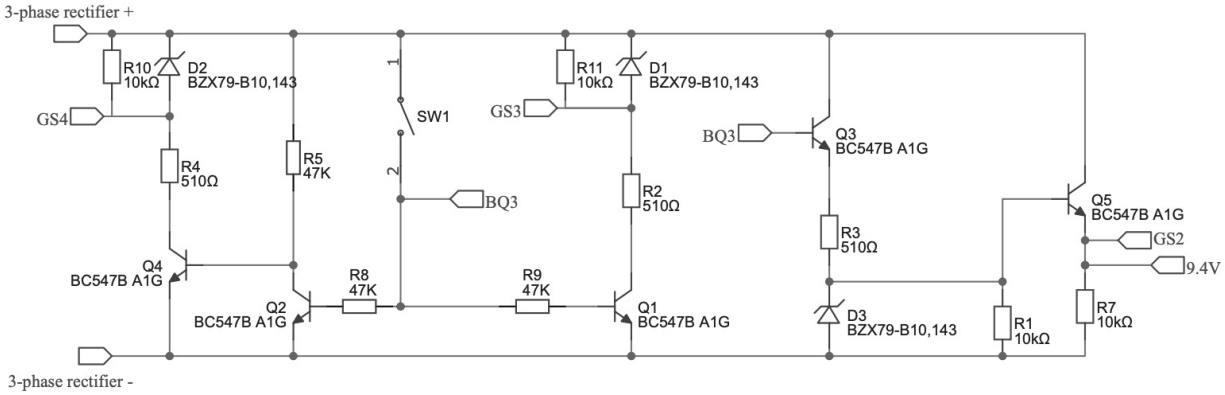

Figure 5.17: Control circuit

When the switch SW1 is closed transistor Q1, Q2 and Q3 are turned on. This allows current to flow through the 10 V zener diode D1 and D3. Zener D1 provides a V_{GS} of -10 V for MOSFET S3 to turn on. Zener D3 provides a V_{GS} of 9.4 V, due the diode drop of the emitter follower Q5, causing MOSFET S2 to turn on as well. Since transistor Q2 is turned on, transistor Q4 is turned off resulting in no current flowing through zener D2 and provides a V_{GS} of 0 V for MOSFET S4 keeping it turned off. This allows for the two supercapacitor banks to be connected in parallel and allow charging operation.

When the switch SW1 is opened, transistors Q1,Q2 and Q3 are turned off. With current not flowing through zener diodes D1 and D3 the V_{GS} of 0 V to be provided to MOSFETs S3 and S2 turning them off. While transistor Q2 is off, transistor Q4 is turned on letting current pass through zener D2 providing a V_{GS} of -10 V causing MOSFET S4 to turn on. This results in the two supercapacitor banks to be connected in series to allow hill climb assist.

It should be noted here that the motor controller draws a high current, close to 25 A during start up. Due to the continuous current rating of a single P-channel MOSFET is 27 A, two MOSFETs are connected in parallel to share the current at switch S4. MOSFETs can be paralleled directly (without ballasting resistors in source leads), because their negative temperature coefficient of I_D at fixed V_{GS} guarantees automatic redistribution of drain currents in a paralleled way[8, p.212]. MOSFETs exhibit negative tempco of I_D at high drain currents, or relatively large values of V_{GS}, as shown in Figure5.18.

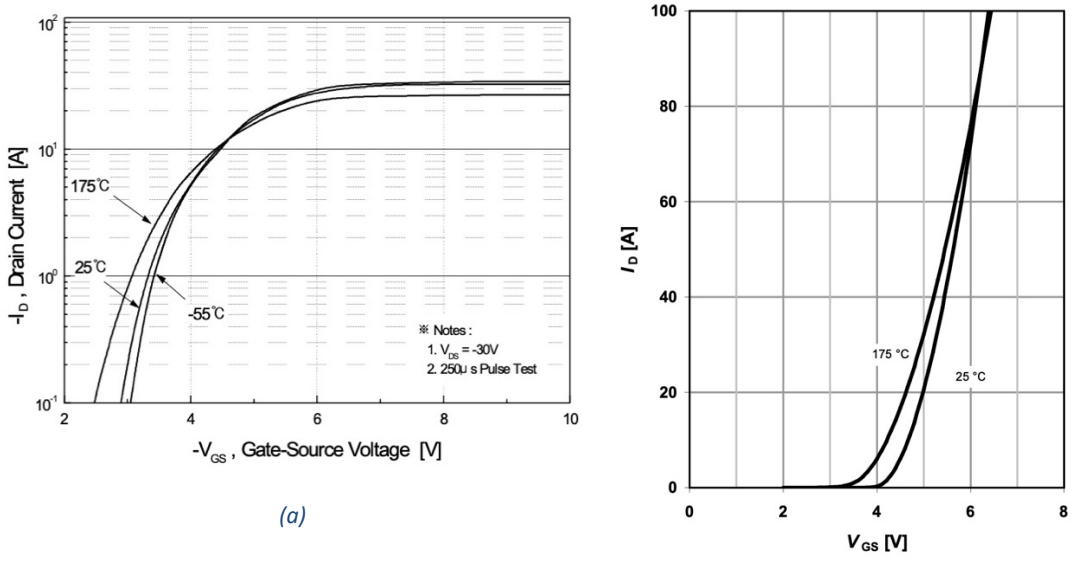

(a) *(b)*

Figure 5.18: Transfer characteristics (a) P-Channel MOSFET[20] (b) N-Channel MOSFET[19]

5.7.2 Current limiting

A quick glance at Figure 5.7(b) shows that the torque increases proportional to the current drawn in the motor windings. The current drawn by a charging supercapacitor is governed by,

$$i_c(t) = \frac{E}{R} e^{-\frac{t}{RC}} \tag{5.9}$$

Where, *E* is the charging voltage, *R* is the resistance of the charging loop, *C* is the capacitance and *t* is the time elapsed.

The current drawn by the supercapacitor changes with its state of charge, decreasing exponentially until fully charged. As a rider has limited power capability, an effective method should be utilized to keep the torque during charging constant and low. One such method explored is the use of pulse-width modulation (PWM) to limit the current. PWM can be obtained by either software or through analogue means. For the current project analogue circuits were developed by utilizing the 555 timer IC and operational amplifiers.

5.7.2.1 PWM using 555 timer IC

The 555 timer IC was connected as shown in Figure 5.19 to operate in its "Astable" mode. A slight modification to the circuit present in its datasheet [21] was made by the inclusion of a diode between the IC's discharge and threshold pins. This modification allowed for the duty cycle to be adjusted from 0 – 100 %. The equations governing the on and off times are shown below.

$$T_{ON} = 0.693(R_1)C_1 \tag{5.10}$$

$$T_{OFF} = 0.693(R_2)C_1 \tag{5.11}$$

The relationship between T_{ON} and T_{OFF} can be represented by,

$$(1 - Duty)T_{ON} = (Duty)T_{OFF} \tag{5.12}$$

To calculate the resistors required for required duty cycle, combining equation (5.9) and (5.10) with equation (5.11) provides the following relationship,

$$\frac{R_1}{R_2} = \frac{Duty}{(1 - Duty)} \tag{5.13}$$

The period is given by,

$$T = T_{ON} + T_{OFF}$$

Resulting in the frequency of the PWM signal,

$$Frequency = \frac{1}{T} = \frac{1.44}{(R_1 + R_2)C_1} \tag{5.14}$$

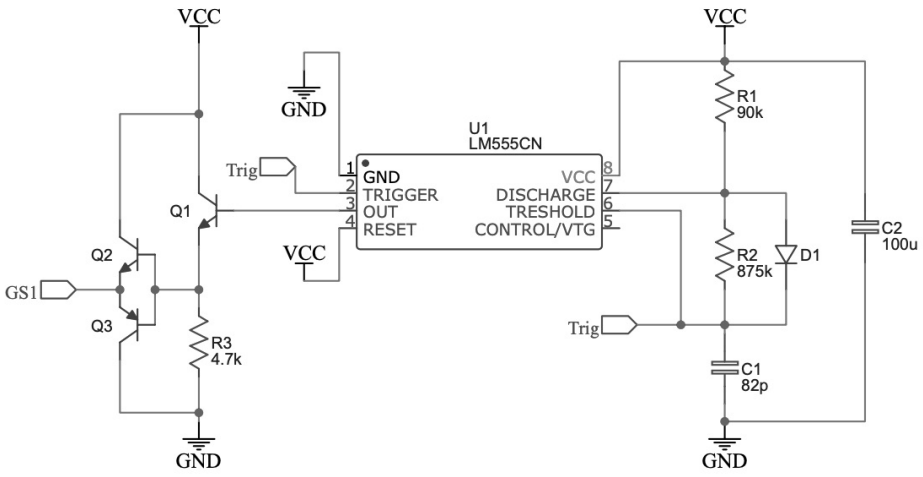

Figure 5.19: 555 timer IC for PWM

Table 5.8: Waveform parameters generated in Figure 5.19

Duty cycle	23%
Frequency	28 kHz

The duty cycle of the PWM signal can be changed by varying the value of the resistors R_1 and R_2. But as per equation (5.13) the frequency of oscillation also changes. Therefore, the 555 timer IC should be use where a fixed PWM signal is required. This does not satisfy the changing current draw depending on the state of charge of the supercapacitor bank requiring a different method of PWM.

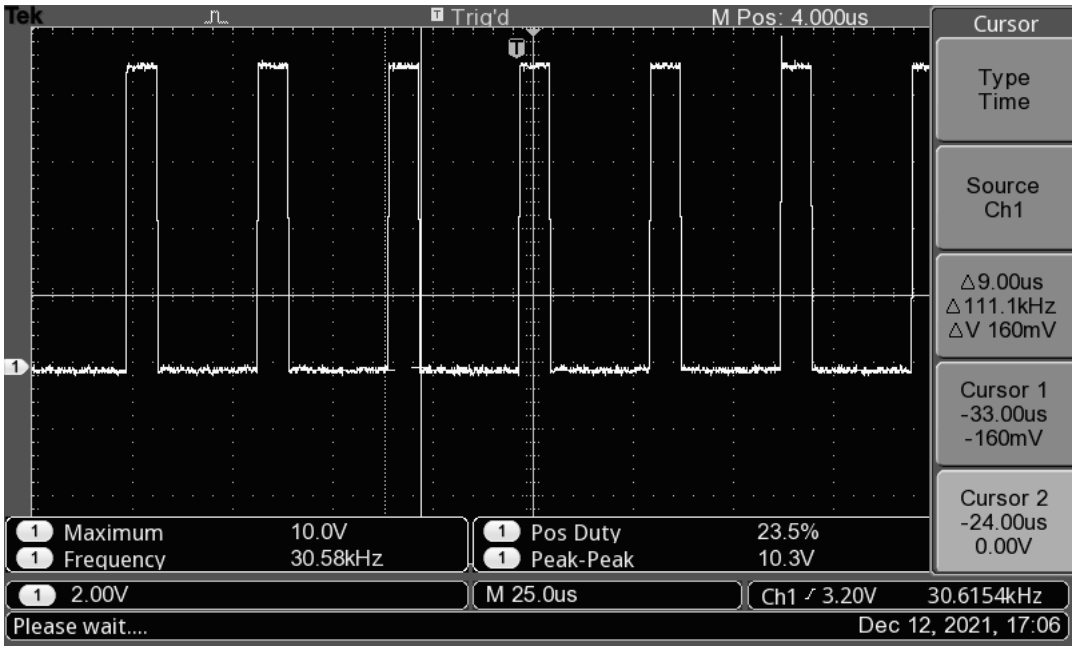

Figure 5.20: PWM waveform obtained by LM555 timer IC

5.7.2.2 PWM using operational amplifiers

An operational amplifier can be used to generate a triangle wave that is compared to a voltage level to generate a PWM signal. Figure 5.21 shows the typical triangle wave generator.

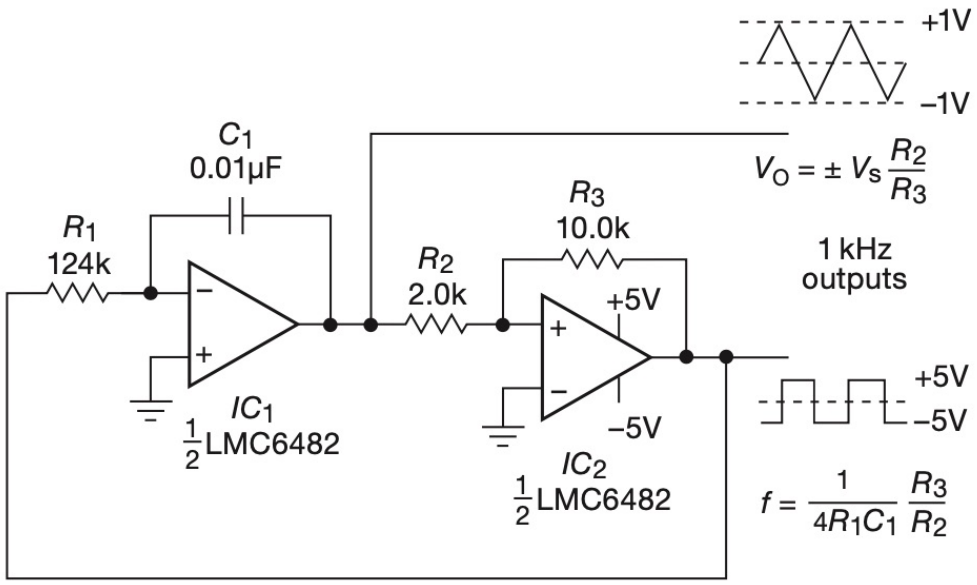

Figure 5.21: Dual supply Triangle wave generator [8, p.239]

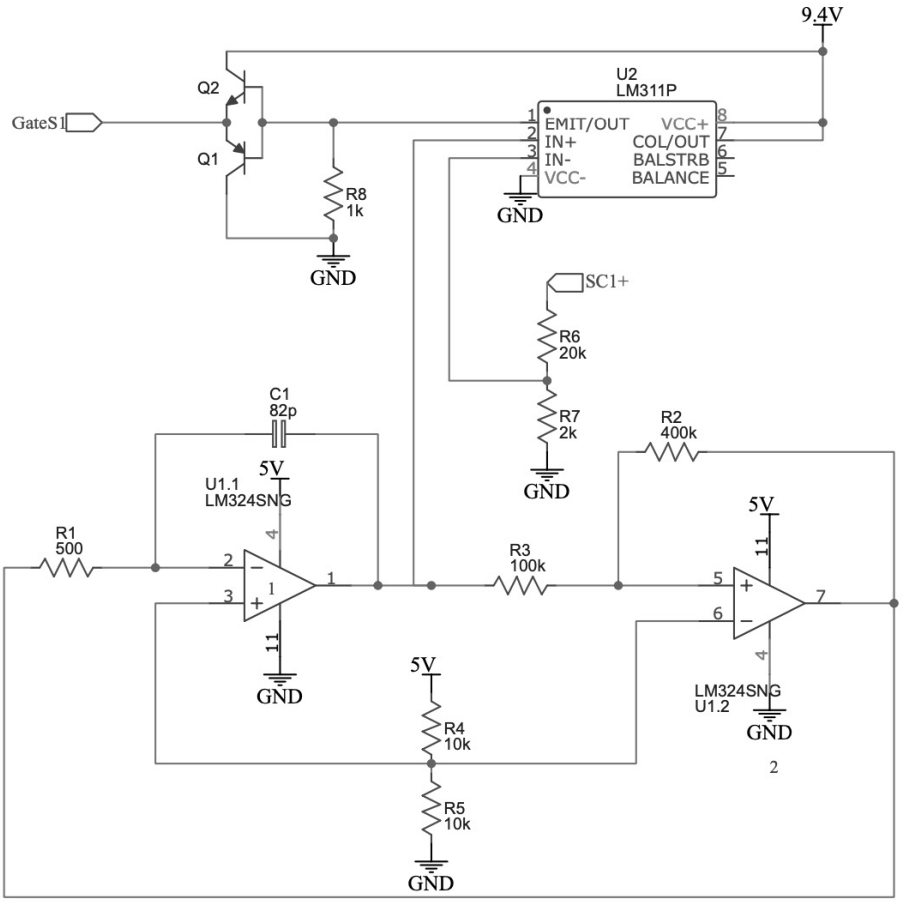

Figure 5.22: Current control circuit

The function generator is constructed using a single supply LM324S [22] op amp, which is powered by the 9.4V voltage rail shown in Figure 5.17. To obtain a single supply rail design [23] a reference voltage of half the supply voltage is fed into the terminals connected to the ground in Figure 5.21 while the negative supply rail is connected to the ground. This results in the triangle wave oscillating around half the supply voltage provide by,

$$V_o = \frac{V_s}{2} \pm V_s \frac{R_2}{R_3} \tag{5.15}$$

The circuit developed is shown in Figure 5.22. The state of charge of supercapacitor bank 1 is compared to the generated triangle wave using a LM311 comparator to provide a varying duty cycle. The PWM signal drives the N-channel MOSFET S1 providing a constant current during the charging period. Sample waveforms for different state of charge is shown in Figure 5.23.

While back emf, *E* = 24 V and total loop resistance, R = 0.400 Ω

Current drawn by supercapacitor bank when both are at 11 V,

$$V_c = 11 = E\left(1 - e^{-\frac{t}{RC}}\right)$$

$$e^{-\frac{t}{RC}} = \left(1 - \frac{11}{24}\right)$$

From Equation (5.9),

$$i_c = \frac{E}{R} e^{-\frac{t}{RC}}$$

$$i_c = \frac{E}{R}\left(1 - \frac{11}{24}\right)$$

$$i_c = 32.5\ A$$

Current drawn by both supercapacitor bank when at 11 V with limiter,

$$I = i_c \times 21.1\% = 6.86\ A$$

Current drawn when supercapacitor bank at 22 V,

$$i_c = 5\ A$$

Current drawn by both supercapacitor bank when at 23 V with limiter,

$$I = i_c \times 44.6\% = 2.23\ A$$

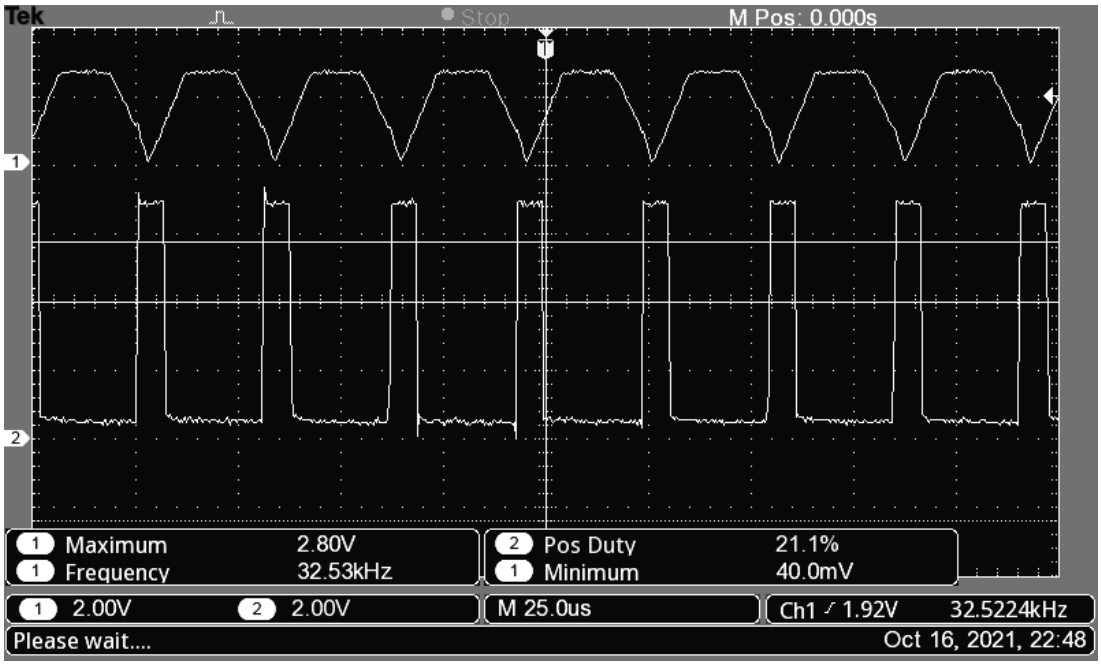

(a)

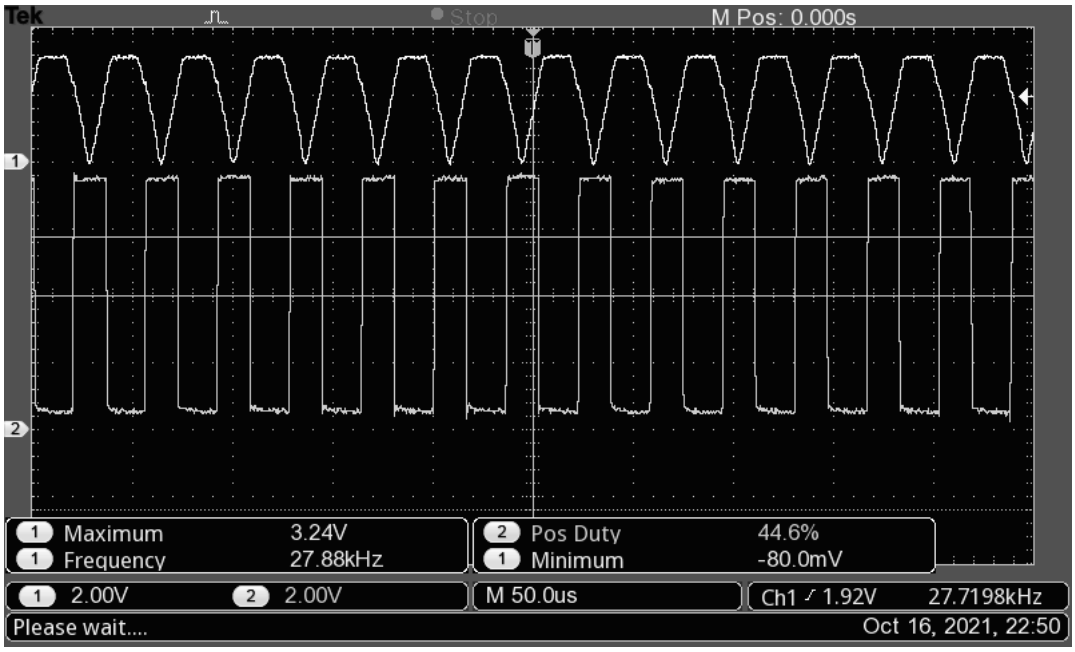

(b)

Figure 5.23: : PWM signal (a) at 11 V (b) at 22V

5.7.3 Snubber circuit

Switch S1 is responsible for closing the circuit for charging the supercapacitors. The BLDC motor is an inductive load and inductive loads are bad news for transistors. Here enters the snubber circuit. The snubber circuit absorbs the inductive load so that the transistor is protected.

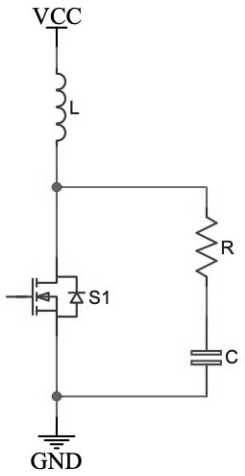

Figure 5.24: Snubber circuit

The snubber capacitor should store the energy in the inductor.

$$E_{inductor} = E_{capacitor}$$

$$\frac{1}{2}LI^2 = \frac{1}{2}CV^2$$

The capacitance should be calculated such that the voltage is less than the breakdown voltage of the transistor. Given that the inductance of the motor and maximum current allowed in the motor windings, a suitable snubber is designed.

Table 5.9: Snubber design criteria

L (µH)	Max current (A)	Breakdown voltage (V)	Chosen voltage (V)
624.8	15 A	60	40

$$C = 2 \times \frac{E_{inductor}}{V^2}$$

$$C = 97.8 \times 10^{-6}\ F$$

$$R = \frac{V}{I} = \frac{40}{15} = 2.7\Omega$$

5.8 Brake energy recovery.

Braking using an electric motor is accomplished by applying torque opposing the direction of travel. This is achieved by absorbing a large amount of current from the motor, either to be dissipated as heat in a load or stored in an energy storage device for future use. Supercapacitors were seen to ideal for a brake energy recovery system due to the low ESR and high current capabilities they afford. The use of one supercapacitor cell with its low voltage between 2.7 – 3.0 V was explored to make sure the motor will store energy and slow down until the back emf was reduced to at least 3.0 V.

5.8.1 Energy dissipation on braking.

Assuming drag forces to be negligible, the energy dissipated during braking will be the total kinetic energy of the moving bicycle. Considering braking on flat ground while travelling at an average speed of 20.72 km/h[14] to a complete stop, the energy dissipated is found using the law of conservation of energy.

$$Brake\ energy\ = Initial\ kinetic\ energy - Final\ kinetic\ energy$$

$$brake\ energy = \frac{1}{2}M\left(v_i^2 - v_f^2\right)$$

$$Brake\ energy\ = 1763\ J$$

Where, M = 106.3 kg, initial velocity, v_i = 5.76 ms^{-1} and final velocity, v_f = 0 ms^{-1}

In a lossless system, this energy is to be stored in a supercapacitor. With an individual cell voltage of V =3.0 V, the capacitance required is found by rearranging the following equation.

$$energy\ stored = \frac{1}{2}CV^2$$

$$C = \frac{1763}{3^2} \times 2 = 391.8\ F$$

A supercapacitor cell was chosen with the following specifications.

Table 5.10: Supercapacitor cell specification

Name	Voltage (V)	Capacitance (F)	ESR (mΩ)	Max current (A)
Vinatech	3.0	500	3.2	288

5.8.2 Brake energy storage.

Preliminary testing consisted of connecting the supercapacitor cell directly to the 3 phase rectifier as shown in Figure 5.25 .

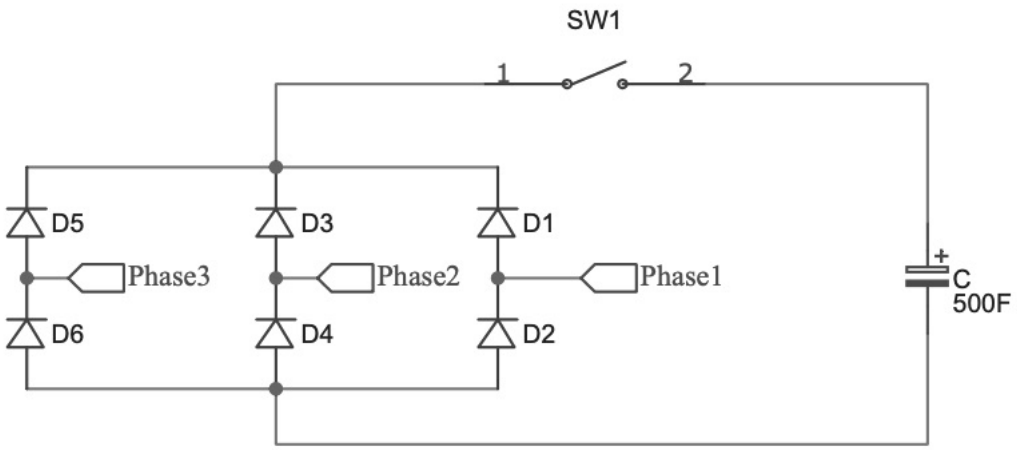

Figure 5.25: Preliminary brake energy recovery testing circuit

The braking torque generated can be found by calculating the current drawn by the supercapacitor.

From Equation (5.9),

$$i_c = \frac{E}{R} e^{-\frac{t}{RC}}$$

$$i_c = \frac{20}{0.385} e^{0} = 51\ A$$

This current draw is at the instant the switch is closed and due to the torque created, will slow down the rotation of the wheel lowering the back emf and consequently lowering the current drawn. This was proved by the braking observed while testing and the voltage gained in the supercapacitor.

The next step was to transfer the energy stored in the braking supercapacitor cell to the main supercapacitor banks, accomplished by boosting the voltage of the braking supercapacitor cell. Boost converter technique, explored in chapter 4, is to be used. It should be mentioned that boost converters are used when the voltage ratio is $1 < V_O/V_I < 5$,

Where V_o is output voltage and V_I is input voltage [9, p.246]. This is determined by the limitation on switching duty cycle, D, where D < 0.8 usually. Even though 48 V of the supercapacitor bank is not within the voltage ratio specified for the boost converter, the energy stored In the inductor during the switch on phase, Figure 5.26(a) should be transferred to the supercapacitor bank during the switch off phase.

Figure 5.26: Two step operation of boost converter: (a) switch on (b) switch off

5.8.2.1 Inductor charging

An inductor was built with an inductance of 10 μH. For charging the inductor,

$$i_L = \frac{V}{R_1}\left(1 - e^{-\frac{t}{\tau}}\right),$$

$$\tau = \frac{L}{R_1} = \frac{10 \times 10^{-6}}{5.8 \times 10^{-3}} = 1.724 \times 10^{-3} s$$

I_L is limited to 10 A as a lab made inductor was used.

$$e^{-\frac{t}{\tau}} = 0.981$$

$$t = 33.66\ \mu s$$

This is the t_{on} for the boost converter switch.

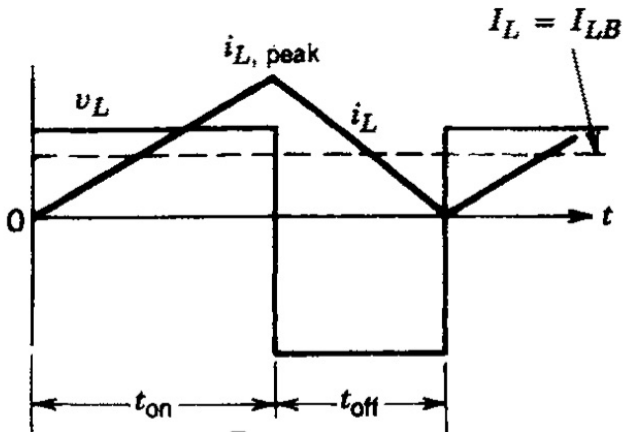

Figure 5.27: Boundary of boost converter continuous conduction mode.[9, p.174]

5.8.2.2 Inductor discharging

During the second phase of the boost converter, assuming discontinuous conduction mode, the energy stored in the inductor is discharged to the supercapacitor bank.

$$\frac{1}{2}LI^2 = \frac{1}{2}C\left(V_f^2 - V_i^2\right) \tag{5.16}$$

Where V_i is the initial voltage and V_f is the final voltage

Considering the supercapacitor bank, of capacitance C = 52.2 F, is charged to V_i = 11 V and inductor current is 10 A, equation (5.16) provides,

$$\Delta V = V_f - V_i = 8.7 \times 10^{-7}\ V$$

The area under the graph, shown in Figure 5.27, in the region t_{off} provides the charge transferred to the supercapacitor,

$$\Delta Q = C\Delta V = 4.54 \times 10^{-5}\ Coloumb$$

t_{off} is then calculated by,

$$\Delta Q = \frac{1}{2} \times 10 \times t_{off}$$

$$t_{off} = 9.08\ \mu s$$

The switching frequency of the boost converter is,

$$f = \frac{1}{T} = \frac{1}{t_{on} + t_{off}} = 23.4\ kHz$$

With a duty cycle (D) of,

$$D = \frac{t_{on}}{T} = 0.79$$

When the supercapacitor bank is charged to V_i = 22 V, when calculated as above t_{off} was,

$$t_{off} = 4.55\ \mu s$$

This is less than the previous value which shows the boost converter circuit when run at frequency of 23.4 kHz with a duty cycle of 0.79 will stay at discontinuous conduction mode.

5.8.2.3 LTSpice simulation of boost converter

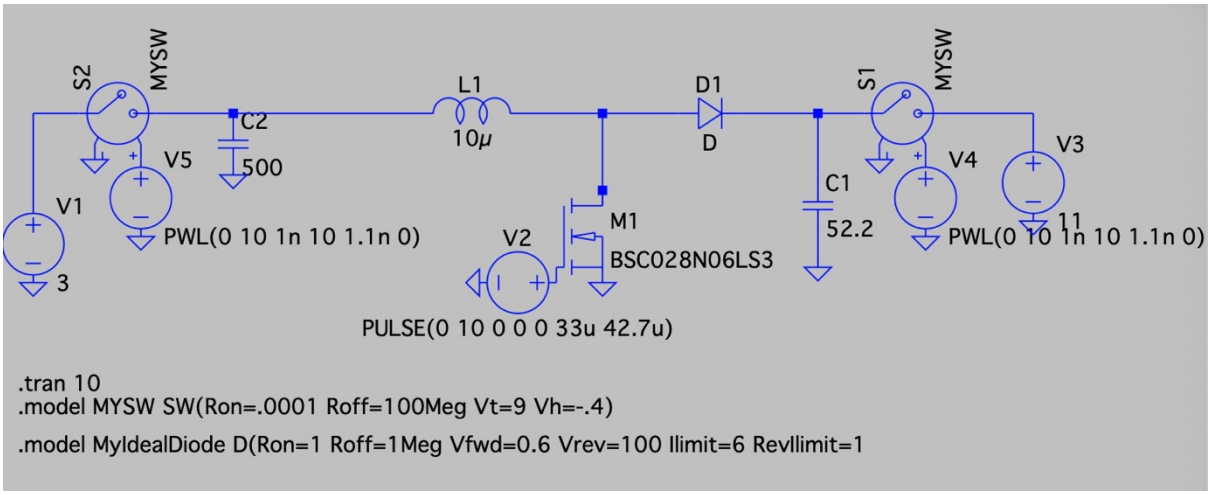

Figure 5.28: LTSpice simulation schematic for boost technique

An LTSPice simulation model of the boost converter is shown in Figure 5.28. The braking supercapacitor is C2 while the main supercapacitor bank is C1. For initial charging of the supercapacitors, voltage control switches were utilized. The basic model of the switch is:

.model MYSW SW(Ron=0.001 Roff=100Meg Vt=9 Vh=-.4)

MYSW represents model name, Ron and Roff represent the on and off resistance of the switch. Ron is set to a low value to make sure the voltage drop is minimized. Vt, trip voltage, and Vh, hysteresis voltage, trips the switch when (Vt - Vh) and (Vt + Vh). To see a notable increase in voltage at C1 the simulation needed to run for a long time, hence the 10 second duration.

However further development of the system was halted due to covid-19 lockdowns.

5.9 Performance of SCA-bicycle

The bike performance for the two scenarios of hill climb and flat ground travel is shown in Figure 5.29. The red curve, covering a distance of 116.8 m, is the performance for hill climb along O'Donoghue Street in Hamilton, with a grade of 5%, at full throttle. The blue curve, covering a distance of 377.4 m, shows the performance on flat ground at full throttle. The black curve shows the discharge rate of the supercapacitor bank.

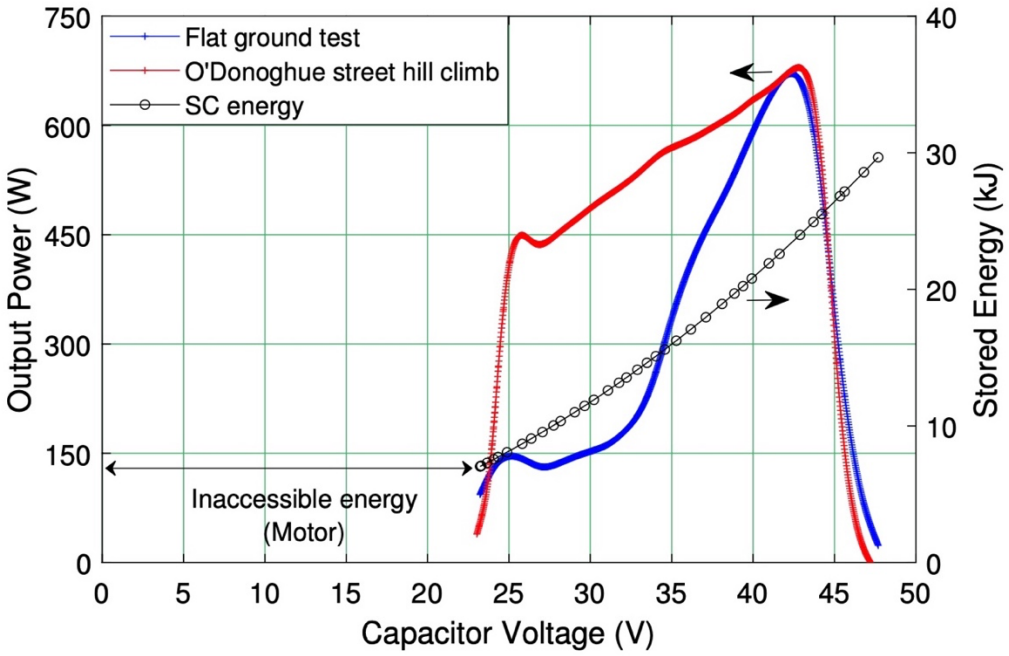

Figure 5.29: Supercapacitor assisted bike performance for hill climb and on flat ground

5.10 Energy stored while riding

Figure 5.30 shows the energy stored and the respective voltage gained in the supercapacitor banks per distance travelled.

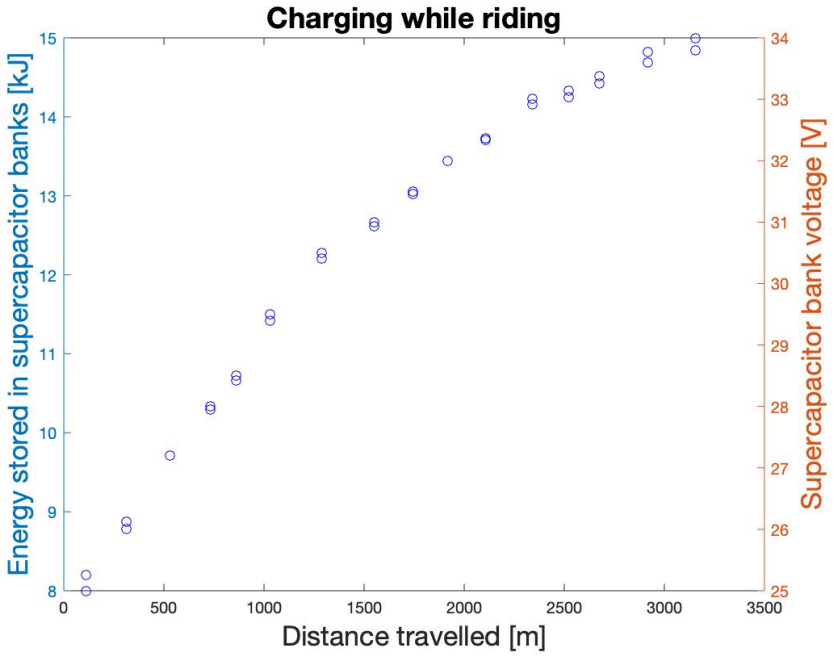

Figure 5.30: Energy stored when riding

The reason for the decreasing energy stored as the distance ridden is due to the power limitation of the average human rider, discussed previously in section 5.4.1. Part of the limited power available for the rider is used to charge the supercapacitor banks. The speed of the motor needs to increase to generate the voltage needed to charge the supercapacitor, shown by the KE rating. When the speed increases so does the forces of air drag, governed by the equation,

$$Drag\ force = F_D = \frac{1}{2}\rho_{air} C_D A v^2$$

Therefore the power used for charging is decreased while the power exerted by the rider is kept constant. Figure 5.31 shows a plot of the power decreasing as the amount of energy stored increases.

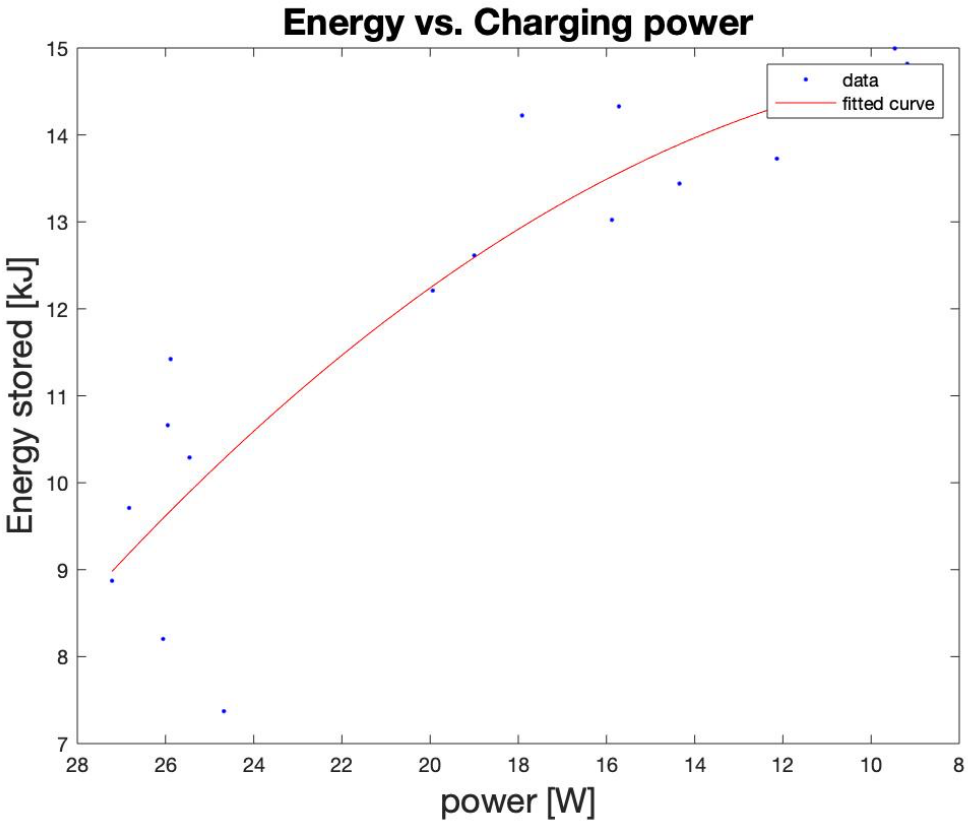

Figure 5.31: Power used for charging

Chapter 6: Conclusion

6.1 Summary of results

The main objectives of the project were,

- To assess the viability of a supercapacitor bank to provide a hill climb assist
- To develop an effective charging system to harvest energy into the supercapacitor bank while riding.
- To develop a brake energy recovery system for more energy harvesting.
- To complete objectives within the time frame of a Master programme of study

The viability of a supercapacitor assisted bicycle was proven and prototype was built with an effective charging system. A global pandemic, due to COVID-19, resulted in major restrictions and lockdowns resulting in halting development of the brake energy recovery system.

6.1.1 Replacing the battery with a supercapacitor bank

A supercapacitor's charge and discharge profile is different to that of a Li-ion battery. This is fundamentally due to the different techniques utilized by each component, with one using electrostatic means while the other is chemical. Li-ion batteries hold their voltage fairly constant during the discharge cycle while supercapacitors have their voltage change linearly under constant current discharge. To utilize the maximum available energy in the supercapacitor bank the full operating voltage range supported by the motor controller was used providing adequate energy for the hill assist.

6.1.2 Developing effective charging system

A prototype circuit for switching between parallel and series arrangement of the supercapacitor banks was successfully developed. The use of analogue circuit design for the MOSFET switching circuitry as well as the PWM signal generation for current limiting depending on the state of charge of the supercapacitor bank ensures reliable operation. Unlocking the potential of the protype circuit could lead it to be used for more power applications. The use of LTSpice simulations provided quick turnaround of circuit prototypes, especially with Covid-19 lockdowns affecting lab access.

6.2 Future work

The performance of the supercapacitor bike prototype had varying power output, with considerably low power near the lower end of the supercapacitor's state of charge. The supercapacitor bank also had energy which was inaccessible due to the operating voltage range of the BLDC motor controller.

Accounting for the regeneration capability of the BLDC motor, a possible solution would be the arrangement of the supercapacitors in parallel at a lower voltage and using a boost converter to provide constant power to the motor controller. Having the supercapacitors in parallel will allow more efficient charging due to the lower equivalent ESR and the lower voltage will allow the BLDC motor to charge them faster at a lower wheel speed than the current prototype, while the boost converter would add the benefit of deep discharging the supercapacitor banks extending the range, albeit by a small margin.

Another avenue could be to use the inductance of the BLDC motor as the boost stage of a boost converter to charge the supercapacitor bank at even lower speeds while also allowing the varying of the charging current. This could allow a braking system to be developed where an intermediate supercapacitor is not required to then charge the main supercapacitor bank. Variable braking could also be achieved by the charging current variability afforded by the boost converter.

References

[1] A. Hughes, B. Drury, "Electric Motors and Drives", *Elsevier*, 4th edition, 2013, pp 1-38

[2] J. G. Hayes, G. A. Goodarzi, "Electric Powertrain", *John Wiley & Sons*, 1st edition, 2018, pp 68-108, 159-298

[3] H. A. Toliyat, G. B. Kliman, "Handbook of Electric Motors", *CRC Press*, 2nd edition, 2004, pp 58-71, 763-772

[4] J. Keljik, "Electricity 4: AC/DC Motors, Controls, and Maintenance", *Delmar Cengage learning*, 10th edition, 2013, pp 1-16 , 113-134

[5] J Louis, "Control of Synchronous Motors", *Wiley*, 2011, pp 285

[6] N. Kularatna, K. Gunawardane, "Energy Storage Devices for Renewable Energy-Based Systems- Rechargeable Batteries and Supercapacitors", *Elsevier*, 2nd edition, 2021, pp 37-96, 173-249

[7] R. A. Mammano, "Fundamentals of Power Supply Design", *Texas Instruments*, 1st edition, 2017

[8] P. Horowitz, W. Hill, "The Art of Electronics", *Cambridge University Press*, 3rd edition, 2015.

[9] N. Mohan, T. M. Underland, W. P. Robbins, "Power Electronics, Converters, Applications and Design", *John Wiley & Sons*, 3rd edition, 2003.

[10] G. A. Rincon-Mora, "Analog IC design with Low-Dropout Regulators (LDO)", *McGraw-Hill*, 1st edition, 2009.

[11] N. Kularatna, "DC power supplies: power management and surge protection for power electronic systems", *CRC Press*, 2012.

[12] N. Kularatna, "Electronic Circuit Design: From concept to implementation", *CRC Press*, 2008.

[13] N. Kularatna, D. Jayananda, " Supercapacitor based Long Time Constant Circuits", *IEEE Industrial Electronics*, June 2020, pp. 40-56.

[14] T. Ariyarathna, "Design of SCALDO based high-current DC power supply(Thesis, Doctor of Philosophy)", *The University of Waikato*, 2021

[15] T. Ariyarathna, N. Kularatna, K. Gunawardane, D. Jayananada, D. A. Steyn-Ross, "Development of Supercapacitor Technology and its Potential Impact on New Power Converter Techniques for Renewable Energy", *IEEE Journal of Emerging and selected topics in Industrial Electronics*, Vol. 2, No. 2, July 2021, pp. 267-276

[16] T. Christen, M. W. Carlen, "Theory of Ragone plot", *Journal of Power Sources 91, 2000, pp.210-216*

[17] D. Jayananda, N. Kularatna, D. A. Steyn-Ross, "Supercapacitor-assisted LED (SCALED) technique for renewable energy systems: a very low frequency design approach with short-term DC-UPS capability eliminating battery banks", *IET Renewable Power Generation*, Vol. 14, Issue 9, June 2020, pp. 1559-1570

[18] N. Kularatna, "Power Electronics Design Handbook: low power components and applications", *Newnes*, London, 1998

[19] Diodes Incorporated, " 40A Trench Schottky Rectifier", SDT40A120CT datasheet, September 2016

[20] D. G. Wilson, "Bicycling science", *The MIT Press*, 3rd edition, 2004

[21] "Bicycle statistics", City of Copenhagen website, *City of Copenhagen*, 13 June 2013

[22] S. Tengattini, A. Y. Bigazzi, "Physical characteristics and resistance parameters of typical urban cyclists", *Journal of sports science*, 2018, vol. 36, no. 20, pp. 2383-2391

[23] A. Campbell, T. Crabtree, E. Halgryn, J. Tritscher, "Supercapacitor Assisted Electric bicycle", *The University of Waikato*, 2019

[24] C. Schmuker, H. Wanner, W. Kircher, W. Hofmeister, A. Simmel, "Vehicle electrical systems," *Automotive Electrics Automotive Electronics*, 5th edition, Robert Bosch GmbH, 2007

[25] M. Uno, H. Toyota, "Equalization Technique Utilizing Series-Parallel Connected Supercapacitors for Energy Storage System", *IEEE*, 2008

[26] Infineon, "OptiMOS™3 Power-Transistor", IPP093N06N3 datasheet, Revision 1.2, January 2010

[27] Fairchild Semiconductor Corporation, "P-channel QFET® MOSFET", FQP27P06 datasheet, Revision C0, March 2013

[28] Fairchild Semiconductor Corporation, "LM555 Single Timer", LM555 datasheet, Revision 1.1.0, January 2013

[29] ON semiconductor, “Single Supply Quad Operational Amplifiers”, LM324S datasheet, Revision 0, October 2014

[30] R. Mancini, “Single-supply op amp design”, *Texas Instruments*, Mixed signal Products, SLOA030A, 2001

[31] J. Caldwell, “Analog Pulse Width Modulation”, *Texas Instruments*, TI Precision Designs, SLAU508, June 2013

[32] H. Chen, “Low-Input Voltage High-current Boost converter with TPS61088”, *Texas Instruments*, TI Designs: PMP9772, TIDU880, April 2015

A. Appendix

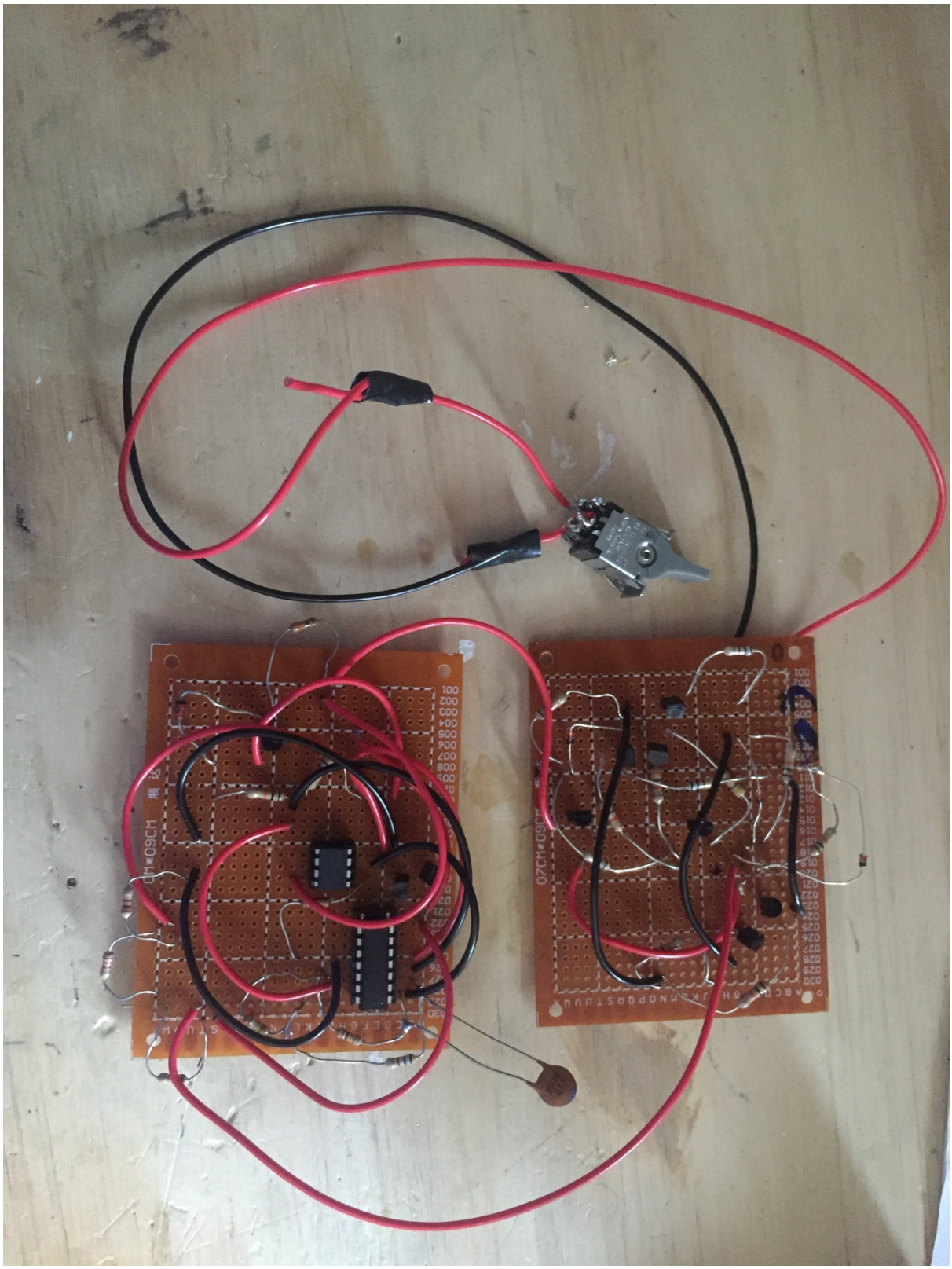

Figure A.1:Op-amp based Current limiting circuit (left) and Control Circuit (right)

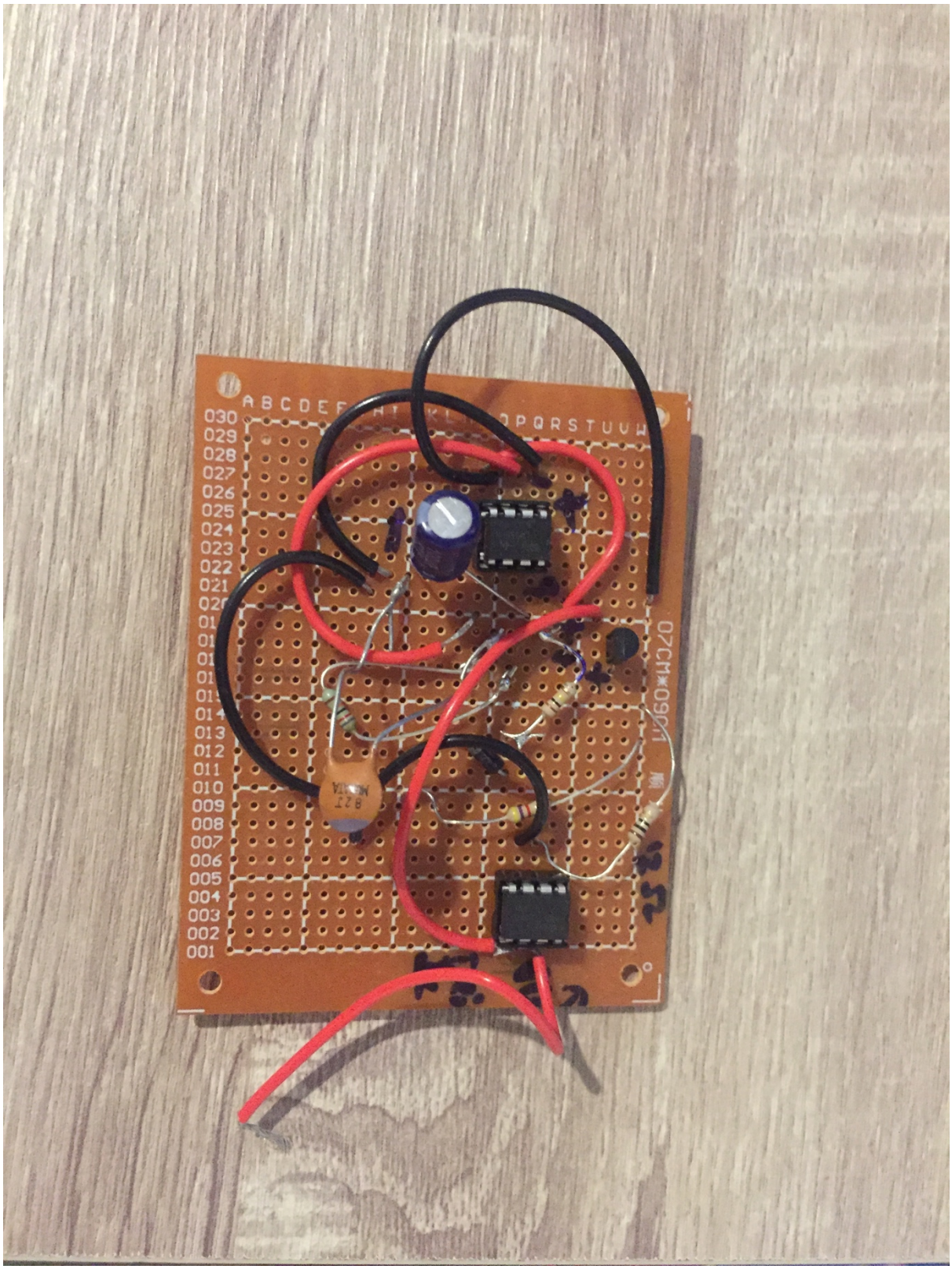

Figure A.2: LM555 timer IC based PWM generator circuit

NEW PRODUCT

SDT40A120CT

40A
TRENCH SCHOTTKY RECTIFIER

Product Summary (Per Leg)

V_{RRM} (V)	I_O (A)	V_F Max (V) @ +25°C	I_R Max (μA) @ +25°C
120	20	0.88	120

Features

- Low Forward Voltage Drop
- Excellent High Temperature Stability
- Soft, Fast Switching Capability
- **Lead-Free Finish; RoHS Compliant (Notes 1 & 2)**
- **Halogen and Antimony Free. "Green" Device (Note 3)**

Description and Applications

The SDT40A120CT provides very low V_F and extremely excellent reverse leakage stability at high temperatures. It is ideal for use as a rectifier, freewheel diode or blocking diode in:

- DC-DC Converters
- AC-DC Adaptors

Mechanical Data

- Case: TO220AB
- Case Material: Molded Plastic, UL Flammability Classification Rating 94V-0
- Terminals: Matte Tin Finish Annealed over Copper Leadframe. Solderable per MIL-STD-202, Method 208 e3
- Weight: 1.85 grams (Approximate)

TO220AB
Top View

TO220AB
Bottom View

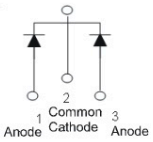

Package Pin Out
Configuration

Ordering Information (Note 4)

Part Number	Case	Packaging
SDT40A120CT	TO220AB	50 Pieces/Tube

Notes:
1. EU Directive 2002/95/EC (RoHS) & 2011/65/EU (RoHS 2) compliant. All applicable RoHS exemptions applied.
2. See http://www.diodes.com/quality/lead_free.html for more information about Diodes Incorporated's definitions of Halogen- and Antimony-free, "Green" and Lead-free.
3. Halogen- and Antimony-free "Green" products are defined as those which contain <900ppm bromine, <900ppm chlorine (<1500ppm total Br + Cl) and <1000ppm antimony compounds.
4. For packaging details, go to our website at http://www.diodes.com/products/packages.html.

Marking Information

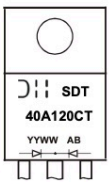

SDT40A120CT = Product Type Marking Code
AB = Foundry and Assembly Code
YYWW = Date Code Marking
YY = Last Two Digits of Year (ex: 16 = 2016)
WW = Week (01 to 53)

Figure A.3: Diode used: SDT40A120CT datasheet

NEW PRODUCT

Maximum Ratings (Per Leg) (@T_A = +25°C, unless otherwise specified.)

Single phase, half wave, 60Hz, resistive or inductive load.
For capacitive load, derate current by 20%.

Characteristic		Symbol	Value	Unit
Peak Repetitive Reverse Voltage Working Peak Reverse Voltage DC Blocking Voltage		V_{RRM} V_{RWM} V_{RM}	120	V
Average Rectified Output Current per Device	(Per Leg) (Total)	I_O	20 40	A
Non-Repetitive Peak Forward Surge Current 8.3ms Single Half Sine-Wave Superimposed on Rated Load		I_{FSM}	250	A

Thermal Characteristics (Per Leg)

Characteristic	Symbol	Value	Unit
Typical Thermal Resistance (Note 5) Package = TO220AB	$R_{\theta JC}$	2	°C/W
Operating and Storage Temperature Range	T_J, T_{STG}	-55 to +150	°C

Electrical Characteristics (Per Leg) (@T_A = +25°C, unless otherwise specified.)

Characteristic	Symbol	Min	Typ	Max	Unit	Test Condition
Forward Voltage Drop	V_F	— —	0.81 0.66	0.88 0.73	V	I_F = 20A, T_J = +25°C I_F = 20A, T_J = +125°C
Leakage Current (Note 6)	I_R	— —	5 4	120 25	µA mA	V_R = 120V, T_J = +25°C V_R = 120V, T_J = +125°C

Notes: 5. With 50mm*50mm*23mm Al heatsink.
6. Short duration pulse test used to minimize self-heating effect.

Figure A.4: Diode used: SDT40A120CT datasheet

NEW PRODUCT

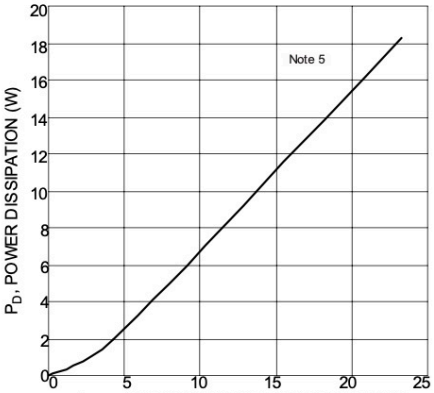

Figure 1 Forward Power Dissipation

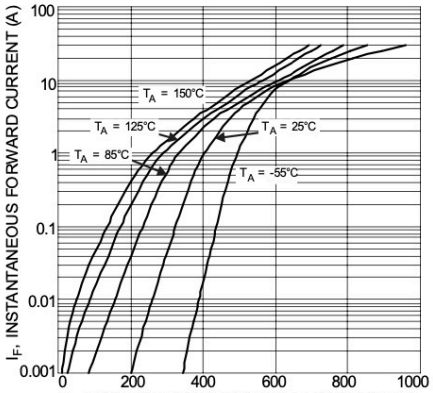

Figure 2 Typical Forward Characteristics

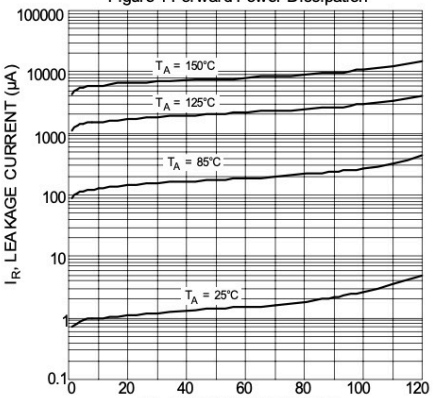

Figure 3 Typical Reverse Characteristics

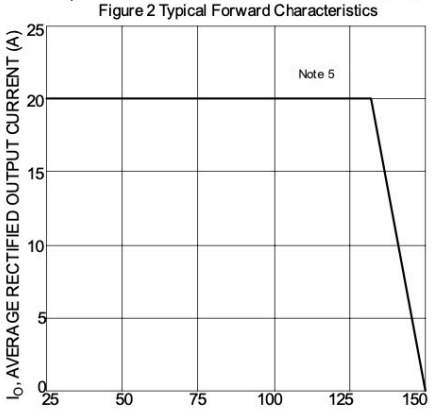

Figure 4 Forward Current Derating Curve

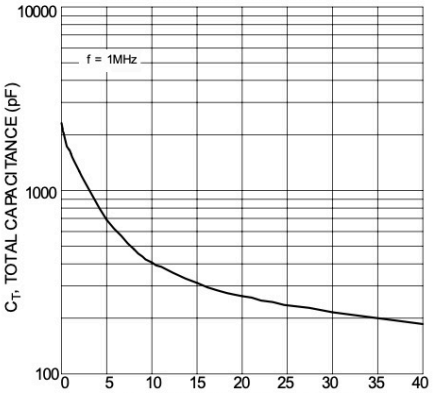

Figure 5 Total Capacitance vs. Reverse Voltage

Figure A.5: Diode used: SDT40A120CT datasheet

OptiMOS™3 Power-Transistor

Features

- for sync. rectification, drives and dc/dc SMPS
- Excellent gate charge x $R_{DS(on)}$ product (FOM)
- Very low on-resistance $R_{DS(on)}$
- N-channel, normal level
- Avalanche rated
- Qualified according to JEDEC[1] for target applications
- Pb-free plating; RoHS compliant
- Halogen-free according to IEC61249-2-21

Product Summary

V_{DS}	60	V
$R_{DS(on),max\ (SMD)}$	9	mΩ
I_D	50	A

RoHS

Halogen-Free

Type	IPB090N06N3 G	IPP093N06N3 G
		
Package	PG-TO263-3	PG-TO220-3
Marking	090N06N	093N06N

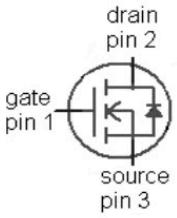

Maximum ratings, at T_j=25 °C, unless otherwise specified

Parameter	**Symbol**	**Conditions**	**Value**	**Unit**
Continuous drain current	I_D	T_C=25 °C[2]	50	A
		T_C=100 °C	50	
Pulsed drain current[3]	$I_{D,pulse}$	T_C=25 °C	200	
Avalanche energy, single pulse	E_{AS}	I_D=50 A, R_{GS}=25 Ω	43	mJ
Gate source voltage	V_{GS}		±20	V
Power dissipation	P_{tot}	T_C=25 °C	71	W
Operating and storage temperature	T_j, T_{stg}		-55 ... 175	°C
IEC climatic category; DIN IEC 68-1			55/175/56	

[1] J-STD20 and JESD22
[2] Current is limited by bondwire; with an R_{thJC}=1.6 K/W the chip is able to carry 74 A.
[3] See figure 3
[4] Device on 40 mm x 40 mm x 1.5 mm epoxy PCB FR4 with 6 cm² (one layer, 70 µm thick) copper area for drain connection. PCB is vertical in still air.

Figure A.6: N-Channel MOSFET used: IPP093N06N3 datasheet

Parameter	Symbol	Conditions	Values			Unit
			min.	typ.	max.	
Thermal characteristics						
Thermal resistance, junction - case	R_{thJC}		-	-	1.6	K/W
Thermal resistance, junction - ambient	R_{thJA}	minimal footprint	-	-	62	
		6 cm² cooling area[4)]	-	-	40	
Electrical characteristics, at T_j=25 °C, unless otherwise specified						
Static characteristics						
Drain-source breakdown voltage	$V_{(BR)DSS}$	V_{GS}=0 V, I_D=1 mA	60	-	-	V
Gate threshold voltage	$V_{GS(th)}$	V_{DS}=V_{GS}, I_D=34 µA	2	3	4	
Zero gate voltage drain current	I_{DSS}	V_{DS}=60 V, V_{GS}=0 V, T_j=25 °C	-	0.1	1	µA
		V_{DS}=60 V, V_{GS}=0 V, T_j=125 °C	-	10	100	
Gate-source leakage current	I_{GSS}	V_{GS}=20 V, V_{DS}=0 V	-	1	100	nA
Drain-source on-state resistance	$R_{DS(on)}$	V_{GS}=10 V, I_D=50 A	-	8.0	9.3	mΩ
		V_{GS}=10 V, I_D=50 A, (SMD)	-	7.7	9	
Gate resistance	R_G		-	0.7	-	Ω
Transconductance	g_{fs}	$\|V_{DS}\|>2\|I_D\|R_{DS(on)max}$, I_D=50 A	28	55	-	S

Figure A.7: N-Channel MOSFET used: IPP093N06N3 datasheet

5 Typ. output characteristics

$I_D=f(V_{DS})$; $T_j=25$ °C

parameter: V_{GS}

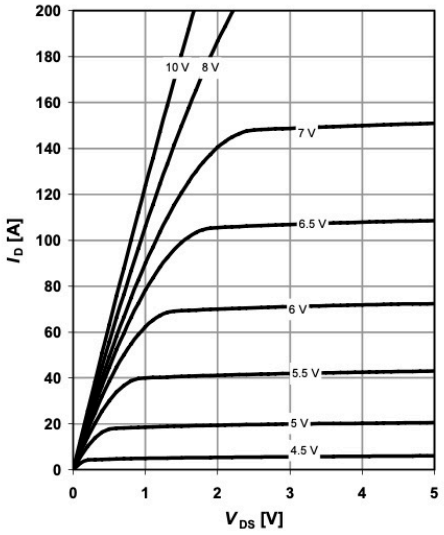

6 Typ. drain-source on resistance

$R_{DS(on)}=f(I_D)$; $T_j=25$ °C

parameter: V_{GS}

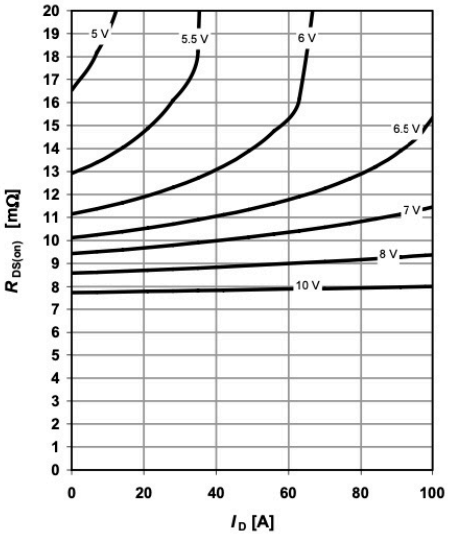

7 Typ. transfer characteristics

$I_D=f(V_{GS})$; $|V_{DS}|>2|I_D|R_{DS(on)max}$

parameter: T_j

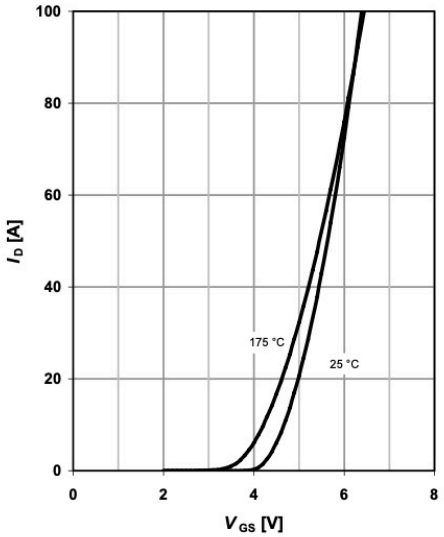

8 Typ. forward transconductance

$g_{fs}=f(I_D)$; $T_j=25$ °C

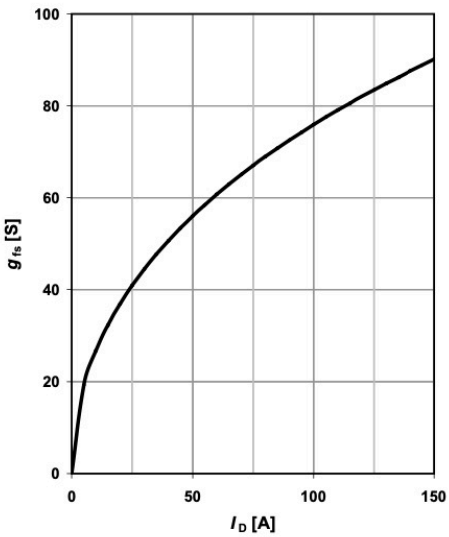

Figure A.8: N-Channel MOSFET used: IPP093N06N3 datasheet

FAIRCHILD SEMICONDUCTOR®

March 2013

FQP27P06

P-Channel QFET® MOSFET

- 60 V, - 27 A, 70 mΩ

Description

This P-Channel enhancement mode power MOSFET is produced using Fairchild Semiconductor®'s proprietary planar stripe and DMOS technology. This advanced MOSFET technology has been especially tailored to reduce on-state resistance, and to provide superior switching performance and high avalanche energy strength. These devices are suitable for switched mode power supplies, audio amplifier, DC motor control, and variable switching power applications.

Features

- - 27 A, - 60 V, $R_{DS(on)}$ = 70 mΩ (Max.) @ V_{GS} = - 10 V, I_D = - 13.5 A
- Low Gate Charge (Typ. 33 nC)
- Low Crss (Typ. 120 pF)
- 100% Avalanche Tested
- 175°C Maximum Junction Temperature Rating

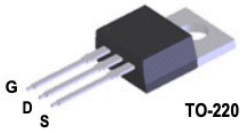

TO-220

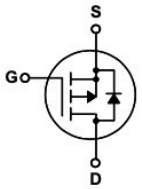

Absolute Maximum Ratings

T_C = 25°C unless otherwise noted

Symbol	Parameter		FQP27P06	Unit
V_{DSS}	Drain-Source Voltage		-60	V
I_D	Drain Current	- Continuous (T_C = 25°C)	-27	A
		- Continuous (T_C = 100°C)	-19.1	A
I_{DM}	Drain Current	- Pulsed (Note 1)	-108	A
V_{GSS}	Gate-Source Voltage		± 25	V
E_{AS}	Single Pulsed Avalanche Energy	(Note 2)	560	mJ
I_{AR}	Avalanche Current	(Note 1)	-27	A
E_{AR}	Repetitive Avalanche Energy	(Note 1)	12	mJ
dv/dt	Peak Diode Recovery dv/dt	(Note 3)	-7.0	V/ns
P_D	Power Dissipation (T_C = 25°C)		120	W
	- Derate above 25°C		0.8	W/°C
T_J, T_{STG}	Operating and Storage Temperature Range		-55 to +175	°C
T_L	Maximum lead temperature for soldering purposes, 1/8" from case for 5 seconds		300	°C

Thermal Characteristics

Symbol	Parameter	FQP27P06	Unit
$R_{\theta JC}$	Thermal Resistance, Junction-to-Case, Max.	1.25	°C/W
$R_{\theta CS}$	Thermal Resistance, Case-to-Sink, Typ.	0.5	°C/W
$R_{\theta JA}$	Thermal Resistance, Junction-to-Ambient, Max.	62.5	°C/W

Figure A.9: P-Channel MOSFET used: FQP27P06 datasheet

Elerical Characteristics

T_C = 25°C unless otherwise noted

Symbol	Parameter	Test Conditions	Min	Typ	Max	Unit
Off Characteristics						
BV_{DSS}	Drain-Source Breakdown Voltage	V_{GS} = 0 V, I_D = -250 μA	-60	--	--	V
ΔBV_{DSS} / ΔT_J	Breakdown Voltage Temperature Coefficient	I_D = -250 μA, Referenced to 25°C	--	-0.06	--	V/°C
I_{DSS}	Zero Gate Voltage Drain Current	V_{DS} = -60 V, V_{GS} = 0 V	--	--	-1	μA
		V_{DS} = -48 V, T_C = 150°C	--	--	-10	μA
I_{GSSF}	Gate-Body Leakage Current, Forward	V_{GS} = -25 V, V_{DS} = 0 V	--	--	-100	nA
I_{GSSR}	Gate-Body Leakage Current, Reverse	V_{GS} = 25 V, V_{DS} = 0 V	--	--	100	nA
On Characteristics						
$V_{GS(th)}$	Gate Threshold Voltage	V_{DS} = V_{GS}, I_D = -250 μA	-2.0	--	-4.0	V
$R_{DS(on)}$	Static Drain-Source On-Resistance	V_{GS} = -10 V, I_D = -13.5 A	--	0.055	0.07	Ω
g_{FS}	Forward Transconductance	V_{DS} = -30 V, I_D = -13.5 A	--	12.4	--	S
Dynamic Characteristics						
C_{iss}	Input Capacitance	V_{DS} = -25 V, V_{GS} = 0 V, f = 1.0 MHz	--	1100	1400	pF
C_{oss}	Output Capacitance		--	510	660	pF
C_{rss}	Reverse Transfer Capacitance		--	120	155	pF
Switching Characteristics						
$t_{d(on)}$	Turn-On Delay Time	V_{DD} = -30 V, I_D = -13.5 A, R_G = 25 Ω (Note 4)	--	18	45	ns
t_r	Turn-On Rise Time		--	185	380	ns
$t_{d(off)}$	Turn-Off Delay Time		--	30	70	ns
t_f	Turn-Off Fall Time		--	90	190	ns
Q_g	Total Gate Charge	V_{DS} = -48 V, I_D = -27 A, V_{GS} = -10 V (Note 4)	--	33	43	nC
Q_{gs}	Gate-Source Charge		--	6.8	--	nC
Q_{gd}	Gate-Drain Charge		--	18	--	nC
Drain-Source Diode Characteristics and Maximum Ratings						
I_S	Maximum Continuous Drain-Source Diode Forward Current		--	--	-27	A
I_{SM}	Maximum Pulsed Drain-Source Diode Forward Current		--	--	-108	A
V_{SD}	Drain-Source Diode Forward Voltage	V_{GS} = 0 V, I_S = -27 A	--	--	-4.0	V
t_{rr}	Reverse Recovery Time	V_{GS} = 0 V, I_S = -27 A, dI_F / dt = 100 A/μs	--	105	--	ns
Q_{rr}	Reverse Recovery Charge		--	0.41	--	μC

Notes:
1. Repetitive Rating : Pulse width limited by maximum junction temperature
2. L = 0.9mH, I_{AS} = -27A, V_{DD} = -25V, R_G = 25 Ω, Starting T_J = 25°C
3. I_{SD} ≤ -27A, di/dt ≤ 300A/μs, V_{DD} ≤ BV_{DSS}, Starting T_J = 25°C
4. Essentially independent of operating temperature

Figure A.10: P-Channel MOSFET used: FQP27P06 datasheet

Typical Characteristics

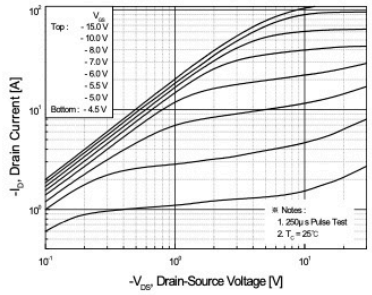

Figure 1. On-Region Characteristics

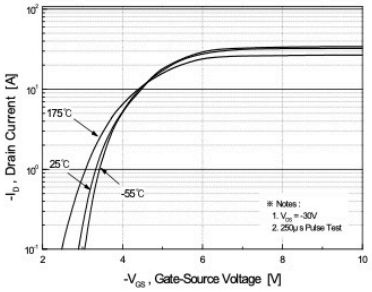

Figure 2. Transfer Characteristics

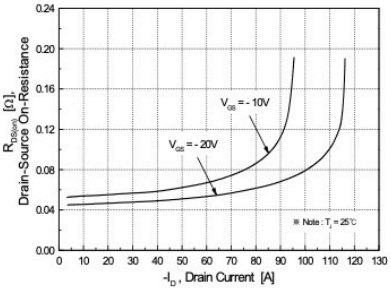

Figure 3. On-Resistance Variation vs. Drain Current and Gate Voltage

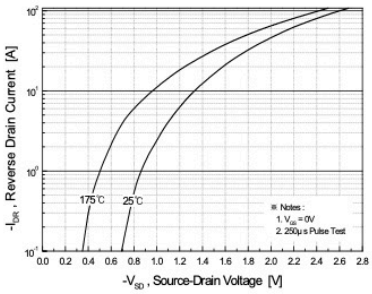

Figure 4. Body Diode Forward Voltage Variation vs. Source Current and Temperature

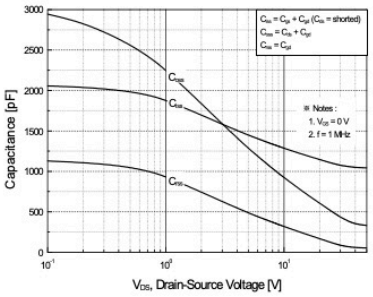

Figure 5. Capacitance Characteristics

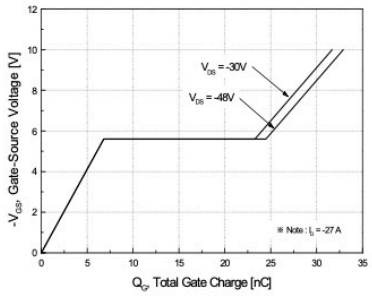

Figure 6. Gate Charge Characteristics

Figure A.11: P-Channel MOSFET used: FQP27P06 datasheet

FAIRCHILD SEMICONDUCTOR®

January 2013

LM555
Single Timer

Features

- High-Current Drive Capability: 200 mA
- Adjustable Duty Cycle
- Temperature Stability of 0.005%/°C
- Timing From μs to Hours
- Turn off Time Less Than 2 μs

Applications

- Precision Timing
- Pulse Generation
- Delay Generation
- Sequential Timing

Description

The LM555 is a highly stable controller capable of producing accurate timing pulses. With a monostable operation, the delay is controlled by one external resistor and one capacitor. With astable operation, the frequency and duty cycle are accurately controlled by two external resistors and one capacitor.

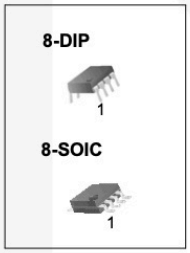

Ordering Information

Part Number	Operating Temperature Range	Top Mark	Package	Packing Method
LM555CN	0 ~ +70°C	LM555CN	DIP 8L	Rail
LM555CM		LM555CM	SOIC 8L	Rail
LM555CMX		LM555CM	SOIC 8L	Tape & Reel

Figure A.12: LM555 datasheet

Electrical Characteristics

Values are at T_A = 25°C, V_{CC} = 5 ~ 15 V unless otherwise specified.

Parameter	Symbol	Conditions	Min.	Typ.	Max.	Unit
Supply Voltage	V_{CC}		4.5		16.0	V
Supply Current (Low Stable) (1)	I_{CC}	V_{CC} = 5 V, R_L = ∞		3	6	mA
		V_{CC} = 15 V, R_L = ∞		7.5	15.0	mA
Timing Error (Monostable) Initial Accuracy (2)	ACCUR	R_A = 1 kΩ to100 kΩ C = 0.1 µF		1.0	3.0	%
Drift with Temperature (3)	Δt / ΔT			50		ppm / °C
Drift with Supply Voltage (3)	Δt / ΔV_{CC}			0.1	0.5	% / V
Timing Error (Astable) Initial Accuracy (2)	ACCUR	R_A = 1 kΩ to 100kΩ C = 0.1 µF		2.25		%
Drift with Temperature (3)	Δt / ΔT			150		ppm / °C
Drift with Supply Voltage (3)	Δt / ΔV_{CC}			0.3		% / V
Control Voltage	V_C	V_{CC} = 15 V	9.0	10.0	11.0	V
		V_{CC} = 5 V	2.60	3.33	4.00	V
Threshold Voltage	V_{TH}	V_{CC} = 15 V		10.0		V
		V_{CC} = 5V		3.33		V
Threshold Current (4)	I_{TH}			0.10	0.25	µA
Trigger Voltage	V_{TR}	V_{CC} = 5 V	1.10	1.67	2.20	V
		V_{CC} = 15 V	4.5	5.0	5.6	V
Trigger Current	I_{TR}	V_{TR} = 0 V		0.01	2.00	µA
Reset Voltage	V_{RST}		0.4	0.7	1.0	V
Reset Current	I_{RST}			0.1	0.4	mA
Low Output Voltage	V_{OL}	V_{CC} = 15 V, I_{SINK} = 10 mA		0.06	0.25	V
		V_{CC} = 15 V, I_{SINK} = 50 mA		0.30	0.75	V
		V_{CC} = 5 V, I_{SINK} = 5 mA		0.05	0.35	V
High Output Voltage	V_{OH}	V_{CC} = 15 V, I_{SOURCE} = 200 mA		12.5		V
		V_{CC} = 15 V, I_{SOURCE} = 100 mA	12.75	13.30		V
		V_{CC} = 5 V, I_{SOURCE} = 100 mA	2.75	3.30		V
Rise Time of Output(3)	t_R			100		ns
Fall Time of Output(3)	t_F			100		ns
Discharge Leakage Current	I_{LKG}			20	100	nA

Notes:

1. When the output is high, the supply current is typically 1 mA less than at V_{CC} = 5 V.
2. Tested at V_{CC} = 5.0 V and V_{CC} = 15 V.
3. These parameters, although guaranteed, are not 100% tested in production.
4. This determines the maximum value of $R_A + R_B$ for 15 V operation, the maximum total R = 20 MΩ, and for 5 V operation, the maximum total R = 6.7 MΩ.

Figure A.13: LM555 datasheet

1. Monostable Operation

Figure 2 illustrates a monostable circuit. In this mode, the timer generates a fixed pulse whenever the trigger voltage falls below $V_{CC}/3$. When the trigger pulse voltage applied to the #2 pin falls below $V_{CC}/3$ while the timer output is low, the timer's internal flip-flop turns the discharging transistor off and causes the timer output to become high by charging the external capacitor C1 and setting the flip-flop output at the same time.

The voltage across the external capacitor C1, V_{C1} increases exponentially with the time constant $t = R_A*C$ and reaches $2\ V_{CC}/3$ at $t_D = 1.1\ R_A*C$. Hence, capacitor C1 is charged through resistor R_A. The greater the time constant R_AC, the longer it takes for the V_{C1} to reach $2\ V_{CC}/3$. In other words, the time constant R_AC controls the output pulse width.

When the applied voltage to the capacitor C1 reaches $2\ V_{CC}/3$, the comparator on the trigger terminal resets the flip-flop, turning the discharging transistor on. At this time, C1 begins to discharge and the timer output converts to low. In this way, the timer operating in the monostable repeats the above process. Figure 3 shows the time constant relationship based on R_A and C. Figure 4 shows the general waveforms during the monostable operation.

It must be noted that, for a normal operation, the trigger pulse voltage needs to maintain a minimum of $V_{CC}/3$ before the timer output turns low. That is, although the output remains unaffected even if a different trigger pulse is applied while the output is high, it may be affected and the waveform does not operate properly if the trigger pulse voltage at the end of the output pulse remains at below $V_{CC}/3$. Figure 5 shows such a timer output abnormality.

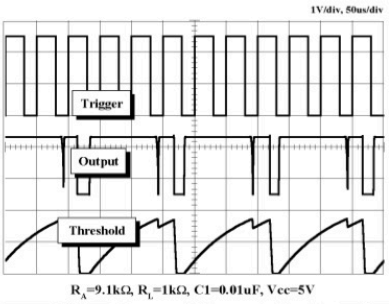

Figure 5. Waveforms of Monostable Operation (abnormal)

2. Astable Operation

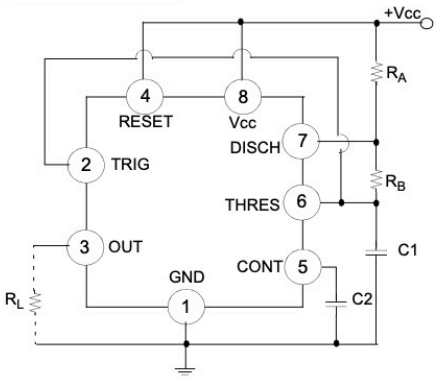

Figure 6. A Stable Circuit

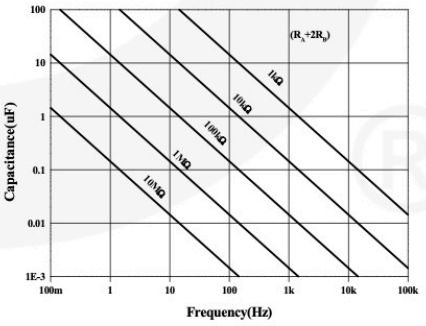

Figure 7. Capacitance and Resistance vs. Frequency

Figure A.14: LM555 datasheet